Risk Minimization for Spreading Processes over Networks via Surveillance Scheduling and Sparse Control

Vera L. J. Somers

A thesis submitted in fulfillment
of the requirements of the degree of
Doctor of Philosophy

Australian Centre for Field Robotics
School of Aerospace, Mechanical and Mechatronic Engineering
The University of Sydney

Submitted August 2021; revised January 2022

Declaration

I hereby declare that this submission is my own work and that, to the best of my knowledge and belief, it contains no material previously published or written by another person nor material which to a substantial extent has been accepted for the award of any other degree or diploma of the University or other institute of higher learning, except where due acknowledgement has been made in the text.

This thesis contains material published in [153–155]. Chapter 3 has been published as part of [155]. However, Figure 3.1 and Examples 3.1 and 3.2 in Section 3.3.3 appeared in [153]. Chapter 4 has been published as part of [155]. Chapter 5 has been published partially in [154] and partially in [155]. This chapter predominantly appeared in [155], however, in particular Figure 5.1, Problem 5.2 and Problem 5.3, including belonging explanations and propositions, and Example 5.3 have been published in [154]. Section A.1.1 has been published as part of [153]. Finally, Figures B.1 and B.2 in Appendix B have been published in [154].

I am the first author of all these papers. The ideas were formulated in collaboration with my supervisor, i.e. second author. However, I implemented the algorithm, created the examples, analyzed the results and wrote the drafts of the papers.

Vera L. J. Somers

19 January 2022

As supervisor for the candidature upon which this thesis is based, I can confirm that the authorship attribution statements above are correct.

Ian R. Manchester

19 January 2022

Abstract

Spreading processes, such as epidemics and wildfires, have an initial localized outbreak that spreads rapidly throughout a network of connected nodes, e.g. global travel networks for pandemics or geographically connected areas for wildfires. The real-world risks associated with such events have stressed the importance and current limitations of methods to both quickly map and monitor outbreaks and to reduce their impact by planning appropriate intervention strategies.

This thesis is, therefore, concerned with risk minimization of spreading processes over networks via surveillance schedules and sparse control. This is achieved by providing a flexible optimization framework that combines surveillance and intervention to bound and minimize the risk of spreading processes.

Here, risk is defined as the risk of an undetected outbreak, i.e. the product of the probability of an outbreak occurring over a time interval and the future impact of that outbreak. The aim is now to bound or minimize the risk of spreading processes by allocation of resources and use of persistent monitoring schedules.

When setting up an optimization framework to tackle this problem, four other aspects have been found to be of importance. First of all, being able to provide targeted risk estimation and minimization for more vulnerable or high cost areas. Second and third, scalability of algorithms and sparsity of resource allocation are essential due to the large network structures. Finally, for wildfires specifically, there is a gap between the information embedded in fire propagation models and utilizing it for persistent monitoring path planning algorithms for efficient remote sensing.

The presented framework utilizes the properties of positive systems and convex optimization, in particular exponential cone programming, to provide flexible and scalable algorithms for both surveillance and intervention purposes.

We demonstrate with different spreading process examples and scenarios, focusing on epidemics and wildfires, that the presented framework gives convincing and scalable results. In particular, we demonstrate how our method can include persistent monitoring scenarios and provide more targeted and sparse resource allocation compared to previous approaches.

Acknowledgements

The past 3.75 years have been an interesting and incredible journey, working on a topic that got exponentially more relevant by the month. Ironically I am also writing this while in lockdown. This thesis journey, however, would not have been possible nor as exciting and successful without the following people.

First of all, I would like to thank my supervisor, Ian Manchester, for his endless support and guidance and whom I probably drove crazy by my minor stalking behavior whenever I had a question or needed a signature on a form. Moreover, for his patience and only minor disapproval of my many, many arguably stupid questions.

Next, a big shout-out to the ACFR crew, in particular: Felix, Fletcher, Jackson, Jacob, James, Jasper, Max, Stuart, Wei and Wilhelm. Friends for life, partners in crime, fellow prisoners, thank you for the endless conversations and discussions, for the climbing, canyoning and pub adventures. It made ACFR a place where I felt at home, although it did get me a serious cryptic crossword and coffee addiction. To my other second home, the Rose, thank you for providing plenty of beer for thought and for the informal control meetings in the pub, who knew pub time could be productive!

To my parents, for always believing in me and to my dad in particular for convincing me that doing a PhD is the best time of your life, you were right! I really wish the borders weren't closed though. The last time I saw my parents in person, little did I know what was about to happen. It was that tipping point between 'interesting thesis topic' and 'holy guacamole, it's a bit too relevant'. Sydney was filled up with smoke. Ash was raining down on the city and in the plane landing into Sydney you could smell that distinctive smell of forest burning. Only a couple months later, I found myself stuck in a lockdown my own model would probably agree with.

Last but not least, a special mention to Cookie and Salem, for being fluffy and cuddly (and needy and distracting). To my Dutch friends, for being there for me from afar and in particular my highschool friends, thank you for visiting. It meant a lot to me! To Jonathon, for supporting me in these last hectic months. To everyone who never really understood what I did, it's okay, neither did I. Does anyone really? To everyone doing a PhD, you got this! And finally to everyone else, who supported me, but I don't have space to mention, thank you!

I swear I didn't start any fires or pandemics.

Contents

List of Figures

List of Tables

Nomenclature

Notation

Vectors and Matrices

a_i, a_{ij}	Element i of vector a or element (i, j) of matrix A
a^T	Transpose of the vector a
A^{-1}	Inverse of matrix A
$\text{diag}(a)$	Diagonal matrix with the elements of vector a on the diagonal
$\hat{a}(t)$	Expected value of a at time t
$\overline{a}$	Upper bound on parameter a
$\underline{a}$	Lower bound on parameter a
$\geq$	$A \geq B \Longrightarrow$ Elementwise inequality: $a_{ij} \geq b_{ij}\ \forall i, j$
	In particular $A \geq 0$ indicates that all elements are nonnegative
$\odot$	The Hadamard product, i.e. element-wise multiplication
$\lambda_{max}(A)$	The spectral abscissa or dominant eigenvalue of the matrix A, i.e. the eigenvalue with maximal real part
$\lvert \cdot \rvert$	Absolute value
$\lvert a \rvert_1$	1-norm, i.e. $\lvert a \rvert_1 := \sum_{i=1}^{n} \lvert a_i \rvert$
$\lVert a \rVert_{\ell_0}$	0-"norm", i.e. the number of non-zero elements of a
$\lVert a \rVert_{\ell_1}$	1-norm, see $\lvert a \rvert_1$
I	The identity matrix of the appropriate dimension
$\vec{1}$	Row vector with all ones of the appropriate dimension

Probability

$Pr\{\cdot\}$	Probability
$E[\cdot]$	Expected value

Miscellaneous

$\mathbb{R}$	The set of real numbers
$\mathbb{R}_+$	The set of nonnegative real numbers
$\mathbb{R}^n$	The set of n-tuples of real numbers
$\mathbb{R}^{n\times n}$	The set of real $n \times n$ matrices
Δ_t	Small time interval
$:=$	Definition
$\Rightarrow$	Implies that
pax	Number of passengers carried

List of Acronyms

ATL	Atlanta
CA	cellular automata
COVID-19	coronavirus disease of 2019
DCA	Washington DC
DS	Dynamics-Sensitive
DOP	Dubins orienteering problem
DP	dynamic programming
GP	geometric program
KKT	Karush-Kuhn-Tucker
LIDAR	light detection and ranging
LP	linear program
MDP	Markov Decision Process
MERS	Middle East respiratory syndrome
MPC	model predictive control
NIMFA	N-Intertwined Mean-Field Approximation
NYC	New York City
ODE	ordinary differential equation
OP	orienteering problem
PHL	Philadelphia
SARS	severe acute respiratory syndrome
SI	Susceptible-Infected
SIR	Susceptible-Infected-Removed
SIS	Susceptible-Infected-Susceptible
TSP	traveling salesman problem
UAV	unmanned aerial vehicle
US	United States

Chapter 1

Introduction

This thesis is concerned with risk minimization of spreading processes via surveillance scheduling and sparse control. This is achieved by providing the joint optimization of surveillance and intervention methods to bound and minimize the risk of spreading processes such as epidemics and wildfires. In this first introductory chapter, we provide background on the problems involved with risk minimization of spreading processes, state the research objective, summarize this thesis's main contributions including related publications and outline the thesis structure.

1.1 Background and Motivation

Epidemics and wildfires claim each year a significant number of lives, have major impacts on the economy and can cause significant disruptions to life as we know it as the outbreak of coronavirus disease of 2019 (COVID-19) and the Australian and Californian wildfire seasons of 2019/2020/2021 have demonstrated [18, 52, 72, 77, 127]. What they both have in common is that they can be thought of and modeled as a spreading process in which an initial localized outbreak spreads rapidly to neighboring nodes in a network [12, 80, 113]. Examples of these 'networks' are social contact networks for epidemics and raster data representing a forest area, i.e. a landscape partitioned into geographically connected grid cells, for wildfires.

The real-world risks associated with these events and other spreading processes, such as computer viruses, have sparked significant research into methods for modeling, prediction and control as indicated by the recent surveys [113, 122, 183]. The aftermath of two decades of multiple deadly coronavirus epidemics alone (SARS, MERS, COVID-19) stresses the importance and current shortcoming of being able to not only quickly map and monitor the spread of infection, but more importantly, get an accurate risk estimate and plan appropriate intervention strategies such as lockdowns, testing and vaccination [52, 127].

For wildfires specifically, future wildfire potential is, unfortunately, only predicted to keep increasing due to a warmer and dryer climate with already an upward trend being noticeable with fires becoming more frequent and severe [41, 77]. Therefore, as indicated by the Australian Bushfires and Natural Hazards CRC [18, 177], there is an interest in using remote sensing for early fire detection and risk reduction. Although many fire propagation models and simulators exist (e.g. [76, 80]) and path planning for spatial monitoring is well advanced (e.g. [129, 152, 179]), the link connecting them is still missing.

The earlier a fire or contagious disease can be detected, the easier it is to minimize the damage [57, 70, 113]. Therefore, it is essential to be able to quickly assess the situation and detect outbreaks early on. Hence, there is a clear need for methods to provide quick situational awareness to assess and minimize the risk of spreading processes.

The large scales these spreading processes typically evolve on, e.g. global travel networks for epidemics, large geographic areas for wildfires, or the internet for computer viruses, imposes another challenge and emphasizes the importance of scalability of computational methods. Furthermore, sparsity of resource allocation solutions is often needed, because it can be difficult or impossible to distribute resources broadly across the network, such as vaccines for epidemics or waterbombing allocations for wildfires.

1.2 Problem Statement

In the previous section we already touched upon some of the problems involved with risk minimization of spreading processes. The main problem is that it is important to be able to both efficiently monitor the network to reduce the risk of undetected outbreaks and to get an accurate risk estimate to plan appropriate intervention.

Four aspects in particular are important when solving this problem. First of all, being able to provide targeted risk estimation and minimization for more vulnerable or high cost areas, such as an elderly community during an epidemic or more populated areas when controlling a wildfire. Second, because spreading processes evolve over large networks, scalability of algorithms is important. Moreover, it can be difficult to distribute resources widely. Hence, sparsity of resource allocation is required. Finally, for wildfires specific, there is currently an inability to be able to directly use fire propagation models for efficient remote sensing, e.g. by deploying unmanned aerial vehicles (UAVs). Hence, there is a gap between the information embedded in spreading models and utilizing it for persistent monitoring path planning algorithms.

In order to address this problem we define our research objective as *'develop a joint optimization framework for both surveillance and intervention purposes that is 1) based on a risk model with node dependent costs for targeted risk minimization, 2) results in sparse outcomes, 3) is scalable to large network sizes and 4) can be connected to persistent monitoring algorithms for robot path planning'*.

In this thesis, we will, therefore, first of all examine the current state-of-the-art and existing literature on risk minimization for spreading processes. Next, we will design a surveillance schedule and determine intervention strategies to bound and minimize the risk of an undetected outbreak of a spreading process. In particular, we will focus on developing scalable algorithms and providing sparse resource allocation for targeted risk minimization. For wildfires specific, we will aim to bridge the gap between spreading models and remote sensing.

1.3 Contributions

In this thesis we provide a flexible optimization framework to bound and minimize the risk of spreading processes via surveillance schedules and sparse resource allocation. The main contributions of this thesis that address the problems and research objective presented in Section 1.2, can be summarized as follows:

- We provide the **joint optimization framework** of both surveillance and intervention via sensor scheduling and sparse control.
- A **risk model** is developed based on the product of the probability of an undetected outbreak with its discounted future cost, with *node dependent weightings*, to provide targeted risk estimation and minimization. In particular node impact is based on richer information than network topology and can deal with different types of network structures.
- **Sparsity** inducing resource models are presented, validated and discussed for the spreading rate, recovery rate and outbreak rate.
- The presented framework provides **scalable algorithms** for both surveillance and intervention purposes by utilizing the properties of positive systems and convex optimization, in particular *exponential cone programming*.
- For wildfires specific, we bridge the gap between spreading models and robotic path planning by developing **revisit maps** based on the risk that can be used in existing path planning algorithms.

We demonstrate the flexibility and use of the proposed approach by providing examples of different spreading processes: epidemics and wildfires. We show how our method leads to a more precisely targeted allocation of resources compared to previous approaches and can incorporate different parameters and scenarios such as a vaccination strategy for epidemics and the effect of vegetation, wind and outbreak rate on a wildfire in persistent monitoring scenarios.

Although we focus on spreading processes, the proposed framework is applicable to any linear positive system for which sparse control applications are needed.

1.4 Publications

The work presented in this thesis has also appeared in the following related publications as declared in the declaration of authorship.

- Somers, V. L. J. and Manchester, I. R. Minimizing the Risk of Spreading Processes via Surveillance Schedules and Sparse Control. *IEEE Transactions on Control of Network Systems*, Under review
- Somers, V. L. J. and Manchester, I. R. Sparse Resource Allocation for Control of Spreading Processes via Convex Optimization. *IEEE Control Systems Letters*, 5(2):547–552, 2021
- Somers, V. L. J. and Manchester, I. R. Priority maps for surveillance and intervention of wildfires and other spreading processes. In *Proceedings of the 2019 International Conference on Robotics and Automation*, pages 739–745. IEEE, 2019

1.5 Thesis Structure

The remainder of this thesis is structured as follows. In Chapter 2 the current state-of-the-art of spreading models, risk minimization for surveillance and intervention and optimization methods is analyzed. In particular, we provide background on spreading models of the two spreading processes we focus on, epidemics and wildfires, and discuss the existing literature and their shortcomings in relation to surveillance and intervention of them. The purpose of this chapter is to provide background on what methods could be used to design an optimization framework for risk minimization of spreading processes, which is the objective of this thesis.

Chapter 3 presents how to model the risk of an undetected outbreak of a spreading process. The risk model is based on the product of the probability of an undetected outbreak starting in a particular area and the impact of the process spreading from that location. We address how to model the outbreak probability and present the used linearized networked spreading model. Furthermore, we define a cost function to obtain targeted risk estimation and discuss how to model and visualize node impact or cost-to-go.

Next, in Chapter 4, we consider the surveillance problem of bounding the risk of an undetected outbreak by use of a revisit schedule. Here the dynamics of the spreading process are fixed and the aim is to identify and bound the future cost of an undetected outbreak spreading from each node. We introduce risk maps and look into the effect of the different parameters on the risk map with two different spreading process examples. Furthermore, we demonstrate how we can use surveillance schedules for persistent monitoring to bound the maximum risk.

We extend this idea in Chapter 5 by including resource allocation for risk minimization. We address the thesis objective and problems discussed earlier in Section 1.2 by formulating the joint optimization framework that minimizes the risk of spreading processes by integrating surveillance schedules and sparse control. To obtain this framework, we define resource models for spreading rate, recovery rate, outbreak rate and surveillance interval rate and discuss how they induce sparsity. Furthermore, we demonstrate how to reformulate the problem to obtain a convex optimization problem, in particular an exponential cone program. Finally, we compare our results to existing methods and we comment on computation and scalability. With multiple examples of spreading processes, i.e. epidemics and wildfires, we convey that the proposed method is easily applicable and provides quick and convincing results.

Finally, Chapter 6 presents the conclusion of this thesis. It summarizes the main results and contributions of this thesis and discusses open problems and directions for future work.

Chapter 2

Background

In order to provide a flexible framework for the optimization of both surveillance and intervention of spreading processes, we first have to look into the state-of-the art of spreading models, surveillance and intervention for risk minimization, and optimization. We, therefore, first present literature and background on models of the two spreading processes we focus on in this thesis: epidemics (Section 2.1) and wildfires (Section 2.2). Next, we review existing literature on surveillance and intervention strategies for risk minimization in respectively Sections 2.3 and 2.4. Finally, in Section 2.5, we provide background on relevant convex optimization methods.

2.1 Epidemic Models

The most well-known spreading models come from the epidemics literature and are the Susceptible-Infected-Susceptible (SIS) model and the Susceptible-Infected-Removed (SIR) model and their variants [7, 66, 83]. Their simplest mathematical description is the classic single group model or compartment model as first introduced by Kermark and Mckendrick [83] and can be described as a Markov process or system of ordinary differential equations (ODEs). To extend these models beyond the population level and model the interactions and connections between individuals, networked versions

of these models have been developed [113, 126, 167]. Finally, threshold conditions of the different models are important to determine the outcome of an outbreak [122].

2.1.1 Susceptible-Infected-Susceptible (SIS)

The simplest epidemic model is the Susceptible-Infected-Susceptible (SIS) model which consists of only two compartments or states: 'susceptible' and 'infectious' [7, 66]. It is assumed that individuals of the modeled population do not acquire immunity after infection and hence, transition back and forth between the 'susceptible' and 'infectious' state as illustrated in Figure 2.1 [166] via the *spreading rate* $\beta > 0$ and *recovery rate* $\delta > 0$. If $\delta = 0$, the model is called an Susceptible-Infected (SI) model and can only transition from 'susceptible' to 'infectious', i.e. infected nodes stay infected.

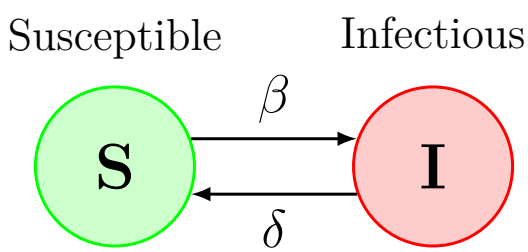

Figure 2.1 – Susceptible-Infected-Susceptible (SIS) model with infection rate β and recovery rate δ.

For the SIS model, the proportion of a population being in the 'susceptible' or 'infectious' state evolves according to the following deterministic ordinary differential equations (ODEs)

$$\dot{\mathcal{S}}(t) = -\beta\mathcal{S}(t)\mathcal{I}(t) + \delta\mathcal{I}(t) \tag{2.1a}$$

$$\dot{\mathcal{I}}(t) = \beta\mathcal{S}(t)\mathcal{I}(t) - \delta\mathcal{I}(t) \tag{2.1b}$$

where $\mathcal{S}(t)$ is the proportion of the population being 'susceptible' at time $t \geq 0$ and $\mathcal{I}(t)$ the proportion that is infectious. This model assumes a homogenous population with a constant population size and $\mathcal{S}(t) + \mathcal{I}(t) = 1$.

This basic deterministic model as originally developed in [83], has two major limitations. First of all, the assumption that an epidemic occurs on a large population that can be estimated by a continuous distribution without the presence of uncertainty or stochasticity. Outbreaks, however, often start as small local outbreaks where the effect of a finite population and uncertainty, such as a small change in the initial local outbreak, can not be neglected and have a significant impact on the outcome of the model. Second, the model does not take into account interactions on an individual node level.

To be able to take the stochasticity of the model into account, we can model an epidemic as a stochastic model with Markov transition probabilities. For a population of n individuals each node $i \in 1, 2, \ldots, n$ has state $X_i(t)$ associated with it that can be either $\mathcal{S}$(susceptible) or $\mathcal{I}$(infectious). This state now evolves according to the following stochastic equations:

$$Pr\left\{X_i(t+\Delta_t) = \mathcal{I} | X_i(t) = \mathcal{S}\right\} = \beta f(X(t))\Delta_t + o(\Delta_t) \tag{2.2a}$$

$$Pr\left\{X_i(t+\Delta_t) = \mathcal{S} | X_i(t) = \mathcal{I}\right\} = \delta\Delta_t + o(\Delta_t) \tag{2.2b}$$

for some scalar function $f : \{\mathcal{S}, \mathcal{I}\}^n \to [0, 1]$ and where Δ_t is a small time period.

It should be noted that (2.2a) describes an exogenous transition, i.e. the state of node i depends on external factors instead of solely its own state, whereas (2.2b) describes an endogenous transition, i.e. this transition between states occurs for each node independent of the state of other nodes [113]. Models that take into account network structure as well as individual node interactions are networked models, which we will discuss further in Section 2.1.3.

2.1.2 Susceptible-Infected-Removed (SIR)

The Susceptible-Infected-Removed (SIR) model as first introduced by Kermark and Mckendrick [83] can be seen as an extension of the SI model, i.e. an SIS model with $\delta = 0$, where an additional state 'recovered' or 'removed' is introduced as demon-

strated in Figure 2.2. Although on a side note, historically it was developed before the SIS model [66, 83].

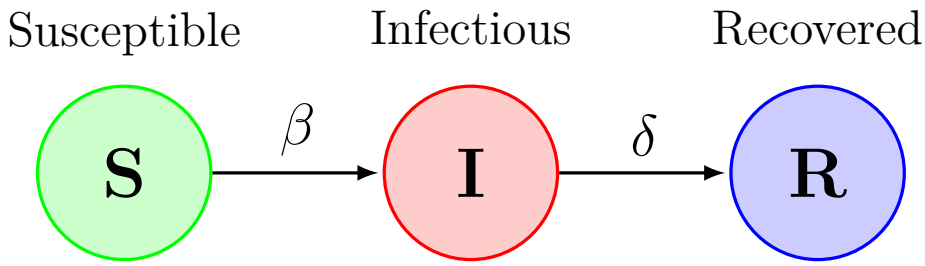

Figure 2.2 – Susceptible-Infected-Removed (SIR) model with infection rate β and recovery rate δ.

The transition between states is again defined by the *spreading rate* $\beta > 0$ and *recovery rate* $\delta > 0$. However, an 'infectious' node in state $\mathcal{I}(t)$ now transitions into the 'recovered' state $\mathcal{R}(t)$ with recovery rate δ instead of going back to the 'susceptible' state $\mathcal{S}(t)$. The deterministic ODEs describing these transitions as first formulated by Kermark and Mckendrick [83] are given by

$$\dot{\mathcal{S}}(t) = -\beta\mathcal{S}(t)\mathcal{I}(t) \tag{2.3a}$$

$$\dot{\mathcal{I}}(t) = \beta\mathcal{S}(t)\mathcal{I}(t) - \delta\mathcal{I}(t) \tag{2.3b}$$

$$\dot{\mathcal{R}}(t) = \delta\mathcal{I}(t). \tag{2.3c}$$

The stochastic model, which is a more realistic model to describe an epidemic as discussed before, can be obtained by replacing (2.2b) of the stochastic SIS model with

$$Pr\left\{X_i(t+\Delta_t) = \mathcal{R} | X_i(t) = \mathcal{I}\right\} = \delta\Delta_t + o(\Delta_t) \tag{2.4}$$

where each node i in the state vector $X(t) = (X_1(t), X_2(t), \ldots, X_n(t))^T$ can be in 3 states, i.e. $X_i(t) \in \{\mathcal{S}, \mathcal{I}, \mathcal{R}\}$. Another option is to model the different states separately where we define $X_i(t)$ as the probability a node i is in the infectious state $\mathcal{I}$ and $Z_i(t)$ as the probability of node i being in the removed state $\mathcal{R}$ as we will discuss further in Chapter 3.

2.1.3 Network Models

In the previous subsection we discussed the unrealistic assumption of the original SIS and SIR models of reducing the entire population into a subset of being in two or three compartments and ignoring individual interactions and connectivity. Networked models consider these individual interactions by associating spreading and recovery rates to individual edges and nodes, where the transitions depend on neighboring nodes. To model these interactions and connectivity, we make use of the basics of graph theory and therefore, first provide some definitions that we will use to describe the networked models.

Note that there is an entire field of study associated with extending compartment and population models to network models with different topologies, which is outside of the scope of this thesis, but for further reading we refer to [126].

Definition 2.1. *A directed graph or digraph $\mathcal{G}(\mathcal{V}, \mathcal{E})$ is a pair consisting of a nonempty set $\mathcal{V}$ of n vertices and a set of edges $\mathcal{E} \subseteq \mathcal{V} \times \mathcal{V}$.*

An *edge* of this graph $\mathcal{G}$ from node $i \in \mathcal{V}$ to node $j \in \mathcal{V}$ is defined by (i, j) and exists if $(i, j) \in \mathcal{E}$ [122].

Definition 2.2. *The adjacency matrix for a graph $\mathcal{G}$ with n nodes is $A_{\mathcal{G}} \in \mathbb{R}^{n \times n}$ with entries $a_{\mathcal{G}_{ij}} \in \mathbb{R}_+$ where $a_{\mathcal{G}_{ij}} = 1$ if and only if $(i, j) \in \mathcal{E}$ and 0 otherwise.*

It follows from Definitions 2.1 and 2.2 that a graph is *undirected* if the adjacency matrix is symmetric, i.e. $a_{\mathcal{G}_{ij}} = 1 \Rightarrow a_{\mathcal{G}_{ji}} = 1$ for all i and j.

Definition 2.3. *The set of in-neighbors of node i is defined as $\mathcal{N}_i = \{j | (j, i) \in \mathcal{E}\}$.*

We can now model the stochastic networked SIS model, where $X_i(t) \in \{\mathcal{S}, \mathcal{I}\} \to [0, 1]$, and instead of (2.2), we obtain

$$Pr\left\{X_i(t + \Delta_t) = \mathcal{I} | X_i(t) = \mathcal{S}\right\} = \sum_{j \in \mathcal{N}_i} \beta X_j(t) \Delta_t + o(\Delta_t) \tag{2.5a}$$

$$Pr\left\{X_i(t + \Delta_t) = \mathcal{S} | X_i(t) = \mathcal{I}\right\} = \delta \Delta_t + o(\Delta_t) \tag{2.5b}$$

for *homogeneous* networks where $\mathcal{N}_i$ is the neighborhood of node i. For *heterogeneous networks* the spreading and recovery rates vary per node and link in the network and therefore, β is replaced with β_{ij} and δ with δ_i.

Networked Mean-Field Approximations

A particularly interesting mathematical adaptation of the SIS model and a method to go from the stochastic networked model to a deterministic set of ODEs is the N-Intertwined Mean-Field Approximation (NIMFA), first described in [167].

Given a graph $\mathcal{G}$ with n nodes, for the basic SIS model, a node is now in two states: 'susceptible', i.e. $X_i(t) = \mathcal{S} = 0$, or 'infectious', i.e. $X_i(t) = \mathcal{I} = 1$. The transition probabilities, following (2.5), are defined using the fact that $X_i(t)$ is a Bernoulli random variable for a small time period Δ_t for a *heterogeneous network* as

$$Pr\left\{X_i(t+\Delta t) = 1 | X_i(t) = 0\right\} = \sum_{j\in\mathcal{N}_i} \beta_{ij} X_j(t)\Delta_t + o(\Delta_t) \tag{2.6a}$$

$$Pr\left\{X_i(t+\Delta t) = 0 | X_i(t) = 1\right\} = \delta_i \Delta_t + o(\Delta_t) \tag{2.6b}$$

$$Pr\left\{X_i(t+\Delta t) = 0 | X_i(t) = 0\right\} = 1 - \sum_{j\in\mathcal{N}_i} \beta_{ij} X_j(t)\Delta_t + o(\Delta_t) \tag{2.6c}$$

$$Pr\left\{X_i(t+\Delta t) = 1 | X_i(t) = 1\right\} = 1 - \delta_i \Delta_t + o(\Delta_t) \tag{2.6d}$$

where β_{ij} is the spreading rate from node j, δ_i the recovery rate and $\mathcal{N}_i$ the neighborhood of node i.

If we define $E[X_i(t)] = Pr\left(X_i(t) = 1\right)$ as the probability of node i being infected, the dynamics of the expectation can be obtained from (2.6) by letting Δ_t go to zero

$$\begin{aligned}\frac{dE[X_i(t)]}{dt} &= -E\left[X_i(t)\delta_i + (1 - X_i(t)) \sum_{j\in\mathcal{N}_i} \beta_{ij} X_j(t)\right] \\ &= -E[X_i(t)]\delta_i + E\left[(1 - X_i(t)) \sum_{j=1}^{n} \beta_{ij} X_j(t)\right]\end{aligned} \tag{2.7}$$

where $\beta_{ij} = 0$ if $(i, j) \notin \mathcal{E}$.

Finally, n coupled nonlinear differential equations can be obtained by using a mean-field approximation:

$$\dot{\chi}_i(t) = (1 - \chi_i(t)) \sum_{j=1}^{n} \beta_{ij}\chi_j(t) - \delta_i\chi_i(t). \tag{2.8}$$

The mean-field approximation is obtained by making the assumption that all random variables have zero covariance, i.e. $E[X_iX_j] = E[X_i]E[X_j]$ for all $i \neq j$. It is proven in [51, 90, 165] that the deterministic model upperbounds the actual infection probabilities.

The set of ODEs (2.8) have an equilibrium point at $\chi = 0$ called the *disease-free equilibrium*. Because in many real epidemics, levels of infection in a population are very small, we can linearize (2.8) around the disease-free equilibrium to obtain the linear model

$$\dot{x}(t) = (B - D)x(t) \tag{2.9}$$

where $x(t) = [x_1(t), ..., x_n(t)]^T$ is the state of the linearized system with $x(0) \in [0, 1]^n$, $B = [\beta_{ij}]$ the matrix of spreading rates, given that $\beta_{ij} = 0$ if $(i, j) \notin \mathcal{E}$, and $D = \text{diag}(\delta_1, \delta_2, \ldots, \delta_n)$ the diagonal matrix of recovery rates. The linear model again upperbounds the nonlinear one [131]. This implies that controlling or stabilizing the linear model has a guarantee of controlling the underlying stochastic epidemic outbreak model.

For the SIR model a set of n nonlinear differential equations can be derived in a similar fashion, which can again be linearized to obtain the linear model. We will discuss the SIR model and linear upperbound further in Chapter 3.

2.1.4 Threshold condition

An important part of epidemiology is being able to predict if and when an epidemic will die out, i.e. if or when the absorbing *disease-free* state will be reached. For the basic compartmental SIS model (2.1)/(2.2) there are two equilibrium states possible:

the system either reaches the *disease-free equilibrium* $\mathcal{I} = 0$ or the *endemic equilibrium* $\mathcal{I} = 1 - \frac{\delta}{\beta}$. The threshold condition for the disease-free equilibrium to be globally asymptotically stable is

$$R_0 = \frac{\beta}{\delta} \leq 1 \tag{2.10}$$

where R_0 is the *basic reproductive number* that describes the average amount of secondary infections that are caused by a single infectious individual [83, 113, 122].

For the SIR model the same threshold condition (2.10) exists, however, there is no endemic equilibrium due to the existence of the 'removed' state. If $R_0 \leq 1$ the outbreak exponentially converges to the disease-free equilibrium $\mathcal{I} = 0$, whereas if $R_0 > 1$ the outbreak will monotonically increase until reaching its peak. Afterwards it will decrease to the disease-free equilibrium $\mathcal{I} = 0$ with nodes being either 'susceptible' or 'removed'.

For networked models, the basic reproductive number R_0 alone is often not sufficient to represent the outcome of the epidemic and updated threshold conditions have been derived. For *homogeneous* networked models the disease-free equilibrium $\chi = 0$ is globally asymptotically stable if and only if

$$R_0 = \frac{\beta}{\delta} \leq \frac{1}{\lambda_{\max}(A_{\mathcal{G}})} \tag{2.11}$$

where $\lambda_{\max}(A_{\mathcal{G}})$ is the maximum eigenvalue of the adjacency matrix [167].

Relating this back to the previous discussion about the NIMFA; if the disease-free equilibrium of the deterministic model is globally asymptotically stable, the underlying stochastic system will reach the disease-free absorbing state in sublinear time [90, 165]. Hence, it also defines a lower bound for the epidemic threshold.

For *heterogeneous* networks, the disease-free equilibrium $\chi = 0$ is globally asymptotically stable if and only if

$$\lambda_{\max}(B - D) \leq 0 \tag{2.12}$$

where $\mathcal{G}$ is assumed to be strongly connected directed, $B = [\beta_{ij}]$ the matrix of spreading rates, such that $\beta_{ij} = 0$ if $(i, j) \notin \mathcal{E}$, and $D = \mathrm{diag}(\delta_1, \delta_2, \ldots, \delta_n)$ the diagonal

matrix of recovery rates [85, 178].

More detail on the stability of the disease-free equilibrium can be found in [85, 122].

Threshold conditions are particularly critical when trying to intervene with the spreading process and the basic reproduction number R_0 is often used in press conferences [33, 102] when talking about COVID-19 outbreaks to indicate the seriousness of the variation or current outbreak and the need for less or more measures such as lockdown restrictions.

2.1.5 Other Models

The described stochastic, deterministic and networked SIS and SIR models are the most common epidemic models and will be used in this thesis. However, there are many other extensions and variations to these models. A common extension is to include birth and death rates or adding additional compartments, e.g. 'exposed' or 'asymptomatic' [68, 122].

For the networked models there are multiple variations. First of all, metapopulation models where nodes represent subpopulations instead of individuals. They are modeled in a similar way to networked models, but are often extended by modeling the dynamics within populations as well [113, 126]. Second, all presented network models assume continuous time, but discrete time versions as presented in [122] might be more suitable depending on the epidemic data available. Finally, instead of deterministic network models, stochastic agent based models are a different approach to modeling the individual connections and interactions. For a comparison between agent based models and metapopulation models, we refer to [1].

2.2 Wildfire Models

The basics for fire spread modeling were set out by Rothermel in [141] and [142], with an additional model for crown fires later described in [143]. Almost all current

available fire models and simulators use these basics to a certain extent and tune their rate of spread model parameters on his research. The current fire spread models can be split into two categories regarding their landscape presentations: continuous and discrete [157, 159] of which discrete models or more specifically stochastic cellular automata (CA) models are similar to epidemic SIS and SIR models.

2.2.1 Continuous Landscape Representation

Continuous landscape fire spread models use wave propagation to model wildfires [157]. This is done by applying Huygens' wavelet principle by considering fire spread similar to light wave propagation. Instead of light waves propagating from each other, each point on a fire perimeter is considered as a possible new fire ignition source [5, 159]. This model is, together with Rothermels' models for fire spread [141, 143], the basis for FARSITE [47], the fire simulator used by the U.S. Forest Service.

The main disadvantages of continuous landscape representations are that they are very complex models that need homogeneous data to perform well. That is, fire spread parameters, such as vegetation, fuel available and wind conditions, are assumed to be the same for the entire area or landscape that is considered. However, the real environment is often not homogeneous but heterogeneous, which introduces errors into the system that accumulate over time if no correction factors are used [159]. Using a discrete representation of the landscape helps address these issues.

2.2.2 Discrete Landscape Representation

Within discrete landscape representation models, a split can be made between regular, e.g. a grid, and irregular structures, e.g. triangulation. On this discrete landscape the rate of spread can be calculated by either considering the shortest path or using probabilities for fire transition from one cell to another. The first, the shortest path method, is applied by Stepanov and Smith [157] for a wildfire model using a Delaunay triangulation that can serve as a good first approximation of wildfire propagation time.

The latter is commonly known as cellular automata (CA) and is similar to the stochastic epidemic SIR model. It is easier to implement than all previously described methods, has a low computational cost and is suitable for heterogeneous conditions [159]. Furthermore, it has been shown to give quantitatively accurate predictions when compared to real wildfire spread [81]. It is, therefore, one of the most popular and common wildfire propagation models and forms the basis for Australis [82], the simulator developed for the Western Australia Deparment of Fire and Emergency Services.

Cellular Automata Models

Cellular Automata (CA) models are stochastic models based on fire transition probabilities from one cell to another. Each cell is in one of a finite number of states and can transition to another state in discrete time based on a number of rules. The most simplified version would be that a cell is 'on fire' or 'unburned' and 'susceptible' to fire. Compare this to an SIS model (Section 2.1.1) where 'susceptible' is 'susceptible to fire' and 'infectious' is now 'on fire' . Similar to SIR models (Section 2.1.2) a third state 'recovered' or 'removed' can be added by adding a 'burned' state.

An example set of rules of how the state $X_i(t)$ of cell i transitions could be

> *Rule 1*: IF $X_i(t)$='on fire' THEN $X_i(t+1)$='burned' with probability δ_i
>
> *Rule 2*: IF $X_i(t)$= 'unburned' AND neighbor j is 'on fire' THEN $X_i(t+1)$='on fire' with a probability β_{ij} [3].

Here δ_i is the recovery or removed rate and β_{ij} is the spreading rate from cell j to i based on wind velocity and direction, vegetation, fuel available and other factors influencing fire spread.

We visualize the spreading options to neighboring cells in Figure 2.3 for a lattice grid, which is common in fire CA models. The fire can spread to the 8 surrounding grid cells with probability β_{ji}. That is, if a cell is on fire as demonstrated in Figure 2.3

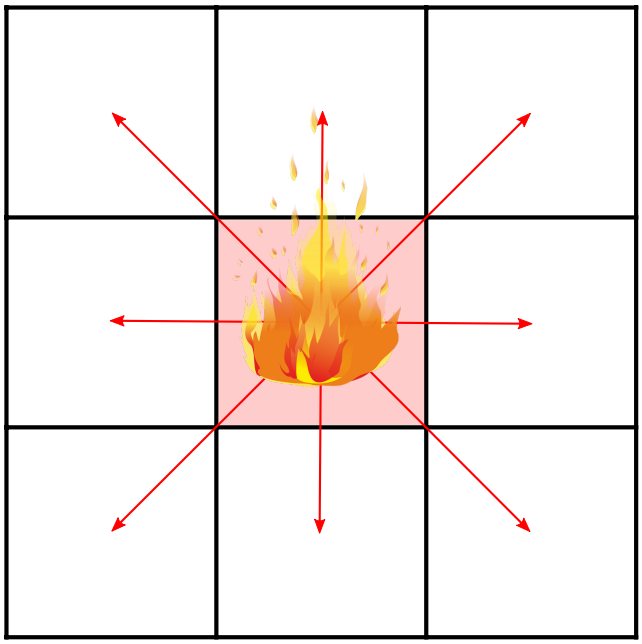

Figure 2.3 – Fire can propagate to its 8 direct neighbors on a square grid.

for a simple grid example, at each discrete time step t of the simulation, the fire can spread to each surrounding grid cell j with independent probability β_{ji}.

One of the first CA models suitable for both homogeneous and inhomogeneous forests was described by Karafyllidis and Thanailakis in [80] where they use hypothetical forests to validate the model. Another example of a successful cellular automata model with a regular grid structure that can include the state of fuel present is the model described by Alexandridis et al. [3] that is validated on the Spetses Island fire in 1990.

Instead of using a square grid, Hernández Encinas et al. [65] proposed a CA model with hexagonal cells. It has low computational cost, weather and land topography are included, it can implement different rates of spread and a first comparison with real fire spreading data gives good results.

A downside of regular grids is that they can only model the fire spread in limited directions, due to its structure, which can lead to fire shape distortions and lower accuracy. Therefore, Johnston et al. [76] proposed a fire spread model using an irregular grid that obtains the same accuracy as wave propagation methods, but has

a lower computational cost.

A disadvantage of CA models is that stochastic discrete models are not directly amenable for optimization-based analysis and decision-making as each simulation will have a different outcome. However, we can overcome the stochastic CA models' optimization and decision-making issues by using their deterministic approximations similar to epidemic modeling.

We can model this grid as a directed graph $\mathcal{G}(\mathcal{V}, \mathcal{E})$ with n nodes, where each cell is a node $i \in \mathcal{V}$ and an edge $(i, j) \in \mathcal{E}$ exists if cells are connected. For a small time interval Δ_t a surrounding cell j can now catch fire with probability $\beta_{ji}\Delta_t$ and the node i, that is on fire, can burn out with probability $\delta_i\Delta_t$ and we have reached a similar model as the ones discussed in Section 2.1.

2.2.3 Wildfire Simulators

In the previous subsections we already mentioned a couple of different simulators such as Farsite [47] and Australis [82]. We in particular want to highlight the Australis wildfire simulator to demonstrate and convey that CA models can be very accurate in simulating real wildfires.

As mentioned previously, the Australis wildfire simulator is based on a CA model and fire can spread as demonstrated in Figure 2.4. If cell A is 'on fire', Figure 2.4a, fire can spread to its surrounding cells. If cell A is 'susceptible' to fire and its neighbors are 'on fire', fire can spread towards cell A with a predetermined probability.

This simulator was validated by comparing simulated fire spreading with historical wildfire data in [81], an example of this comparison is shown in Figure 2.5.

Furthermore, the research by Kelso et al. [81] proposes a method for evaluating wildfire simulators. To obtain this accuracy in prediction, existing wildfire simulators, such as Australis, take into account vegetation maps, elevation, terrain, fuel maps and weather conditions to obtain accurate transition probabilities [81, 109].

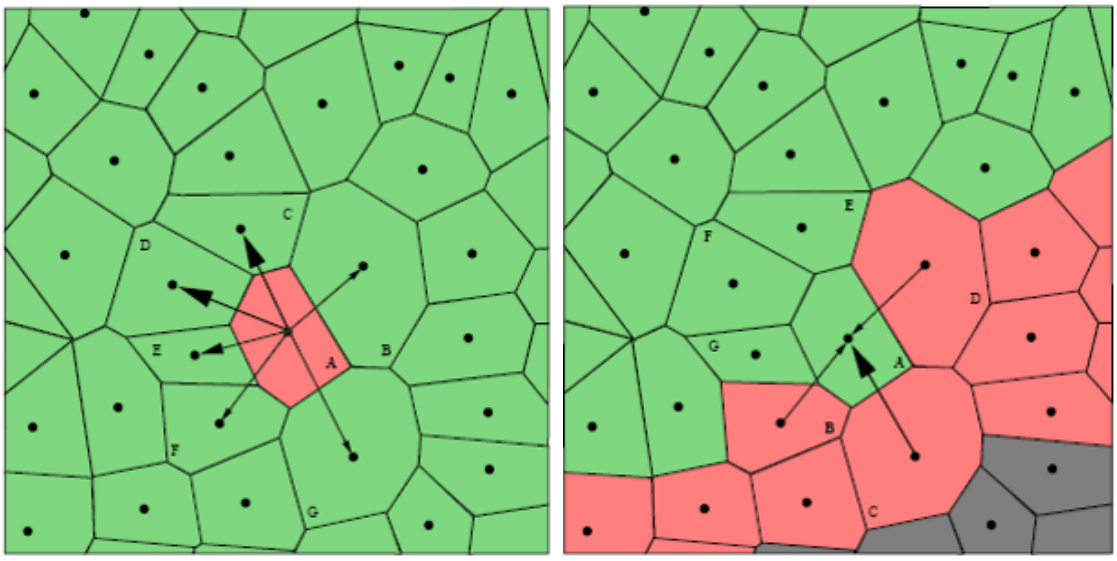

(a) Fire can spread from a single cell A to its neighbors [82]

(b) Fire can spread to cell A from neighboring cells on fire [82]

Figure 2.4 – The Australis wildfire simulator [82] is based on a CA model. Fire can spread from or to cell A based on which neighboring cells are on fire and, in this case, a southeasterly wind. Green is 'susceptible' to fire, red indicates 'on fire' and black is 'burned'. Figures are taken from [82].

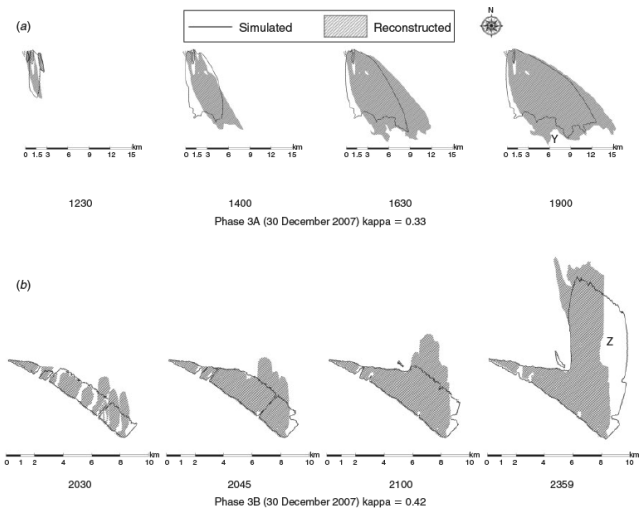

Figure 2.5 – Example of a wildfire simulation evaluation of the Australis simulator by Kelso et al. [81].

Remote sensing can provide estimates for fuel mapping or biomass estimation as shown by many studies, e.g. [4, 26, 109]. In [109] the sensitivity of fire simulators to different fuel and probability models is tested and the authors conclude that the use of

airborne laser scanning, i.e. light detection and ranging (LIDAR), and multispectral data over Landsat and other satellite imagery, see [4, 109], has significantly increased the accuracy of fuel maps, increasing the appeal of the aforementioned CA models.

2.3 Surveillance

Given a spreading process and its known model, there are two main problems that can be considered. First of all *Surveillance Scheduling*, i.e. how to estimate the state of the process. Especially since spreading processes evolve on large networks, a sampling schedule is needed to determine the state of the outbreak. The second problem is *Intervention*, i.e. how to modify the spreading process and reduce the impact of its outbreak, which we will discuss in Section 2.4.

2.3.1 Critical Nodes

Both for surveillance scheduling and intervention it is important to determine which nodes in a graph are most influential in regards to an outbreak of a spreading process. This is often approached by ranking nodes, for which many different methods exist. The most common ones are based on graph topology, where the most straightforward method is to look at the degree of a node [98]. The higher the degree of a node, i.e. the number of neighbors (Definition 2.3), the more critical the node. Another option is to define neighbors of randomly picked nodes as critical, since neighbors of random nodes are most likely to have a high degree [98].

More sophisticated versions of this are point centrality [50, 69, 125] and the k-shell index [86]. Point centrality metrics are common in analysis of social networks and can be split into three different categories: degree, as already discussed, closeness, i.e. the closeness of a node to all other nodes in a directed graph (Definition 2.1), and betweenness centrality, which looks at if a node is on the shortest path of pairs of other random nodes in the graph [50, 69]. The k-shell index, described by Kitsak et al. [86], focuses on the location of the nodes instead of solely on the neighbors (i.e.

degree) to determine the influential nodes. The k-shell index of a node is obtained by looking at the remaining degree after pruning of nodes with a lower degree than the current layer.

However, these methods struggle in defining critical nodes in regular graph structures such as grids, where all nodes have similar degrees. Moreover, in [97] it is shown that considering topological features alone is in most cases not enough to indicate influential nodes.

Other options include reproduction number [113] and PageRank [25, 103, 118]. Reproduction number R_0, as discussed in Section 2.1.4, is the average number of secondary infections that occur from a single node. Hence, nodes can be ranked by simulating their impact. Although it works well as a metric to find high impact nodes, it is not computational efficient [113, 135]. PageRank is the algorithm behind the Google search rankings, which consists of a random walk problem, where the more often a node is visited on a random walk, the higher the rating [103, 118].

Furthermore, in wildfire models it is particularly important to consider spatially-varying spreading rates, due to the effects of vegetation, terrain, and weather.

Methods that, therefore, go beyond simple topological features and take into account both network structures and dynamical parameters such as spreading rate are Dynamics-Sensitive (DS) centrality [97] and eigenvector centrality [178]. DS centrality determines the importance of a node by considering a weighted sum of walks from a node to all other nodes in the graph by taking into account both the spreading rate and spreading time, where longer walks have a lower weighting [97]. In eigenvector centrality, the elements of the eigenvectors corresponding to the maximum eigenvalue of the adjacency matrix, i.e. *spectral radius*, provide a measure of node impact [114, 132, 167, 168, 178]. This relates back to the threshold condition of heterogeneous networks (2.12) and will be further discussed regarding intervention and minimizing the dominant eigenvalue in Section 2.4.1.

2.3.2 Outbreak Probability

Another aspect of surveillance scheduling, besides only finding the critical nodes, is the likelihood of an outbreak. While the outbreaks of unknown and new epidemics are hard to predict, the likelihood of experiencing outbreaks of known diseases can be modeled. In [28] the likelihood of a severe acute respiratory syndrome (SARS) outbreak is modeled by analyzing different stochastic outcomes of an outbreak with the same initial conditions. That is, the more often these stochastic simulations result in high case numbers in a given location, the higher the likelihood of an outbreak. Hence, new critical outbreak locations can be found.

Wildfires, on the other hand, are in some sense more predictable due to the known conditions that cause a fire to start. Fire ignition probabilities are studied in [133]. Here, the authors purely look into determining fire probability maps using weather and fire danger variables and compare them to historical data. They indicate, however, a need to connect their maps to additional topographic variables, i.e. combining outbreak probability with node impact and spreading models.

Other stochastic and deterministic fire susceptibility mapping approaches using machine learning and logistic regression are researched in [53, 74, 89]. In [177] satellite data is used to estimate the live fuel moisture content, one of the primary factors influencing wildfire fuel flammability.

2.3.3 Surveillance Scheduling

Surveillance scheduling, or *sensor scheduling*, consists of finding an optimal schedule for taking measurements at individual nodes to estimate or influence the state of the total system, given a limited budget on the number of nodes that can be sensed at the same time.

In the literature, sensor scheduling is often considered from a control theoretical perspective. E.g. sensor and actuator placement to optimize controllability and observability for dynamical networks is studied in [160]. For linear dynamical systems

tractable algorithms are developed in [170] and a simple example in an application for active mapping is presented. Similarly, periodic sensor scheduling for an infinite time horizon of continuous time linear systems is presented by Ha and Choi [61]. For discrete time linear systems a greedy algorithm is presented in [75] and Huber and Hanebeck [71] accomplish prioritizing sensor nodes and sensor schedules by exploiting the monotonicity of the Riccati equation in combination with a branch-and-bound technique.

Sensor scheduling applied to spreading processes on the other hand is more limited. For epidemics, sensor scheduling could be interpreted as a testing schedule or the selection of individuals to be tested for which an interest has arrived since COVID-19 [130]. For wildfires, sensor scheduling or more specifically, *persistent monitoring* using UAVs is a more active area of research.

Persistent monitoring

Persistent monitoring literature for wildfires can be roughly split into two categories based on their main goal: 1) fire mapping and fire perimeter estimation, and 2) optimal path planning. The first category is outside the scope of this thesis, but examples of boundary estimation and fire perimeter tracking algorithms are given in [78, 151]. The second category, path planning, is relevant for this thesis, because it is part of our thesis objective to bridge the gap between existing spreading models and UAV path planning. We, therefore, need to look into the current state-of-the-art of path planning methods.

For the persistent monitoring problem different path planning algorithms and solutions exist [2, 17, 23, 59, 129, 136, 146, 152, 179]. They can be split into two main categories; either all nodes are visited in an optimal order and frequency or a trade-off is made which nodes to visit based on their impact.

If all nodes are visited, the most straightforward and simple persistent monitoring model is the 'boustrophedon' path, more commonly known as a lawnmower pattern [23]. When no further information about an outbreak is available this method is often

used as a baseline with decent results. Another option is to approach the problem as a traveling salesman problem (TSP) [48], i.e. finding the shortest, most efficient path between nodes. This problem is NP-hard, but many different efficient heuristic algorithms have been proposed [60, 93, 95]. For a grid pattern with equal distances and no weights associated with the nodes, this will often result in a lawnmower pattern. TSPs for the Dubins vehicle, i.e. turn-rate limited, are developed in [146].

A more sophisticated approach for a predetermined path is given in [152], where a linear program (LP) is solved to compute a speed controller to minimize the maximum field value over the environment. Alamdari et al. [2] provide a solution to the persistent monitoring problem in discrete environments by minimizing the maximum latency between observations. Here maximum latency is the maximum time between visits to the same node. This is done by first creating a relaxed graph, i.e. relaxing the weights of the nodes to be powers of 2, and ranking the nodes of the relaxed graph in different priority classes. Afterwards different walks are created for which a traveling salesman path is found. These walks together form the final path, such that the highest priority nodes are visited in each subwalk and the lowest priority nodes are only visited once during the complete tour. The results outperform a classic TSP.

An example of a routing problem in which a trade-off is made which nodes to visit is the orienteering problem (OP). Here the goal is to find a path that visits a subset of nodes that maximizes the total collected sum, where each node has a weight associated with it [59]. Different variations exist. An example of a flight time and path length trade-off algorithm is the Dubins orienteering problem (DOP) discussed in [129]. The proposed solution is based on the variable neighborhood search. Yu et al. [179] give a nonlinear extension to the OP called the correlated orienteering problem, which is solved with a mixed integer quadratic program.

2.4 Intervention

In the previous section we discussed how to determine the state of the system and find nodes that are influential and critical in case of an outbreak of a spreading process.

The next step is to utilize this knowledge and look into strategies to influence the system and reduce the impact of the spreading process within a budgeted constraint. We are particularly interested in methods that provide sparse and scalable control due to the large scale these spreading processes typically evolve on.

2.4.1 Topological Control

The most intuitive idea to reduce the impact of an outbreak is by either removing the optimal combination of nodes or edges or to influence the system by lowering the epidemic threshold (see Section 2.1.4). Removing nodes and edges from a graph is most likely to be costly in the real world. Therefore, an optimal solution is required to make sure a minimum number of nodes and edges is selected to obtain the desired reduction in outbreak.

Node and Link Removal

The problems of minimizing the spreading rate by removing either a fixed number of nodes or edges, i.e. links, in the network turn out to be respectively NP complete and NP-hard [168]. This fact has motivated the study of heuristics methods based on node-rankings of various forms [34, 62, 94, 101].

Many heuristics use the metrics that were discussed in Section 2.3.1 to identify critical nodes to remove based on topological features, e.g. point centrality [69, 125] and PageRank [25, 103]. In [148] the susceptible size of the population is optimized based on a variation of the betweenness centrality. In [42] a different approach is taken by solving a non-convex quadratically constrained quadratic program for optimal link removal.

Lindmark and Altafini [94] identify parameters for controllability of a network, where the main result is again based on topological features, i.e. the highest ratio of weighted outdegree versus indegree. Similarly, in [34] leader selection and its influence on stability and optimal performance in directed graphs is explored. Moreover, the authors

study combination drug therapy and solve this by influencing the main diagonal of the dynamic matrix.

However, these approaches have drawbacks as identified previously in Section 2.3.1. That is, they are not suitable for regular graph structures like grids and using topological features alone is not enough to indicate critical nodes. In general, these approaches will, therefore, not be optimal in any sense and tend to perform poorly [97, 113, 181]. Furthermore, the assumption of complete node or link removal is often unrealistic and impractical in the real world, because this implies that it is possible to perfectly isolate or remove an individual or area from the network.

Spectral Abscissa

A method that goes beyond simple topological features is minimizing the *spectral radius*, i.e. minimizing the dominant eigenvalue of the adjacency matrix $\lambda_{\max}(A_{\mathcal{G}})$, or more specifically, minimizing the *spectral abscissa*, i.e. minimizing the dominant eigenvalue of the linear dynamics, $\lambda_{\max}(B - D)$ (2.12). This results in a reduction in overall spreading rate across the network and is based on the intuitive approach of lowering the epidemic threshold [114, 132, 167, 168, 178]. The effect of minimizing the spectral abscissa (2.12) is to maximize the exponential decay rate of the system towards the disease-free equilibrium [113].

In [171] and [172], the authors recognise the importance of spatial control and develop constrained optimization methods, employing Lagrange multipliers, for allocating resources to minimize the dominant eigenvalue of the system matrices.

However, in many cases it is crucial to take into account node dependent costs for targeted outbreak risk minimization. For example, higher cost may be associated with nodes representing populated areas when controlling a wildfire or more vulnerable members of the community, such as the elderly or immunocompromised, in an epidemic. This is not taken into account when minimizing the spectral abscissa.

2.4.2 Optimal Control

A more suitable approach and realistic assumption is to reduce the impact of an outbreak by tuning and controlling the spreading rates and recovery rates. This can be achieved by applying resources to the nodes and edges. Examples of resources include waterbombing and backburning for wildfires and social distancing, lockdowns and vaccination for epidemics. Various solutions to the optimal control problem of regulating infection spread over networks are presented in [12, 31, 35, 36, 63, 84, 96, 99, 113, 114, 132, 137, 162, 182].

For example, the control input can be taken as the fraction of the population treatment or resource allocation is provided to as done for SIS and SIR models in [44, 49, 107]. Using Pontryagin's maximum principle an optimal solution is found where the result is a bang-bang controller. An optimal control solution based on multiple switches is presented by [84] to regulate infection levels by adapting recovery rates of the nodes. Di Giamberardino and Iacoviello [35] applied classical control strategy to the cost function to develop an optimal vaccination model that has a switching cost depending on the state and severity of the disease and outbreak.

A different approach was taken by Bloem et al. [12], who considered an SI(R) model for computer networks infected by a virus. A linear-quadratic regulator is proposed to solve the problem of spreading minimization via patching. In [99] the authors present a Jacobi type distributed algorithm for suppressing epidemic spread over networks. Distributed feedback control for two competing viruses is studied in [96].

Most of these presented methods give good working results for small scale examples, but have limitations in regards to scalability. More recently limitations on feedback control have been identified in [175, 176]. It is proven that a large class of distributed controllers cannot guarantee convergence to the disease-free equilibrium utilizing the recovery rate as the control input.

Linear spreading processes are positive systems [8], which enables control based on *linear programming* [16, 138] and *geometric programming* [15], which allows global optima to be found with efficient numerical methods and significantly improved scal-

ability compared to general linear systems. Optimal resource allocation via geometric programming has, therefore, been studied in [63, 73, 114, 115, 117, 132, 182].

In particular we like to highlight [132], which is the first paper to describe how the problem of containing spreading processes under budget constraints can be reformulated as a geometric program (GP) using the linear SIS dynamics. Two problems are considered, 1) minimize the impact of the outbreak given a fixed budget by finding the optimal resource allocation and 2) find the minimal amount of resources required to control the spreading process. Extensions were proposed in [63] for unknown contact rates. Hung et al. [73] consider the problem where two levels of recovery rates exist with different amounts of resources required. Again the problem is reformulated as a conic geometric program. In [115] a convex optimization framework is proposed for SIR models where the expected number of infections is minimized.

However, most of these papers consider minimizing the spectral radius, spectral abscissa or similar instead of node dependent costs. In addition, most of the discussed methods do not result in sparse resource allocation, exceptions being [31] which formulated a knapsack problem for a multi epidemic problem and sparse resource allocation was obtained, and [162] in which optimal sparsity is obtained for the special case of diagonally symmetrizable system matrices. We will, therefore, discuss convex optimization, geometric programming and sparsity further in more detail in Section 2.5.

2.4.3 Other Methods

Most of the discussed intervention methods come from the epidemics literature. For wildfires specific, different intervention approaches have been proposed. A general wildfire resource allocation approach is suggested by Griffith et al. [58]. They model the wildfire dynamics as a CA model and suppression as a Markov Decision Process (MDP), where they use both a Monte Carlo tree search and a model predictive control (MPC) method to find the optimal suppression team allocation. The authors test the presented methods for examples up to a maximum grid size of 30x30 and 32 oppressive teams and conclude that the optimization method outperforms the Monte

Carlo tree search for larger examples due to increase of the state space dimension.

More common is to focus on wildfire fuel management, where the available fuel is minimized, which reduces the spreading rate and outbreak probability. For small scale examples, mixed integer programming has been shown to give good results. However, for larger state dimensions, heuristics have to be considered [91, 101, 105, 174]. For a complete overview, we refer to [54, 104].

2.5 Convex Optimization

In the previous Sections 2.3 and 2.4 we identified different methods for surveillance and intervention of spreading processes. The most promising methods, e.g. linear programs (LPs) and geometric programs (GPs), require the problem to be phrased as an optimization problem in order to solve it.

Optimization problems are widely used in civil, mechanical, aerospace and chemical engineering to solve optimal design problems arising in for example scheduling, estimation and signal processing, communications and networks, finance, supply chain management, automatic control systems and many more [14].

A particular interesting field of optimization problems, due to their reliability and numerical efficiency, is called *convex* optimization, which we will discuss in this section. In particular we review two subclasses of convex optimization in more detail, namely linear programming and geometric programming, that will be used to set up our optimization framework.

Notation

This section has some different notation compared to the rest of this thesis in line with the literature. In particular, x corresponds to the vector of decision variables of the optimization problem to be consistent with other optimization literature. For the remainder of this thesis, however, x is the state variable of the linearized dynamics.

Similarly, β is not the spreading rate, p not the node impact and c not the cost, but are used as indicated within this section.

2.5.1 Convex Programming

An optimization problem is a problem of the form

$$\underset{x}{\text{minimize}} \quad f_0(x) \tag{2.13a}$$

$$\text{such that} \quad f_i(x) \leq b_i, \qquad i = 1, \ldots, m, \tag{2.13b}$$

where $x = (x_1, \ldots, x_n)$ is the vector of optimization variables, $f_0 : \mathbb{R}^n \to \mathbb{R}$ the cost or objective function, $f_i : \mathbb{R}^n \to \mathbb{R}$ the constraints functions and $b_1, \ldots, b_m$ are constants that are the bounds for the constraints.

A vector $x^\star$ is a solution of the minimization problem (2.13) or it is said to be *optimal*, if it has the smallest value for the objective (2.13a) out of all vectors that satisfy the constraints (2.13b) [14].

A *convex* optimization problem is an optimization problem of the form (2.13) where the objective and constraint functions are convex, i.e.

$$f_i(\alpha x + \beta y) \leq \alpha f_i(x) + \beta f_i(y) \tag{2.14}$$

for all $x, y \in \mathbb{R}^n$ and all $\alpha, \beta \in \mathbb{R}$ with $\alpha + \beta = 1$, $\alpha \geq 0$, $\beta \geq 0$ [14].

The main advantage of convex optimization problems is that they can be solved reliably and numerically very efficient using interior-point methods or other effective methods specifically for convex optimization. The algorithms that exist for convex optimization can solve large convex problems with thousands of variables within seconds and by exploiting problem structure, such as sparsity, even larger problems with ten thousands of variables and constraints can be solved quickly in the same time frame [14]. Furthermore, convex optimization has as a guarantee that a local optimum is automatically also a global optimum [9], which is a major advantage in the

case of iterative algorithms as there is no doubt whether a local or global optimum is found.

2.5.2 Linear Programming

Linear programming is one of the most well known subclasses of convex optimization and has been around for a long time due to its ease of implementation and variety of applications in a number of fields. LPs have been more widely introduced since 1947 and been used in commercial applications since 1952, from the petroleum industry for oil extraction calculations to more recently financial management such as portfolio analysis. One of the first methods suggested to solve them is the simplex method for which a starting basic feasible solution is needed. Since the 1980s, interior point methods have become more popular and with increased capacity and efficiency of computers, large LPs can be solved extremely numerically efficient these days [14, 32].

The mathematical definition of a linear program (LP) is an optimization problem of the form (2.13) where the objective and constraint functions $f_0, \ldots, f_m$ are linear, i.e.

$$f_i(\alpha x + \beta y) = \alpha f_i(x) + \beta f_i(y) \tag{2.15}$$

for all $x, y \in \mathbb{R}^n$ and all $\alpha, \beta \in \mathbb{R}$.

Comparing the condition for a linear program (2.15) to the condition for convex optimization (2.13), it is evident that, therefore, any linear program is a convex optimization problem and linear programming is a subclass of convex optimization.

The standard mathematical form of a linear optimization problem is:

$$\underset{x}{\text{minimize}} \quad c^T x \tag{2.16a}$$

$$\text{such that} \quad a_i^T x \leq b_i, \qquad i = 1, \ldots, m, \tag{2.16b}$$

where $c, a_1, \ldots, a_m \in \mathbb{R}^n$ and $b_1, \ldots, b_m \in \mathbb{R}$.

2.5.3 Geometric Programming

A geometric program (GP) is an optimization problem in which the objective and constraints can be rewritten as positive sums of exponentials. It is, therefore, a subclass of *exponential cone programming* or relative entropy programming [21].

GPs are not convex in their natural form, but can be transformed to a convex optimization problem [14]. The key principle for geometric programming is the way the objective function and constraints are defined. Therefore, we need the following preliminaries.

Definition 2.4. *A monomial function or monomial is a real-valued function of the form* $f(x) = cx_1^{a_1}x_2^{a_2}\cdots x_n^{a_n}$ *where* $c > 0$ *and* $a_i \in \mathbb{R}$ *[14].*

Definition 2.5. *A posynomial function or posynomial is a sum of one or more monomials, i.e.* $f(x) = \sum_{k=1}^{K} c_k x_1^{a_{1k}} x_2^{a_{2k}} \cdots x_n^{a_{nk}}$ *where* $c_k > 0$ *[14].*

Lemma 2.1. *Monomials and posynomials are convex in log scale [14].*

A geometric program can now be defined as an optimization problem of the form

$$\begin{aligned} \underset{x}{\text{minimize}} \quad & f_0(x) && && (2.17a) \\ \text{such that} \quad & f_i(x) \leq 1, && i = 1, \ldots, m, && (2.17b) \\ & g_i(x) = 1, && i = 1, \ldots, p, && (2.17c) \end{aligned}$$

where f_i are *posynomials*, g_i are *monomials* and all variables are positive, i.e. $x_i > 0$ [14, 15].

The reason for this formulation follows from Lemma 2.1. Geometric programs, which by themselves are quasi-convex, can now be solved by converting them into log-scale, since as stated by Lemma 2.1 posynomials are convex in log-scale, transforming the GP into a convex optimization program.

Hence, taking the transformation $y_i = \log(x_i)$, this results in the following convex

optimization problem:

$$\begin{aligned} \underset{y}{\text{minimize}} \quad & \log\left(f_0(e^y)\right) && && (2.18a) \\ \text{such that} \quad & \log\left(f_i(e^y)\right) \leq 0, && i = 1, \ldots, m, && (2.18b) \\ & \log\left(g_i(e^y)\right) = 0, && i = 1, \ldots, p. && (2.18c) \end{aligned}$$

The attractiveness of geometric programs lies in the convexity of the reformulated optimization program, which makes it possible to solve large scale problems in a computationally efficient manner.

Note that if the objective and constraint functions (2.17) are all monomials, the geometric program reduces to a linear program (2.16). That is, geometric programming can be considered a generalization of linear programming.

2.5.4 Exponential Cone Programming

Exponential cone programming or relative entropy programming [21] is a type of cone programming. Cone programs are a type of optimization problems in which a linear functional is minimized over the intersection of an affine subspace and a convex cone, i.e. the objective and constraints are subject to both linear and conic constraints [9, 14, 21]. In exponential cone programming, these conic constraints are given by the exponential cone.

Conic optimization problems are a special class of convex optimization problems and can also be understood as a reformulation of convex optimization problems [55]. Therefore, before we explain the exponential cone further, let us start with a more straightforward understanding of conic optimization.

LPs can also be seen as a cone program where the convex 'cone' $\mathcal{K}$ is the nonnegative

orthant $\mathbb{R}^n_+$. Hence, (2.16) becomes

$$\begin{aligned} \underset{x}{\text{minimize}} \quad & c^T x && && (2.19a) \\ \text{such that} \quad & a_i^T x \leq b_i, && i = 1, \dots, m, && (2.19b) \\ & x \in \mathcal{K} && && (2.19c) \end{aligned}$$

where $\mathcal{K}$ is the nonnegative orthant $\mathbb{R}^n_+$.

If the conic constraints are now given by the exponential cone, we obtain an exponential cone program. The three dimensional exponential cone is a convex subset of $\mathbb{R}^3$ defined as

$$\mathcal{K}_{exp} = \left\{(x_1, x_2, x_3) : x_1 \geq x_2 e^{\frac{x_3}{x_2}}, x_2 > 0\right\} \cup \left\{(x_1, 0, x_3) : x_1 \geq 0, x_3 \leq 0\right\}. \tag{2.20}$$

The exponential cone can be utilized to model and set up a variety of constraints.

Geometric programs, as discussed in the previous subsection, are exponential cone programs. To give an example of how to set up an exponential cone program, we, therefore, revisit the GP (2.18) from the previous subsection.

Given $f(x) = \sum_{k=1}^{K} c_k x_1^{a_{1k}} x_2^{a_{2k}} \cdots x_n^{a_{nk}}$, see Definition 2.5, the posynomial constraints (2.18b) of the GP can be rewritten to the form

$$\log\left(\sum_{k=1}^{K} \exp\left(a_k^T y + \log(c_k)\right)\right) \leq 0 \tag{2.21}$$

where $a_k = (a_{1k}, ..., a_{nk})$.

Introducing the new variable u_k for each monomial appearing in the posynomial constraints and a fixed variable $t_k = 1$, we can rewrite the log-sum-exp constraint (2.21) to

$$u_k \geq \exp(a_k^T y + \log(c_k)), \quad \left(\text{or} \quad (u_k, 1, a_k^T y + \log(c_k)) \in \mathcal{K}_{exp}\right) \tag{2.22}$$

$$\sum_k u_k = 1. \tag{2.23}$$

Recently there has been an increased interest in exponential cones and commercially available software such as MOSEK [108] has included exponential cone programming in their software from v9 released in 2019 to solve them efficiently with good numerical performance [30].

2.5.5 Sparsity and Optimization

As mentioned previously, sparsity of resource allocation is desired due to the large scale networks spreading processes evolve on and the often limited budget of resources. We, therefore, look into how to incorporate this into our optimization framework to encourage sparse outcomes.

Sparsity implies that we want to minimize the number of non-zero elements, i.e. the ℓ_0 "norm". For a linear system, given an $m \times n$ matrix Φ, where $m < n$ and vector $x \in \mathbb{R}^n$ for which we desire a sparse outcome, this leads to the following optimization problem

$$\underset{x}{\text{minimize}} \quad \|x\|_{\ell_0} \tag{2.24a}$$

$$\text{such that} \quad y = \Phi x \tag{2.24b}$$

where $\|x\|_{\ell_0} = |\{i : x_i \neq 0\}|$ [20]. (Here, $|\cdot|$ indicates the cardinality instead of the absolute value.)

However, this optimization problem (2.24) is non-convex and generally very challenging to solve [20]. In general, the problem of designing sparse feedback gains for linear systems is non-convex and computationally challenging [92].

A common alternative is, therefore, to minimize the ℓ_1 norm instead, i.e.

$$\underset{x}{\text{minimize}} \quad \|x\|_{\ell_1} \tag{2.25a}$$

$$\text{such that} \quad y = \Phi x \tag{2.25b}$$

where $\|x\|_{\ell_1} = \sum_{i=1}^{n} |x_i|$ [20].

This optimization problem can be rewritten as a linear program (LP) and more importantly is convex and can be solved efficiently. ℓ_1 type constraints are known to encourage sparsity [19, 39, 161] and due to their convexity more practical than ℓ_0 norm constraints and objectives.

If the goal is maximum sparsity, sparsity can be further increased using reweighted iterations [20]. This approach has previously been applied to networked epidemics for a multi-competitive virus model in [123]. The reweighted ℓ_1 minimization problem is given by

$$\underset{x}{\text{minimize}} \quad \left\| \frac{x^k}{|x^{k-1}| + \epsilon} \right\|_{\ell_1} \tag{2.26a}$$

$$\text{such that} \quad y = \Phi x \tag{2.26b}$$

where k is the iteration number and ϵ a small positive constant to improve numerical stability.

The problem is now solved iteratively till the outcome either converges or after a set number of iterations. This reweighted iteration program has no guarantee of convergence or global optimality but has been found to be very effective in practice [20].

2.6 Conclusions

This chapter has presented background literature on modeling spreading processes and discussed different theories and approaches that can be used for surveillance and intervention of them. It can be concluded that spreading models are commonly modeled as Markov processes. The most well-known and documented models are the Susceptible-Infected-Susceptible (SIS) and Susceptible-Infected-Removed (SIR) model, coming from the epidemics literature. Similarly for wildfires, cellular automata (CA) models are most suitable, since they have a low computational cost and deal well with heterogeneous data. However, for surveillance and intervention purposes

the stochastic model is not directly suitable. It is, therefore, common that stochastic models are approximated as ODE models, which in turn can be approximated by linear models, which are proven to be an upperbound and therefore, usually the object of study.

In Section 2.3 we found that existing methods to indicate influential nodes in a network are either topological dependent or cannot take into account node dependent cost. Furthermore, surveillance scheduling literature is still limited for spreading processes. For intervention, as discussed in Section 2.4, a suitable approach includes regulating spreading and recovery rate of the process via convex optimization, in particular exponential cone programming. However, these approaches do not necessarily provide sparse control for targeted intervention in large networks. We, therefore, discussed sparsity and convex optimization in Section 2.5.

In the remaining chapters we will, therefore, present a risk model with node dependent cost in Chapter 3, our proposed surveillance model in Chapter 4 and our joint flexible optimization framework via surveillance scheduling and sparse control using exponential cone programming in Chapter 5.

Chapter 3

Risk Modeling

In this chapter we discuss how to model the risk of an undetected outbreak of a spreading process. Here, risk is the product of the probability of an outbreak starting in a particular area and the impact of the process spreading from that location. We, therefore, first discuss outbreak probability in Section 3.1. Next, we elaborate on how we can model the spread from the outbreak location as a linearized SIR model in Section 3.2. In Section 3.3 we will discuss how to model the node impact or cost-to-go and finally, we present the risk model in Section 3.4.

3.1 Outbreak Rate

Let us consider a network graph $\mathcal{G}(\mathcal{V}, \mathcal{E})$ with n nodes in the set of nodes, or vertices, $\mathcal{V}$ and edge set $\mathcal{E}$, where at each node $i \in \{1, 2, ..., n\}$ an outbreak can occur. We model the probability of an outbreak occurring at a node i within a time interval as a Poisson process [140, Chapter 2]. A Poisson process is a counting process with rate $\lambda > 0$, in which $N(t)$ represents the total number of events up to time t, such that

1. $N(0) = 0$,
2. The process has independent increments, i.e. $Pr\{N(t+s) - N(s)\}$ for any $s \geq 0$, $t > 0$ is independent of $N(s)$,

3. The number of events $N(t)$ happening in any interval of length t is Poisson distributed with mean λt. That is, for all s, $t \geq 0$

$$Pr\left\{N(t+s) - N(s) = m\right\} = e^{-\lambda t}\frac{(\lambda t)^m}{m!} \quad m = 0, 1, \ldots \tag{3.1}$$

In our model outbreaks occurring at each node i are modeled as independent Poisson processes with rates λ_i.

Lemma 3.1. *For any interval t the probability of at least one event occurring within this time interval has a linear upperbound λt.*

Proof. The probability of at least one event occurring within time interval t is a consequence of the Poisson definition and given by

$$\begin{aligned} Pr\left\{N(t+s) - N(s) > 0\right\} &= 1 - Pr\{N(t+s) - N(s) = 0\} \\ &= 1 - e^{-\lambda t}. \end{aligned} \tag{3.2}$$

The derivative at $t = 0$ equals λ, making it a smooth function. For a Poisson rate $\lambda > 0$ the second derivative of (3.2) equals $-\lambda^2 e^{-\lambda t} \leq 0$ and hence is concave. Therefore, the linear approximation will be an upperbound, i.e.

$$1 - e^{-\lambda t} \leq \lambda t. \tag{3.3}$$

□

For a small interval, this is a tight upper bound.

3.2 SIR Spreading Model

We model an outbreak spreading according to a cellular automata (CA) model. Cellular automata simulations such as [3, 76, 80] (Section 2.2.2) use an underlying stochastic model with Markov transition probabilities. We consider a basic Susceptible-Infected-Removed (SIR) model [83], see Section 2.1.2, and each node

$i \in \{1, 2, ..., n\} \in \mathcal{V}$ has states $X_i(t)$ (infected) and $Z_i(t)$ (removed) associated with it. A node can now be in three states: *infected*, i.e., $X_i(t) = 1$, $Z_i(t) = 0$, *susceptible to infection*, i.e., $X_i(t) = 0$, $Z_i(t) = 0$, or *removed*, i.e., $X_i(t) = 0$, $Z_i(t) = 1$.

The transition probabilities of the infected and removed states $X(t)$ and $Z(t)$ associated with the continuous time Markov chain model [140, Chapter 5] are defined for a small time period Δ_t as

$$Pr\{\,(X_i(t+\Delta_t), Z_i(t+\Delta_t)) = (1,0)|\,(X_i(t), Z_i(t)) = (0,0)\} = \sum_{j\in\mathcal{N}_i} \beta_{ij} X_j(t)\Delta_t + o(\Delta_t) \quad (3.4a)$$

$$Pr\{\,(X_i(t+\Delta_t), Z_i(t+\Delta_t)) = (0,1)|\,(X_i(t), Z_i(t)) = (1,0)\} = \delta_i \Delta_t + o(\Delta_t) \quad (3.4b)$$

where β_{ij} is the spreading rate, δ_i the rate of removal and $\mathcal{N}_i$ the neighborhood of node i.

We will now derive the linear networked SIR model similarly to the derivation in Section 2.1 for the SIS model.

Lemma 3.2. *Let us define $E[X_i(t)] = P(X_i(t) = 1)$ as the probability of a node i being infected at time t and $\dot{z}$ as the rate of removal. If $\chi_i(0) = E[X_i(0)]$ then the upperbound of the stochastic probabilities, i.e. $\chi_i(t) \geq E[X_i(t)]$ for all $t \geq 0$, can be established via the following coupled differential equations*

$$\dot{\chi}_i(t) = (1 - \chi_i(t) - z_i(t)) \sum_{j=1}^{n} \beta_{ij}\chi_j(t) - \delta_i \chi_i(t) \quad (3.5a)$$

$$\dot{z}_i(t) = \delta_i \chi_i(t). \quad (3.5b)$$

There are multiple ways to approach the proof of Lemma 3.2. The networked nonlinear ODEs (3.5) can be either derived from the deterministic compartment model (2.3) or by using a mean-field approximation of the Markov chain model [83, 122]. We will use the latter, similar to Section 2.1.3.

Proof. Using the Kolmogorov forward equations [140, Chapter 5], $E(X_i(t)) = P(X_i(t) =$

1) and letting the asymptotically small time interval Δ_t go to zero, we can obtain the exact dynamics of the expectation

$$\begin{aligned}\frac{dE[X_i(t)]}{dt} &= -E[X_i(t)]\delta_i + E[(1 - X_i(t) - Z_i(t)) \sum_{j\in\mathcal{N}_i} \alpha_{ij}\beta_{ij}X_j(t)] \\ \frac{dE[Z_i(t)]}{dt} &= \delta_i E[X_i(t)]. \end{aligned} \tag{3.6}$$

Now, taking the mean-field approximation and assuming that $E[X_iX_j] = E[X_i]E[X_j]$ for all i $\neq$ j, the deterministic model can be approximated from this stochastic model [113, 132, 178]. Similar derivations for the homogeneous differential equations for the SIR model are given in [83] and for heterogeneous equations in [113, 122, 178]. It is proven in [167, 178], by showing that $E[X_iX_j] \geq E[X_i]E[X_j]$ for all $i \neq j$, that $\chi_i(t) \geq E[X_i(t)]$ for all $t \geq 0$. □

This approximation is based on assuming that all the random variables have zero covariance. This is generally not the case, but it has been found to provide tight bounds in practice which improve further with network size [164, 167].

Furthermore, the upperbound obtained by using the mean-field approximation has positive implications for controlling the underlying stochastic process. That is, stabilizing the mean-field approximation implies stabilizing the underlying model.

A linear model can be obtained by linearizing the deterministic model (3.5) around the *infection-free equilibrium* point ($\boldsymbol{\chi} = 0$, $\mathbf{z} = 0$). Hence, we obtain

$$\dot{x}_i(t) = \sum_{j=1}^{n} \beta_{ij}x_j(t) - \delta_i x_i(t) \tag{3.7a}$$

$$\dot{z}_i(t) = \delta_i x_i(t). \tag{3.7b}$$

We can combine (3.7a) for all i as

$$\dot{x}(t) = Ax(t) \tag{3.8}$$

with initial condition $x(0)$ where $x(t) = [x_1(t), ..., x_n(t)]^T$ with $t \geq 0$, is the state of

the system and the state matrix A is defined by the linearized spreading dynamics

$$a_{ij} = \begin{cases} -\delta_i \leq 0 & \text{if} \quad i = j, \\ \beta_{ij} \geq 0 & \text{if} \quad i \neq j, (i,j) \in \mathcal{E}, \\ 0 & \text{otherwise} \end{cases} \tag{3.9}$$

where $\mathcal{E}$ is the set of edges of the graph. Therefore, the off-diagonal entries a_{ij} are determined by the spreading rate β_{ij} and the adjacency matrix of the graph, whereas the diagonal entries are given by $-\delta_i$, the recovery rate. Because all off-diagonal entries a_{ij} are assumed to be nonnegative, A is Metzler and the system is positive, i.e. if $x_i(0) \geq 0$ for all i, then $x_i(t) \geq 0$ for all $t \geq 0$ [8].

Lemma 3.3. *Let $\chi(t)$ be the solution of (3.5a) $\forall i$ with initial condition $\chi(0)$ and let $x(t)$ be the solution of (3.8). The linear function (3.8) upperbounds the nonlinear one (3.5a), i.e. $x(t) \geq \chi(t)$ for $t \geq 0$ when $x(0) \geq \chi(0)$.*

Proof. Because $\beta_{ij} \geq 0$, $\delta_i \geq 0$, $x(t) \geq 0$ and $z(t) \geq 0$ for all i and j, it holds that

$$\sum_{j=1}^{n} \beta_{ij} x_j(t) - \delta_i x_i(t) \geq (1 - x_i(t) - z_i(t)) \sum_{j=1}^{n} \beta_{ij} x_j(t) - \delta_i x_i(t). \tag{3.10}$$

Hence, the linear model upperbounds the nonlinear one if $x(0) \geq \chi(0)$ [132]. □

It should be noted that the linear SIR model for the infected state (3.7a)/(3.8) is similar to the linear SIS model (2.9).

How the linear model (3.7) behaves in comparison to the nonlinear (3.5) and stochastic cellular automata model (3.4) is shown in Figure 3.1. The stochastic fire spread displayed is the expectation over multiple runs. It can be seen that the linear model upperbounds the nonlinear deterministic one, which upperbounds the stochastic model. Closer to the equilibrium point the linear model more closely approximates the stochastic process whereas over time the error accumulates. That is, the linear model accurately captures the initial exponential growth phase of an outbreak, but

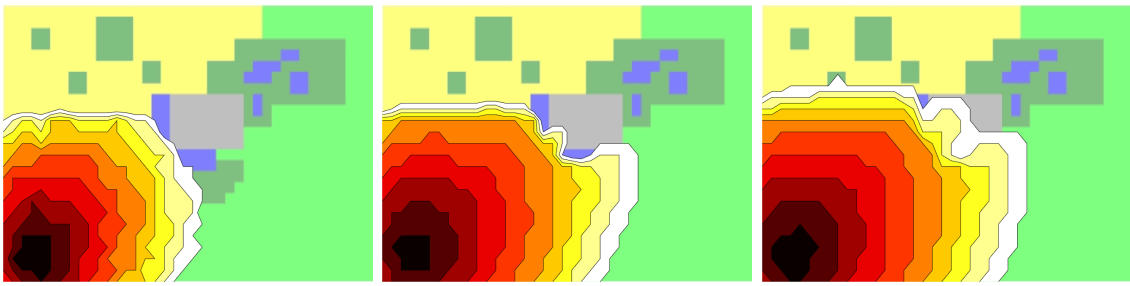

(a) Cellular Automata **(b)** Nonlinear **(c)** Linear

Figure 3.1 – Fire spread comparison of the different models on a fictional landscape. The different colors indicate spreading over time, where lighter indicates further in time.

becomes less accurate as a large percentage of nodes is affected. Nevertheless, its predictions still provide upperbounds on the true probabilities of infection, so controlling the linear model can still provide rigorous guarantees. Therefore, it is common to study the linear model as a proxy for the underlying stochastic spreading process.

3.3 Node Impact

The question now remains how to define the node impact or cost-to-go of the nodes in the graph. We use the property of positive systems that they have *linear* and hence *separable* Lyapunov and storage functions, which has previously been used for scalable methods of robust control and identification [16, 138, 163]. We note that this property also extends to certain classes of nonlinear systems [38, 100].

3.3.1 Cost function

Given that an outbreak has occurred, we associate the following cost function with the Markov process

$$J_M(X(0)) = \int_0^\infty e^{-rt} CE[X(t)]dt \tag{3.11}$$

where $C = [c_1, ..., c_n]$ is a row vector defining the cost associated with each node i, with each $c_i \geq 0$. For example, in a wildfire the cost of a populated area burning is

much higher than open grassland. Similar in an epidemic an elderly population in a nursing home might be more vulnerable and hence, associated with a higher cost of infection. The variable r is the *discount rate* and since X_i is bounded, $r \geq 0$ is finite.

The cost function for the nonlinear model can be defined by

$$J_{NL}\left(\chi(0)\right) = \int_0^\infty e^{-rt} C\chi(t)dt \tag{3.12}$$

and for the linear model by

$$J_L\left(x(0)\right) = \int_0^\infty e^{-rt} Cx(t)dt. \tag{3.13}$$

where we assume that r is large enough such that $A - rI$ is Hurwitz-stable, i.e. all eigenvalues have negative real parts, and hence, J_L is finite. It should be noted that if the Hurwitz condition is not met then the integral defining J_L does not converge, and so the cost is unbounded.

Lemma 3.4. *If $x(0) = \chi(0) = E[X(0)]$ then the cost of the linear model (3.13) upperbounds the cost of the nonlinear model (3.12), which upperbounds the expected cost of the stochastic model (3.11) for all $t \geq 0$,*

$$\int_0^\infty e^{-rt} Cx(t)dt \geq \int_0^\infty e^{-rt} C\chi(t)dt \geq \int_0^\infty e^{-rt} CE[X(t)]dt. \tag{3.14}$$

Proof. From Lemmas 3.2 and 3.3, we have $x(t) \geq \chi(t) \geq E[X(t)]$ and because $C \geq 0$, (3.14) follows. □

Discount Rate

The discount rate $r \geq 0$ can be tuned to emphasize near-term cost over long-term cost and can be understood as $r = \frac{1}{t_d}$, i.e. $J_M = \int_0^\infty e^{-\frac{t}{t_d}} CE[X(t)]dt$, where $t_d \geq 0$ is the discount time constant. A shorter time constant t_d, i.e. a larger discount rate r, indicates short-term cost is prioritized. In surveillance problems discounting is necessary for (3.13) to exist since the spreading process dynamics of interest are

generally unstable.

3.3.2 Cost-to-go

We can now find the *node impact* or *cost-to-go* p via two different methods. Either by direct calculation or via an equivalent linear program (LP).

Lemma 3.5. *If $A - rI$ is Hurwitz-stable, the linear cost-to-go has the following structure,*

$$\int_0^\infty e^{-rt} Cx(t)dt = \sum_{i=1}^{n} p_i x_i(0) \tag{3.15}$$

i.e. $J_L(x(0))$ is finite for all $x(0)$ and a linear function of the initial state, where $p_i x_i(0)$ is the discounted cost-to-go associated with each node i and p is given by

$$p^T = C(rI - A)^{-1}. \tag{3.16}$$

Here, A is the state matrix as defined in (3.9), C is the cost vector, r the discount rate and (3.16) is an upper bound for the stochastic cost-to-go.

Proof. (3.16) implies (3.15) since integrating over the time interval $[0, \infty)$ both sides of

$$\frac{d}{dt}\left(e^{-rt} p^T x(t)\right) = -e^{-rt} Cx(t),$$

gives (3.15), while expanding the left-hand-side gives

$$\begin{aligned} \frac{d}{dt}\left(e^{-rt} p^T x(t)\right) &= -e^{-rt} Cx(t), \\ \Rightarrow e^{-rt} p^T \dot{x}(t) - re^{-rt} p^T x(t) &= -e^{-rt} Cx(t), \\ \Rightarrow p^T (rI - A)x(t) &= Cx(t) \end{aligned}$$

which must hold for all $x(t)$, hence implies (3.16). It follows from Lemma 3.4 that this is an upperbound for the stochastic model. □

Lemma 3.6. *Each element of p is nonnegative and a monotone function of A, i.e. $A_1 \geq A_2 \Rightarrow p_1 \geq p_2$ elementwise.*

Proof. $(rI - A)$ is a positive-stable M-matrix, which is inverse positive [8, p. 134], i.e. all elements of the matrix $(rI - A)^{-1}$ are nonnegative, as are all elements of C by construction. Therefore p_i will always be nonnegative. Furthermore $(rI - A)$ is non-singular and given two non-singular M-matrices M and N, if $M \geq N$, then $N^{-1} \geq M^{-1}$ [46]. Hence if $A_1 \geq A_2$ then $(rI - A_1) \leq (rI - A_2)$ and $(rI - A_1)^{-1} \geq (rI - A_2)^{-1}$. Since all elements of C are nonnegative, $p_1 \geq p_2$. □

Lemma 3.6 implies that reducing the spreading rate or increasing the recovery rate can never increase the node impact and vice-versa. An important application of this is robust solutions: if spreading or recovery rates are uncertain, but known to be in an interval, then worst-case node impact can be calculated using the boundary values of the intervals.

The second method to find the node impact p is via a linear program (LP) which is suitable for extension to include resource allocation. The equivalent LP is

$$\begin{aligned} \text{minimize} \quad & |p|_1 && (3.17a) \\ \text{such that} \quad & p \geq 0, && (3.17b) \\ & p^T A - rp^T \leq -C. && (3.17c) \end{aligned}$$

Lemma 3.7. *The LP (3.17) is equivalent to (3.16).*

Proof. Equivalence can be shown by application of Lemma 3.6. Let $p^\star$ be the node impact calculated using (3.16), then $p^\star \geq 0$ and $p^{\star T} A - rp^{\star T} = -C$ hence $p^\star$ is feasible for the LP, but any other feasible p has $p^T A - rp^T \leq -C$ and hence (via inverse-positivity) $p^T \geq C(rI - A)^{-1} = p^{\star T}$, so

$$|p|_1 = \sum p_i \geq \sum p_i^\star = |p^\star|_1 \tag{3.18}$$

and $p = p^\star$ is optimal for the LP. □

Note that if we are only interested in computing p then the LP representation is redundant: the second inequality constraint in (3.17) can be replaced by an equality,

which is equivalent to (3.16) and no minimization is required. However, in Chapter 5, when we start optimizing over both p and the elements of A, the inequality form is useful as it admits a convex representation whereas the equality does not.

Remark 3.1. *The cost matrix C can be constructed in various ways. One possibility is to use it to represent the expected total number of 'removed' nodes. Indeed, taking the integral of (3.5b) over the interval $[0, \infty)$, and assuming there are no removed nodes at the start, i.e., $z(0) = 0$, this results in*

$$z(\infty) - z(0) = \int_0^\infty \dot{z}(t)dt = \int_0^\infty Dx(t)dt. \tag{3.19}$$

where $D = diag(\delta_1, \delta_2, \ldots, \delta_n)$. Including the option for the discount rate r, i.e. put a higher cost on nodes that are removed earlier, and using the total number of removed nodes as the cost, we obtain

$$\int_0^\infty e^{-rt} Dx(t)dt = \sum_{i=1}^{n} p_i x_i(0). \tag{3.20}$$

3.3.3 Priority Map

To understand the *node impact* p more intuitively and how the different parameters affect it, we will visualize the resulting node impact for two different examples with different sizes and dynamics. We will call the map displaying the node impact a 'priority map'.

16 node grid

Let us consider a graph $\mathcal{G}(\mathcal{V}, \mathcal{E})$ with $n = 16$ nodes, connected as visualized in Figure 3.2a with a spreading rate $\beta = 0.5$ for all $(i, j) \in \mathcal{E}$ and recovery rate $\delta = 0.2$ for all $i \in \mathcal{V}$, where the cost $c_i = 1$ for $i = 16$ and $c_i = 0.1$ for every other node. This results in a system for which $a_{ij} = -0.2$ if $i = j$, $a_{ij} = 0.5$ if $(i, j) \in \mathcal{E}$ and $a_{ij} = 0$ otherwise.

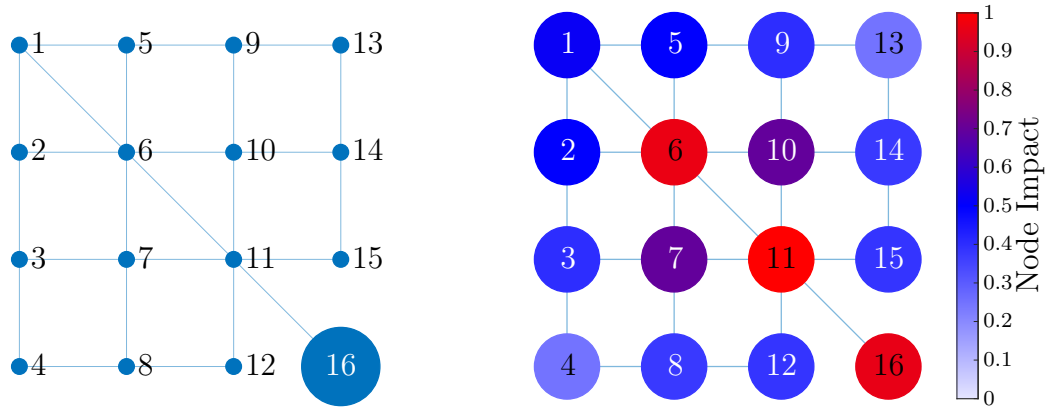

(a) Graph **(b)** Normalized priority map

Figure 3.2 – Example 3.1; Graph and belonging priority map for a network with $n = 16$ nodes with equal spreading rate of $\beta = 0.5$ and recovery rate $\delta = 0.2$ for all nodes. The cost $c_i = 0.1$ for $i = 1, .., 15$ and $c_i = 1$ for $i = 16$.

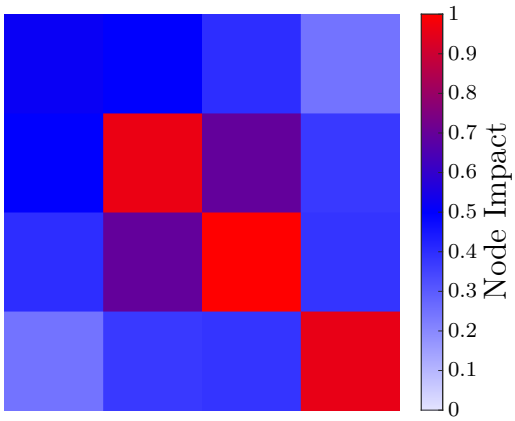

Figure 3.3 – Block format display of the normalized priority map Figure 3.2b for the graph in Figure 3.2a.

Hence, there is a high cost node $i = 16$, which is only connected to node 11. Taking $r = 2$ and solving either (3.16) directly or the LP (3.17), the normalized results are shown in Figure 3.2b.

As expected due to the connectivity, equal spreading and recovery rates and with one high cost node, Figure 3.2b shows high priorities for the diagonal nodes 6 and 11 leading up to the high cost node 16. Another way to display Figure 3.2b, is demonstrated in Figure 3.3 and for larger node examples we will stick to the block format for visibility.

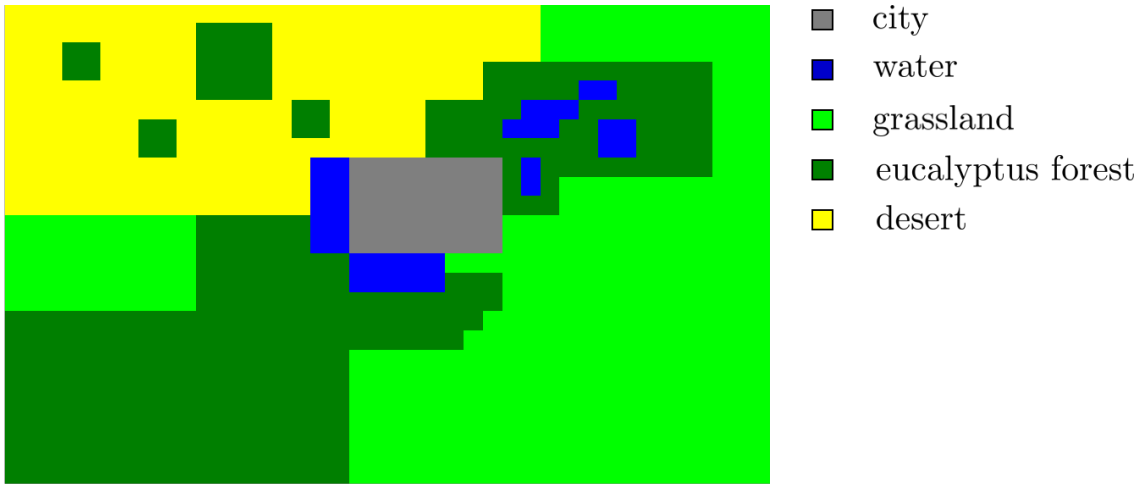

(a) Vegetation Map

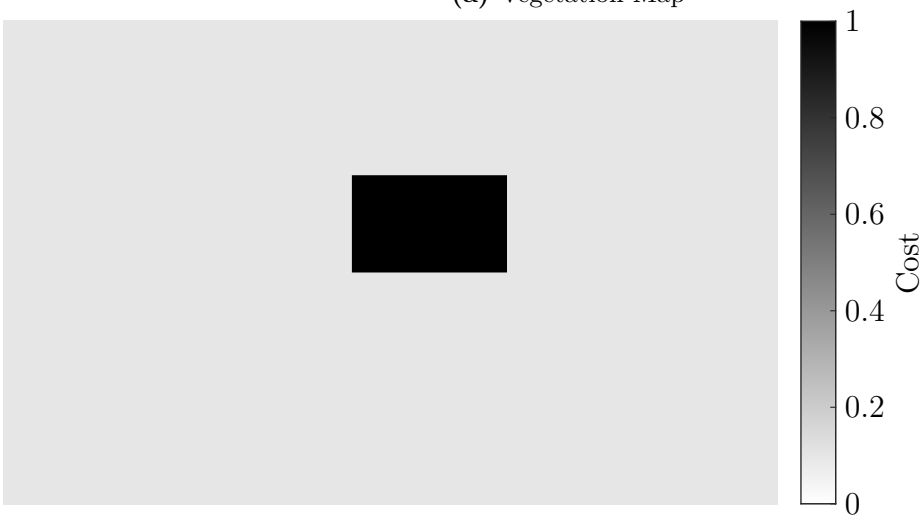

(b) Cost Map

Figure 3.4 – Example 3.2; Fictional landscape with different area types, represented as a grid with $n = 1000$ nodes and corresponding cost map where the city nodes have a high cost associated with them.

1000 node fictional landscape

A more interesting problem is to look at the effect of different spreading rates β, which would be a more realistic representation of actual spreading processes. Therefore, we consider the fictional landscape given in Figure 3.4a consisting of three different vegetation types, a city and water. It can be represented as a network graph with $n = 1000$ nodes. The adjacency matrix and therefore, the edge set $\mathcal{E}$, is based on a 8 node spreading direction grid, i.e., the landscape is seen as a grid where each node is

connected to its 8 neighboring nodes. That is, fire can spread horizontally, vertically and diagonally as explained and visualized previously in Figure 2.3. Boundary nodes have fewer edges accordingly.

The spreading rates are determined based on cellular automata (CA) wildfire models presented in [3] and [80], where the wildfire spreading probabilities are determined based on real wildfire observations. The spreading rates for an edge consist of a baseline spreading rate and vegetation and wind correction

$$\beta = \beta_b \beta_{veg} \beta_w \tag{3.21}$$

where the baseline $\beta_b = 0.5$. A correction factor for the vegetation is taken as $\beta_{veg} = 0.4$, $\beta_{veg} = 1$ and $\beta_{veg} = 1.4$ for respectively desert, grassland and eucalyptus forest. For the city this is $\beta_{veg} = 0.5$ and for the unburnable water areas $\beta_{veg} = 0$ is taken. β_w is calculated following [3]. Finally, β is corrected for spreading between diagonally connected nodes, following [80]. The cost of the city nodes is $c_i = 1$, whereas $c_i = 0.1$ for all other nodes as displayed in the cost map Figure 3.4b.

We now look into adjusting the spreading rate for respectively a southwesterly, southeasterly, northeasterly and northwesterly wind with a speed of $V = 4$ m/s. Taking a discount rate of $r = 3.8$, this results in Figure 3.5, where the effects of wind direction on the node priority map can be seen. A higher wind speed will exaggerate these effects, see Figure 3.6 for $V = 10$ m/s, whereas for lower wind speed the priority maps will look more similar.

In general, the most critical nodes are the nodes in the bottom left corner where the eucalyptus with grassland in between leads up to the city. Other possible hazards are the city itself due to its high cost and the smaller patches of eucalyptus closer to the city. However, this area is smaller and restricted above by slow spreading desert and water. Therefore, it poses less danger in case of fire igniting in the top part of the landscape. For a better interpretation of the priority map, simulations were run starting fires in different priority nodes and the results can be seen in Figure 3.7.

The cost that is taken for the landscape nodes also affects the priority map as shown

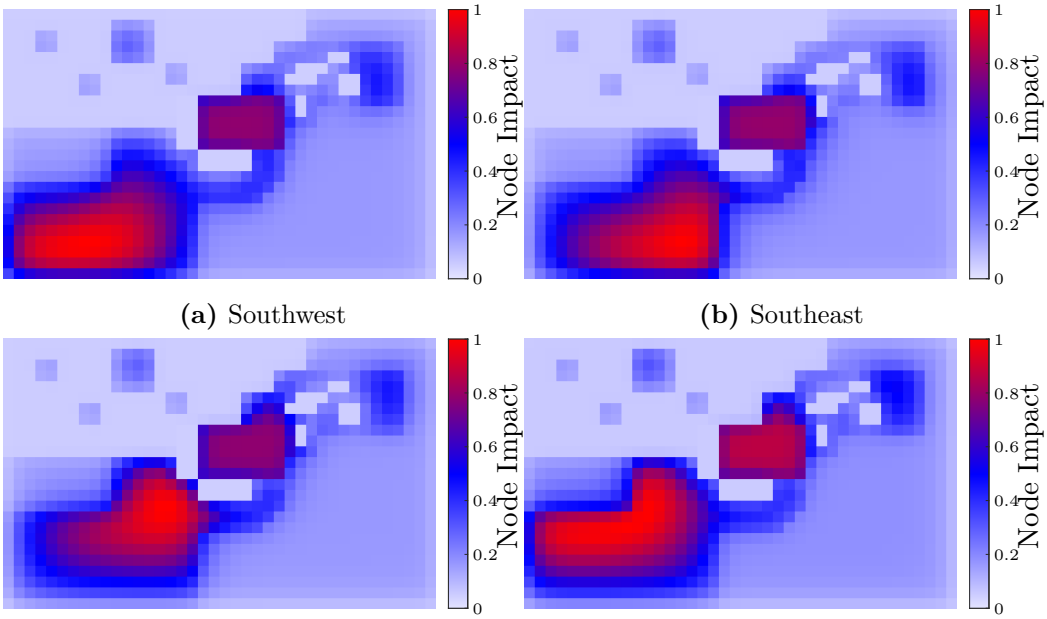

(a) Southwest **(b)** Southeast

(c) Northeast **(d)** Northwest

Figure 3.5 – Normalized surveillance priority map for different wind directions, $\boldsymbol{V = 4}$ **m/s**, for the landscape and cost map in Figure 3.4. Wind direction is indicated as the direction the wind is coming from.

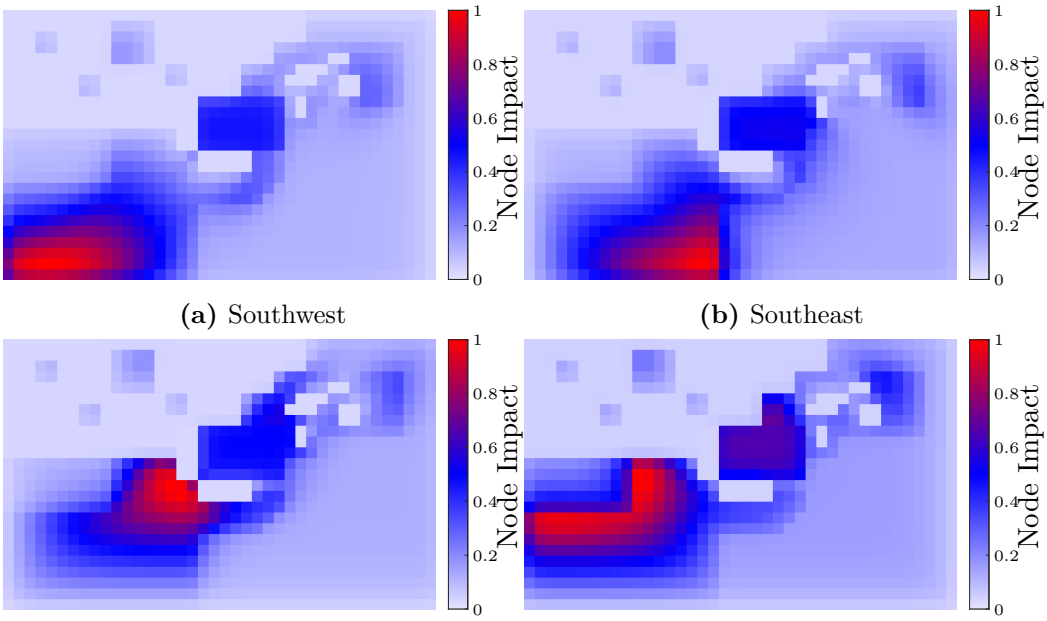

(a) Southwest **(b)** Southeast

(c) Northeast **(d)** Northwest

Figure 3.6 – Effect of a higher wind speed, $\boldsymbol{V = 10}$ **m/s**, on the priority map, compared to Figure 3.5, for the landscape and cost map in Figure 3.4.

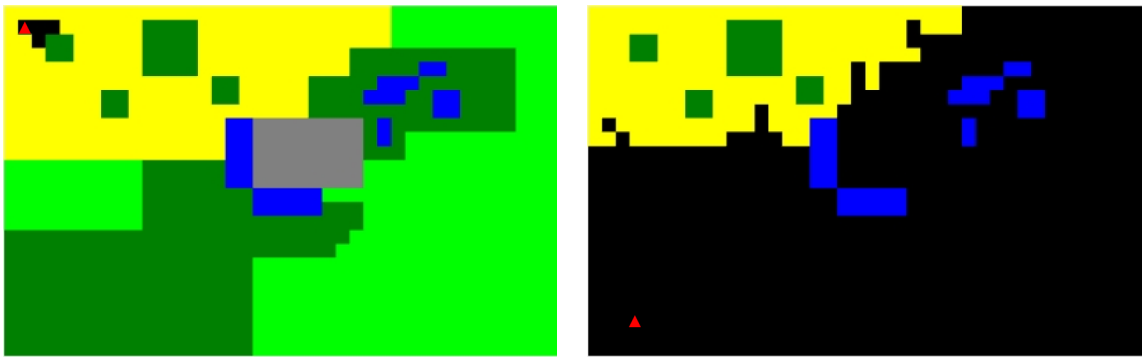

(a) Low priority node **(b)** High priority node

Figure 3.7 – Fire spread simulations of starting fires (red triangle) in different priority nodes in the top and bottom left corner for optimal wind conditions for fire spread to the city. Black indicates burned area.

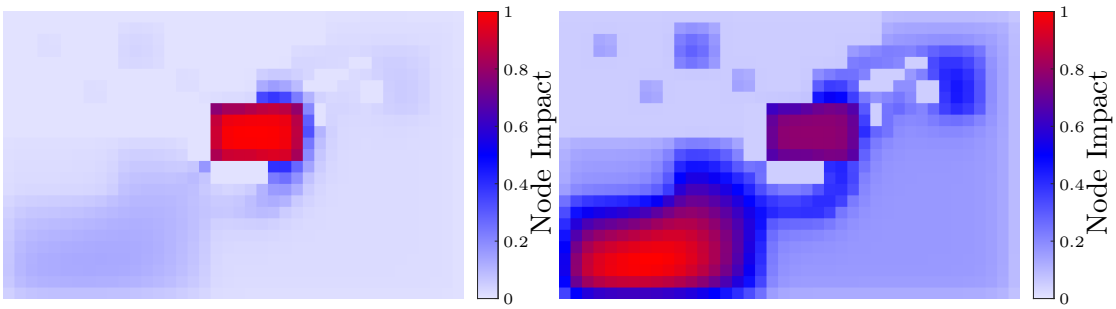

(a) $c_i = 0.01$ **(b)** $c_i = 0.1$

Figure 3.8 – Effect of different cost c_i of the landscape nodes on the priority map of the landscape in Figure 3.4a with southwesterly wind of $V = 4$ m/s and $r = 3.8$.

in Figure 3.8. With a high cost on the landscape nodes, they are prioritized over the city, because more landscape burning down will now result in a higher total cost.

Discount Rate

In Section 3.3.1 we discussed the discount rate r in (3.11) and (3.13). We visualize the effect of the discount rate in Figure 3.9 with again $c_i = 0.1$ for landscape nodes, $c_i = 1$ for city nodes and a southwesterly wind of $V = 4$ m/s, where the minimal discount rate equals $r = 3.3103$ before $rI - A$ becomes singular. A higher discount rate prioritizes the near future and hence, prioritizes what is happening in the city, i.e. the highest cost area of the landscape, over what possible outbreaks in other parts of the graph

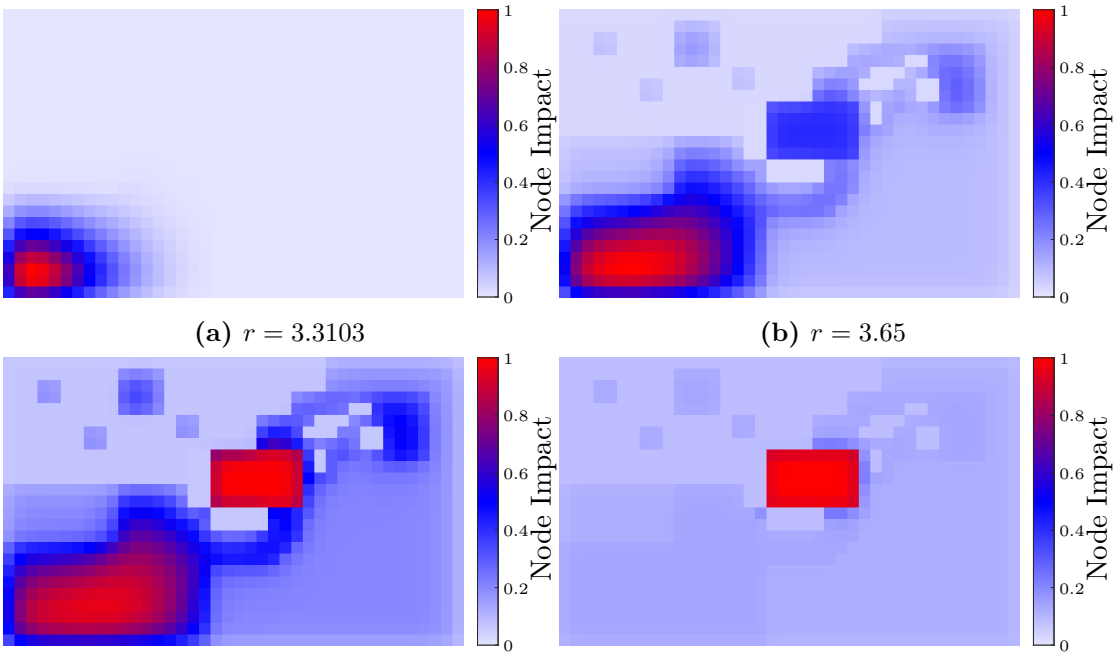

(a) $r = 3.3103$ **(b)** $r = 3.65$

(c) $r = 3.9$ **(d)** $r = 10$

Figure 3.9 – Effect of discount rate r on the priority map for the landscape and cost map in Figure 3.4 with southwesterly wind of $V = 4$ m/s.

could lead to. The limiting case of $r \to \infty$ would result in $\lim_{r\to\infty} \frac{1}{r} C^T(rI - A) = C$, i.e. $p \to \frac{1}{r} C$.

3.4 Risk Model

We can now define a risk model associated with the spreading process on the graph $\mathcal{G}$. The risk R_i at each node i is defined as the product of the probability of at least one outbreak occurring within a time interval (3.2) and the resulting cost of that outbreak (3.11).

Using Lemma 3.1 and Lemma 3.5, we obtain

$$R(t) = p \odot \lambda t. \tag{3.22}$$

Remark 3.2. *Instead of using the probability that at least one outbreak occurs within a given time interval for a Poisson process, we can also define likelihood of an outbreak*

more general with the estimated probability of infection $\hat{x}_i(0)$. The risk vector can now be defined as:

$$R = \hat{x}(0) \odot p. \tag{3.23}$$

Spectral Abscissa

In this thesis we will often compare our proposed risk model to minimizing the spectral abscissa (see Section 2.4.1)

$$J_\lambda = \lambda_{max}(A). \tag{3.24}$$

We will, therefore, define the following corollary to show the relationship between the discount rate r in our model and minimizing the spectral abscissa.

Corollary 3.1. *The constraints on the cost function of the linear model (3.13) and the linear cost-to-go (3.15) are feasible if and only if $A - rI$ is Hurwitz-stable, i.e. $\lambda_{max}(A) \leq r$. Because A is Metzler, λ_{max} is real and unique. Therefore, minimizing the spectral abscissa (3.24) can be upperbounded by minimizing the discount rate r. Hence, the widely-used approach of minimizing the the spectral abscissa can be seen as a special case of the optimization framework we propose in Chapter 5.*

Minimizing the spectral abscissa is common in literature (e.g. [114, 132, 167, 168, 178]), as discussed in Section 2.4.1. The main difference and advantage of our risk model over the spectral abscissa is that it can take into account node dependent costs.

Feasibility

The linear cost-to-go (3.15) used to define the node impact p in the risk model (3.22) is feasible if and only if $A - rI$ is Hurwitz stable. If $A - rI$ is not Hurwitz stable, the linear model (3.13) has infinite cost. This doesn't necessarily imply the nonlinear cost (3.12) is unbounded as the linear model (3.7) is an upperbound of the nonlinear model (3.5), which in turn upperbounds the expected state of the underlying stochastic model (3.4), see Lemma 3.4. However, it has been observed that the mean-field

approximation tends to closely approximate the stochastic model and the gap on the bound decreases with increasing network size [164, 167] and we refer to Figure 3.1 and discussion in Section 3.2 for a fire spread example comparing the stochastic, nonlinear and linear model, showing close agreement between the three.

3.5 Conclusions

In this chapter we defined a risk model based on the product of the outbreak rate and the node impact for a given time interval. We proposed to model the outbreak rate as a Poisson process, where we take the linear upperbound of at least one event occurring within a time interval. Furthermore, we discussed why the linear spreading model is a suitably proxy for studying the underlying stochastic model. Next, we defined a cost function, where we found that the cost function associated with the linear model upperbounds the cost function associated with the stochastic model. We used the properties of positive systems to find the linear cost-to-go or node impact vector, which we discussed further by giving examples of a 'priority map' that shows the node impact or cost-to-go for different cost and spreading parameters and we discussed the effect of the discount rate. Finally, we presented and discussed feasibility of our proposed risk model and how it differs from other risk models, such as the spectral abscissa, by taking into account node dependent costs.

Chapter 4

The Surveillance Problem

In the previous chapter we defined the risk model, where risk consists of the probability of an outbreak starting in a particular area and the impact of the process spreading from that location. In this chapter we consider the problem of bounding the risk of an undetected outbreak by use of a revisit schedule. We will, therefore, first present the surveillance problem and the main theoretical result in Section 4.1, afterwards in Section 4.2 we will discuss two examples of how the risk map and surveillance schedules can be implemented. We look into the effect of different parameters on the risk with a small 16 node example. Finally, with a large 4000 node wildfire example we demonstrate how a revisit schedule can bound the maximum risk.

4.1 Problem Statement

The risk R_i at each node i is defined as the product of the probability of at least one outbreak occurring within a time interval (3.2) and the resulting cost of that outbreak (3.11) as discussed in Chapter 3. We now want to bound the risk and minimize the cost of an undetected outbreak by use of a revisit schedule. That is, we want to find the largest revisit interval τ_i for each node i, such that the risk of an undetected outbreak remains bounded by some $R_{\max} > 0$. We take the assumption that at each revisit we can sense the state of the system, whereas in between visits we receive no

information. That is, at time of visiting the risk of an undetected outbreak is reduced back to a small number ϵ_R, to include sensor inaccuracy, for that node.

Problem 4.1 (Surveillance Problem)**.** *For each node i find the largest revisit interval τ_i, such that the risk of an undetected outbreak remains bounded by R_{max}. Here, the risk R_i at each node i is defined as the product of the probability of at least one outbreak occurring* (3.2) *and the resulting cost of that outbreak* (3.11)*.*

The main theoretical result is

Theorem 4.1. *Suppose that $A - rI$ is Hurwitz-stable, the risk of an undetected outbreak at node i remains bounded by R_{max} for any revisit interval $\tau_i = t_i(k+1) - t_i(k)$ satisfying*

$$\tau_i = t_i(k+1) - t_i(k) \leq \frac{R_{max} - \epsilon_R}{p_i \lambda_i} \tag{4.1}$$

where $t_i(k)$ is the kth time node i is visited, λ_i the Poisson rate of an outbreak occurring at node i, p_i the node impact, and ϵ_R a small number to include sensing uncertainty.

Proof. Using Lemma 3.1 we can upperbound the probability of an outbreak occurring at a node i by $\lambda_i \tau_i$. That is, the estimated outbreak probability over the interval $\tau_i = t_i(k+1) - t_i(k)$, where $t_i(k)$ is the kth time node i is visited, is

$$\hat{x}_i(t) = \lambda_i (t_i(k+1) - t_i(k)). \tag{4.2}$$

The node impact or cost-to-go p_i is given in Lemma 3.5. Therefore, taking into account the risk is reduced to a small number ϵ_R at each revisit, the risk at each node is bounded by

$$R_i(t) \leq p_i \lambda_i \left(t_i(k+1) - t_i(k)\right) + \epsilon_R \leq R_{\max}. \tag{4.3}$$

□

To bound the risk as defined in Theorem 4.1, we can revisit the node location to reduce the uncertainty. How often to revisit depends on the Poisson rate of the outbreak λ_i and cost-to-go p_i. We can visualize this as demonstrated in Figure 4.1.

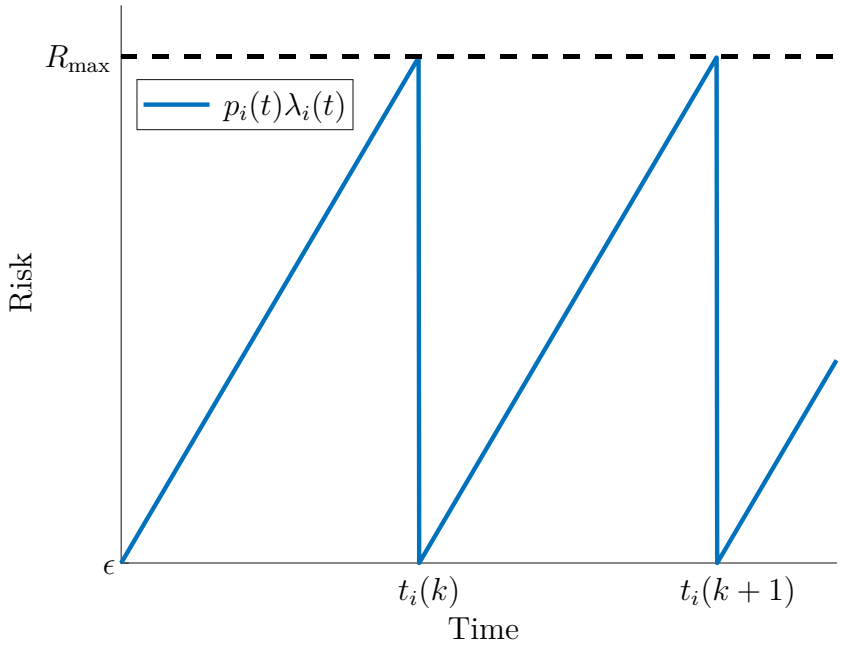

(a) $p_i(t)\lambda_i(t)$

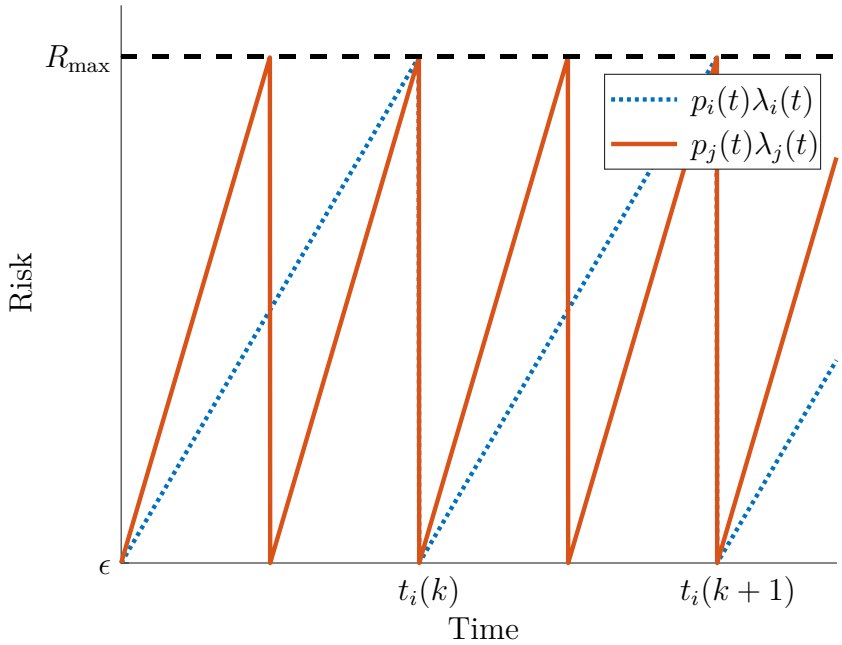

(b) $p_j(t)\lambda_j(t)$

Figure 4.1 – Theorem 4.1 visualized. To keep the risk bounded at $R_{\max}$ (4.1), node j, indicated with the orange line, has to be visited twice as often compared to node i, i.e. the blue (dotted) line.

In Figure 4.1a we have set the risk bound to $R_{\max}$ and we have to revisit at least every $t_i(k+1) - t_i(k)$ interval to prevent the risk of an undetected event going over the set bound. If for a node j, $p_j\lambda_j$ is twice as high as $p_i\lambda_i$, indicated in Figure 4.1b with the orange line, we have to revisit this node twice as often to get the same bound on the risk.

It should be noted that if the Hurwitz assumption is not met, the cost is unbounded, Theorem 4.1 is not valid and no revisit interval can be found, see 'Feasibility' subsection in Section 3.4.

Remark 4.1. *For epidemics, revisiting can be interpreted as testing an individual for infection of a specific disease, e.g. COVID-19. Hence, each time that a node gets tested the risk of an undetected outbreak is reduced.*

4.2 Results

In this section we illustrate how the proposed surveillance model can be implemented with two different examples. First, we look into the effect of different parameters on the risk with a small 16 node example. Next, we discuss a large wildfire example of 4000 nodes, and demonstrate how we can go from the risk map to bounding the risk and incorporate robotic path planning methods for surveillance.

4.2.1 Risk Map

Let us consider a graph with $n = 16$ nodes, connected as visualized in Figure 4.2. We now want to investigate the effect of the different parameters, i.e. cost c_i, outbreak rate λ_i and spreading rate β_{ij}, on the risk. We first set all parameters the same for all nodes and edges, i.e. we take $c_i = 1$, $\beta_{ij} = 0.5$ and $\lambda_i = 1$ $\forall i$, and then introduce one by one node dependent cost, spreading rate and outbreak rate. The resulting risk maps for $r = 2$ are displayed in Figure 4.2.

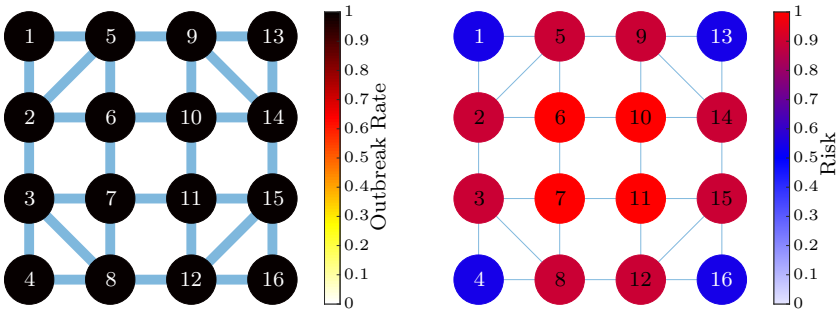

(a) All nodes have equal cost $c_i = 1$ and outbreak rate $\lambda_i = 1$, all edges have spreading rate $\beta_{ij} = 0.5$

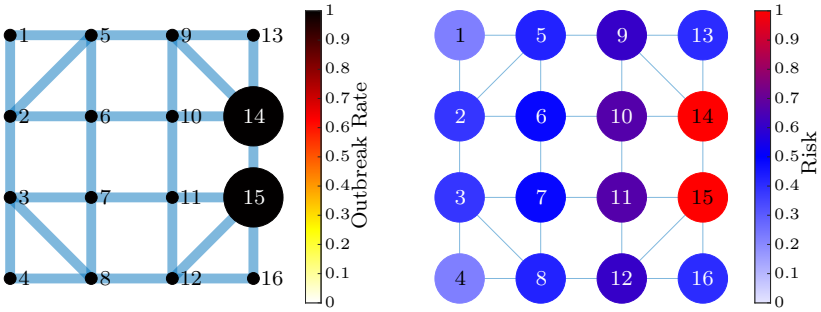

(b) High cost nodes $i = 14, 15$, equal outbreak rate $\lambda_i = 1$ for all nodes and equal spreading rate $\beta_{ij} = 0.5$ for all edges

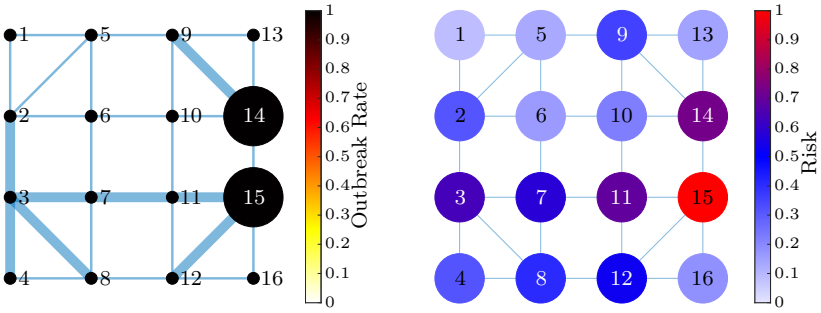

(c) Spreading rate as indicated by edge width on the left, high cost nodes $i = 14, 15$, equal outbreak rate $\lambda_i = 1$

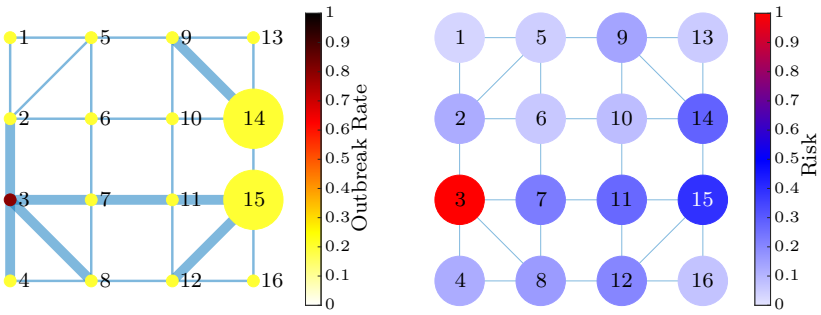

(d) Outbreak rate, spreading rate and cost as indicated on the left

Figure 4.2 – Example 4.1; The effect of cost c_i, outbreak rate λ_i and spreading rate β_{ij} on a graph with $n = 16$ nodes. On the left is the graph where node color indicates outbreak rate, node marker size indicates cost and edge width spreading rate. The resulting risk map is displayed on the right, where node color indicates risk R_i.

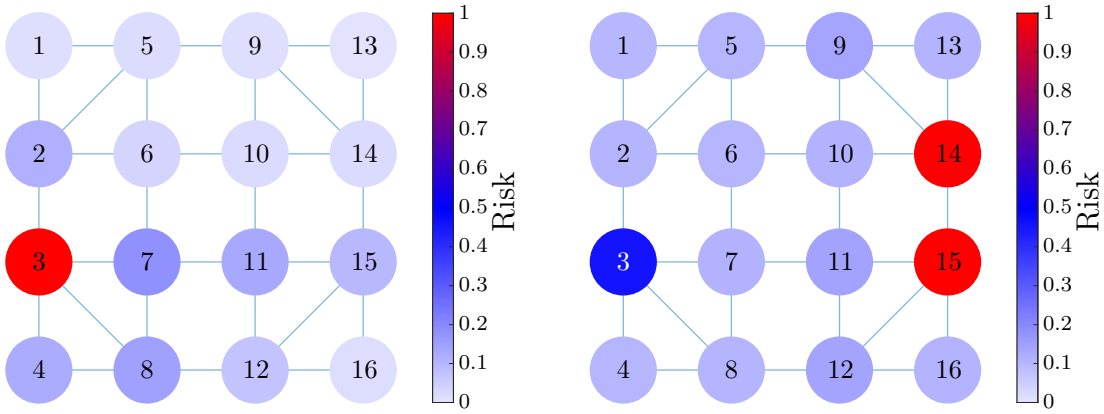

(a) $r = 1.6439$ **(b)** $r = 20$

Figure 4.3 – Effect of the discount rate r on the risk map of Figure 4.2d.

It can be seen that uniform spreading rate, cost and outbreak rate result in risk based on node degree, see Figure 4.2a.

If we introduce a cost $c_i = 1$ for nodes $i = 14, 15$ and $c_i = 0.1$ otherwise, see Figure 4.2b, we obtain high risk nodes $i = 14, 15$ which correspond to the high cost nodes.

Including higher spreading rates $\beta_{ij} = 0.8$ at specified edges and a lower spreading rate of $\beta_{ij} = 0.2$ elsewhere, see Figure 4.2c, we obtain high risk node $i = 15$, which corresponds to both high cost and high spreading rate.

Finally, we set outbreak rate as indicated by the colorbar with a high likelihood of an outbreak starting in node $i = 3$. It can be seen in Figure 4.2d that the high risk node $i = 3$ now corresponds to the high outbreak node.

We can visualize the effect of the discount rate (see Section 3.3.1) for Figure 4.2d by comparing the resulting risk map for a low and high discount rate, see Figure 4.3. Here, the minimum discount rate equals $r = 1.6439$ before $rI - A$ becomes singular. A higher discount rate, see Figure 4.3b, prioritizes the near future and hence, prioritizes what is happening in the high cost nodes over what possible outbreaks in other parts of the graph could lead to.

4.2.2 Surveillance Scheduling

Next, we consider a wildfire example to demonstrate risk maps, revisit maps and surveillance scheduling in combination with persistent monitoring. Similar to Example 3.2, we consider a fictional landscape with varying vegetation, a city and water as visualized in Figure 4.4a and cost c_i given in Figure 4.4b. However, to take it a step further and make it more realistic, we increase the size of the example to a network graph of $n = 4000$ nodes and consider gradual transitions between vegetation areas, see Figure 4.4a, instead of the previous ad hoc representation. Furthermore, we take into account the outbreak rate λ_i as illustrated in Figure 4.4c to obtain the risk map.

The adjacency matrix and therefore, the set of edges $\mathcal{E}$, is again based on a 8 node spreading direction grid, i.e., the landscape is seen as a grid where each node is connected to its direct horizontal, vertical and diagonal neighbors, see Figure 2.3. The recovery rate $\delta = 0.5$ for all nodes, whereas β is again derived using data from cellular automata wildfire models presented in [3] and [80], where the wildfire spreading probabilities are determined based on real wildfire observations. For the spreading dynamics $\beta_{veg} = 2 \cdot \text{Vegetation}$, where the vegetation value is indicated in Figure 4.4a and $\in [0, 1]$ for respectively minimal and maximal vegetation. For the city $\beta_{veg} = 0.5$ is taken and for the nonburnable water areas $\beta_{veg} = 0$. Finally, β is corrected for spreading between diagonally connected nodes, following [80].

The spreading rate is, furthermore, adjusted for respectively a westerly, northerly, easterly and southerly wind with a speed of $V = 8$ m/s. Taking a discount rate of $r = 4$, this results in Figure 4.5, where the effects of wind direction on the risk map can be seen. Large spreading rates, caused by e.g. eucalyptus forest, in combination with wind direction form the most direct hazards to the high cost city nodes.

It should be noted that the generated risk maps are for a revisit rate of 1, i.e. $\frac{1}{\tau} = 1$. If we now want to minimize the maximum risk by 50% by using a revisit schedule, i.e. $R_{\max} = 0.5R_i$ where R_i is the risk in Figure 4.5a, we can obtain the smallest revisit rate using Theorem 4.1, assuming ϵ_R is negligible. The results are displayed in Figure 4.6.

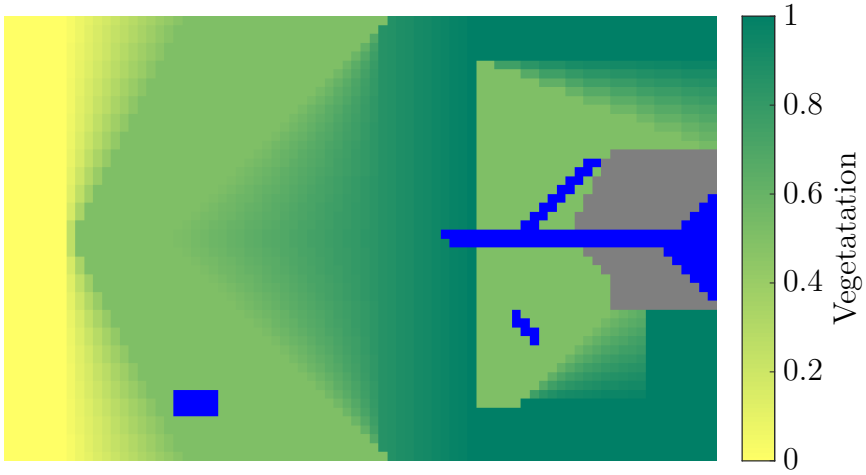

(a) Vegetation Map; blue indicates water, grey city area.

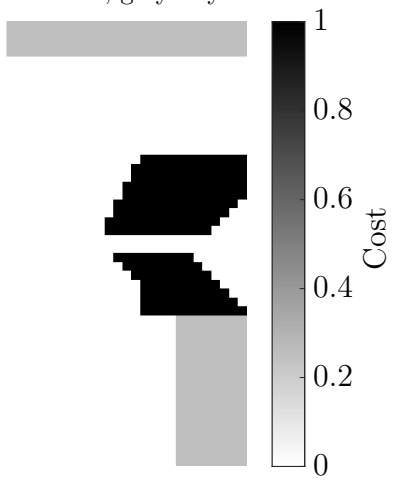

(b) Cost Map

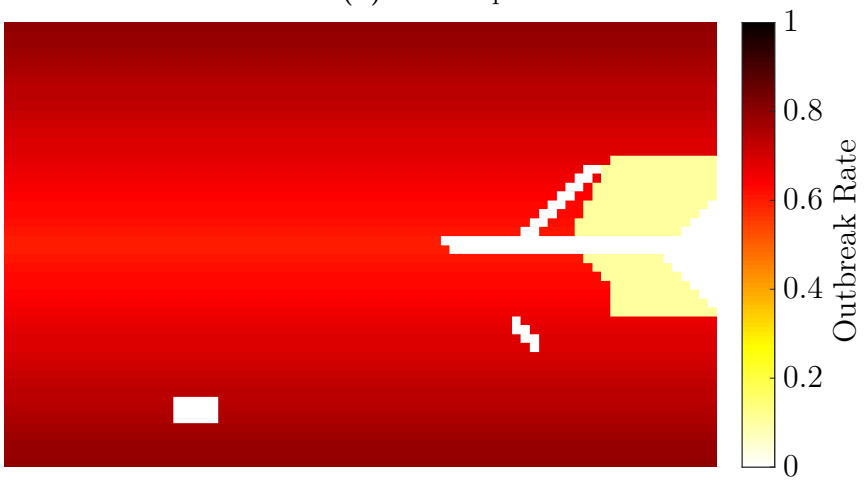

(c) Outbreak Rate

Figure 4.4 – Example 4.2; Wildfire spreading over a graph with $n = 4000$ nodes representing a simplified landscape with its corresponding cost map and outbreak rate.

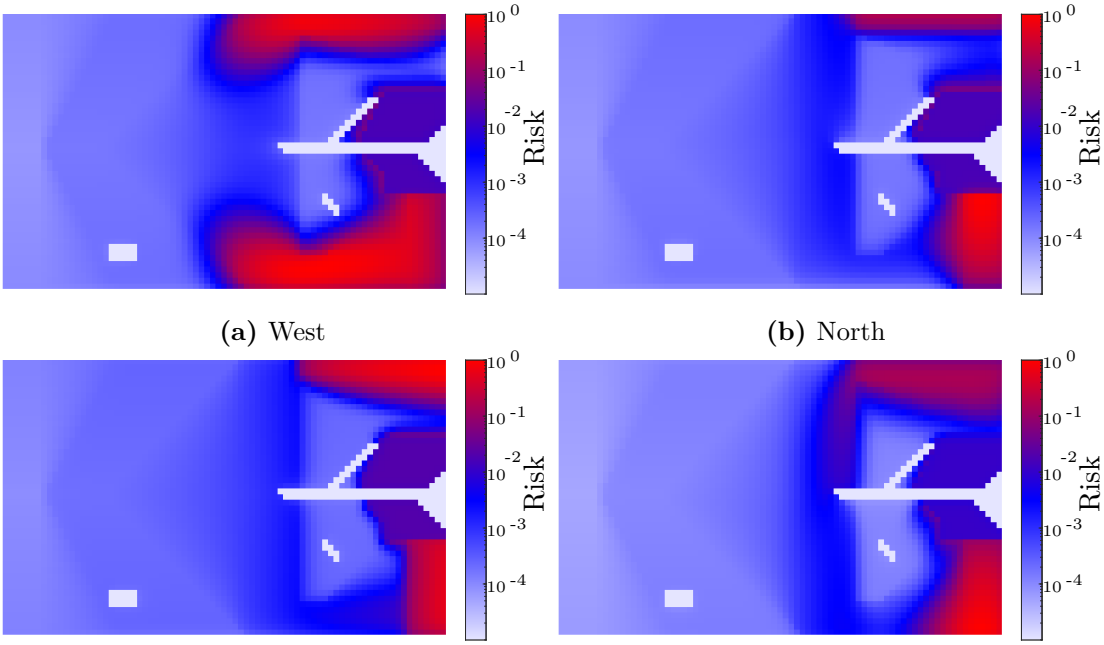

(a) West **(b)** North

(c) East **(d)** South

Figure 4.5 – Logarithmic surveillance risk map for different wind directions for the landscape in Figure 4.4. Wind direction is indicated as the direction the wind is coming from.

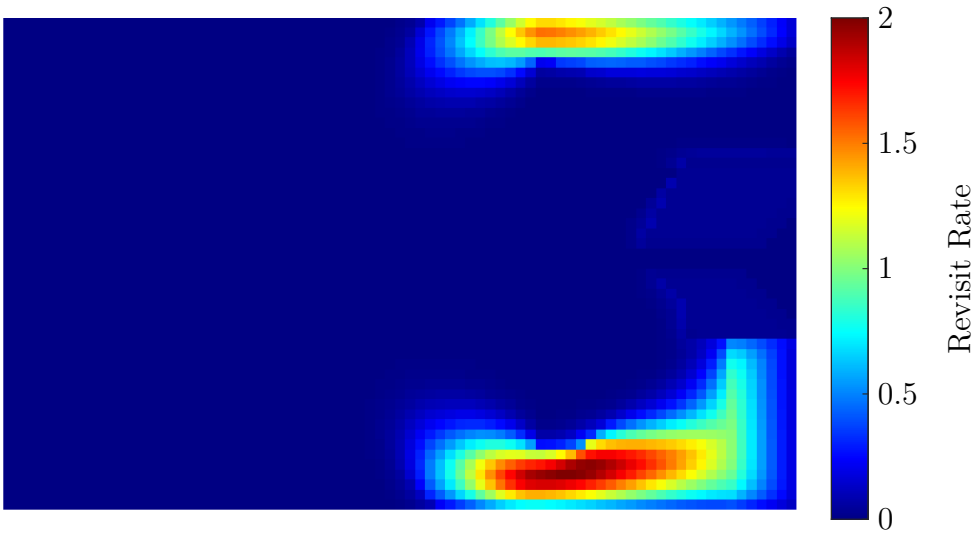

Figure 4.6 – Minimum revisit rate $\frac{1}{\tau_i}$ needed to reduce the maximum risk of Figure 4.5a by 50%.

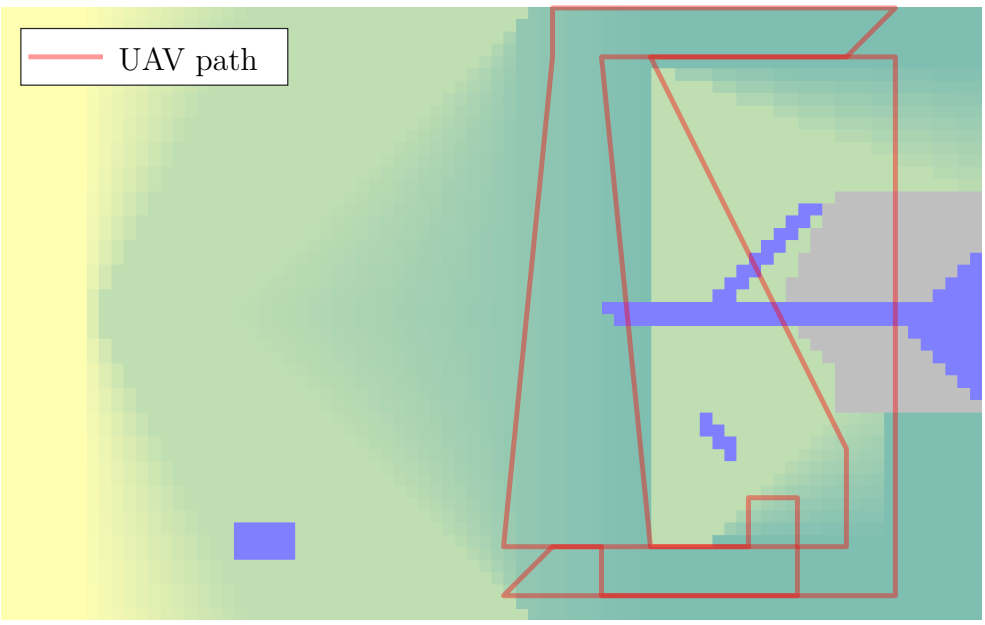

Figure 4.7 – Persistent monitoring path consisting of two subwalks using the minimum maximum latency walk [2] on the revisit map given in Figure 4.6. Darker red lines indicate multiple subwalks visit this section.

We can use this revisit rate to find a persistent monitoring path, see Figures 4.7 and 4.8. We consider a simplified scenario, with no restrictions on flight time and path length, and assume the UAV is able to monitor a 4x4 square of nodes at the same time. To match this sensing assumption, we take the maximum revisit rate of 4x4 squares of nodes of Figure 4.6, rounded to the nearest integer, as input.

As discussed in Section 2.3.3 for the persistent monitoring problem different algorithms and solutions exist [124, 152, 179]. To show how a risk map or revisit map can be used for persistent monitoring we show the implementation of one of these existing algorithms.

Alamdari et al. [2] for example provide a solution to the persistent monitoring problem in discrete environments by minimizing the maximum latency between observations. Here maximum latency is the maximum time between visits to the same node, i.e. the revisit interval τ. Their method ranks nodes into different subclasses based on their value, where the higher the value and subclass the more often the node will be visited as explained in more detail in Section 2.3.3.

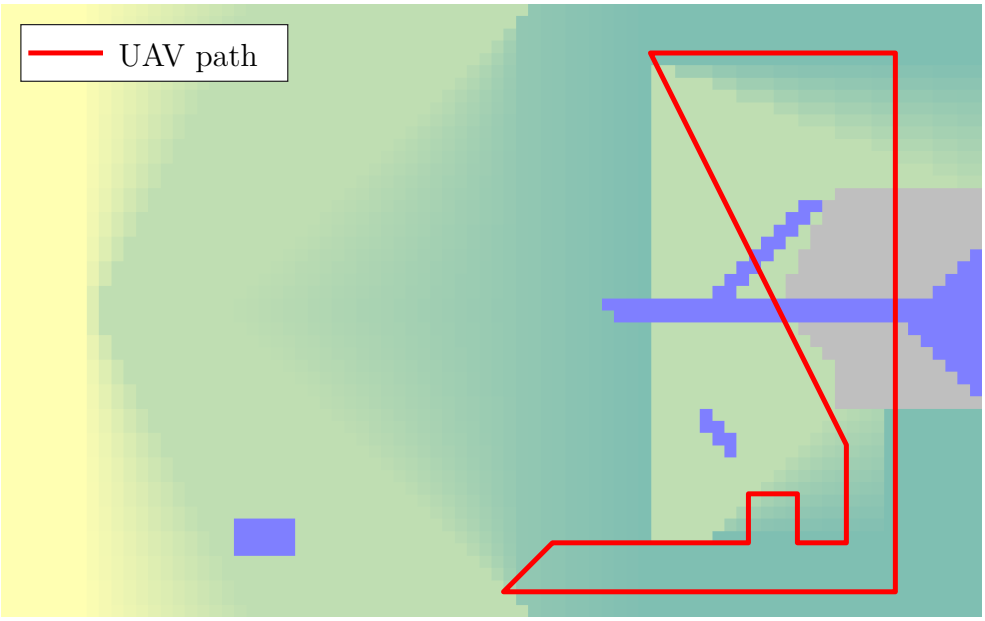

(a) Subwalk 1

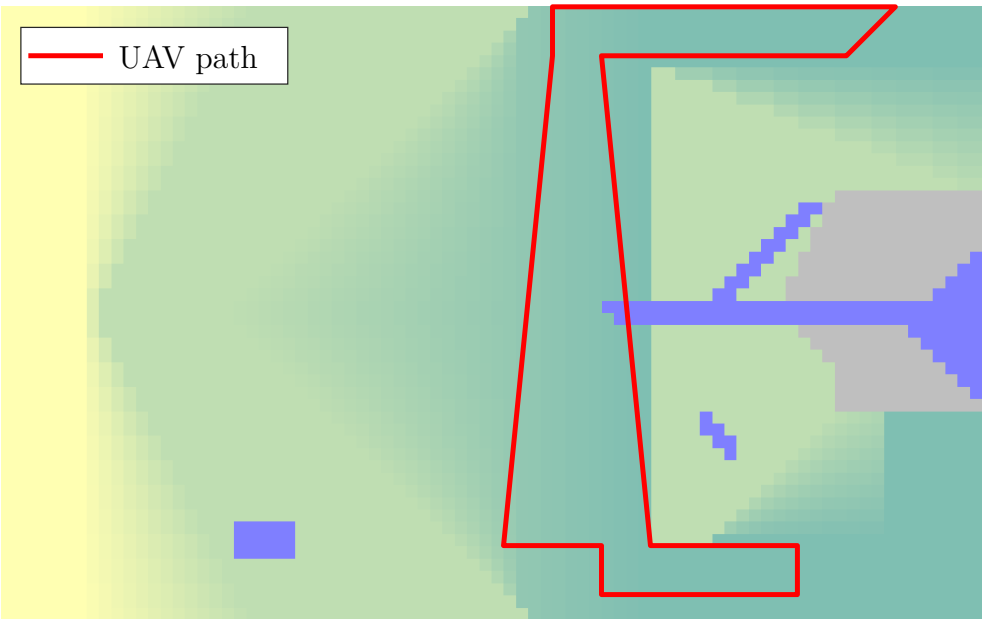

(b) Subwalk 2

Figure 4.8 – Two different subwalks of the persistent monitoring path given in Figure 4.7.

Implementing the algorithm proposed in [2], the minimum maximum latency walk for persistent monitoring as visualized in Figure 4.7 is obtained. Darker red lines indicate that multiple subwalks visit that section. This particular persistent monitoring path consists of two subwalks, which are illustrated in Figure 4.8.

It should be noted that the risk map, e.g. Figure 4.5, could also be taken directly as an input to flight time and path length trade-off algorithms such as the Dubins orienteering problem (DOP) [129].

4.3 Conclusions

In this chapter we formulated the surveillance problem. In the surveillance problem, the dynamics of the spreading process are fixed and the aim is to identify and bound the future cost of an undetected outbreak spreading from each node. This can be done by use of risk maps and finding the largest revisit interval for each node that we can use in surveillance schedules. We demonstrated this by first showing the effect of different parameters and discount rate on the risk map, afterwards we discussed a larger realistic wildfire example and demonstrated how to implement persistent monitoring path planning to bound the risk. In the next chapter, i.e. Chapter 5, we will extend this by including resource allocation for risk minimization.

Chapter 5

The Intervention Problem

In the previous chapter, we discussed how to bound the risk of an undetected outbreak by use of a revisit schedule. In this chapter, we consider allocating resources to reduce the risk and determine the associated surveillance workload needed. We, therefore, first define the resource model in Section 5.1. Next, we formulate the intervention problem and its convex representation in respectively Section 5.2 and Section 5.3. In Section 5.4 we discuss sparsity and reweighted ℓ_1 minimization. Finally, we present results for both epidemic and wildfire examples in Section 5.5. We demonstrate how the optimization framework can integrate both resource allocation and surveillance schedules, compare our results to minimizing the spectral abscissa and the original stochastic model and comment on computation and scalability.

5.1 Resource Allocation Model

In this section we discuss our proposed resource allocation model. Resources, e.g. lockdowns, vaccination, fire containment lines, can be allocated to modify the spreading and recovery rates β_{ij} and δ_i, the outbreak Poisson rate λ_i and the revisit interval

τ_i. We assume bounded ranges of possible values

$$0 < \underline{\beta}_{ij} \leq \beta_{ij} \leq \overline{\beta}_{ij}, \tag{5.1a}$$

$$0 < \underline{\delta}_i \leq \delta_i \leq \overline{\delta}_i < \overline{\Delta}, \tag{5.1b}$$

$$0 < \underline{\lambda}_i \leq \lambda_i \leq \overline{\lambda}_i, \tag{5.1c}$$

$$0 < \underline{\tau}_i \leq \tau_i \leq \overline{\tau}_i. \tag{5.1d}$$

Here $\overline{\beta}_{ij}$ and $\underline{\delta}_i$ are the unmodified rates of the system (3.8).

Remark 5.1. *Note that $\overline{\Delta} > \overline{\delta}$ as introduced in (5.1b) is often restricted to 1 for (networked) spreading processes where the recovery rate δ can not exceed 1 due to either restrictions on the discrete or nonlinear continuous dynamics, used time frames and/or values to indicate the spreading process [122, 132].*

The resource model we propose is defined by the following functions:

$$f_{ij}\left(\beta_{ij}\right) = w_{ij}\log\left(\frac{\overline{\beta}_{ij}}{\beta_{ij}}\right), \tag{5.2a}$$

$$g_i\left(\overline{\Delta} - \delta_i\right) = w_{ii}\log\left(\frac{\overline{\Delta} - \underline{\delta}_i}{\overline{\Delta} - \delta_i}\right), \tag{5.2b}$$

$$h_i\left(\lambda_i\right) = \omega_{\lambda_i}\log\left(\frac{\overline{\lambda}_i}{\lambda_i}\right), \tag{5.2c}$$

$$\psi_i\left(\tau_i\right) = \omega_{\tau_i}\log\left(\frac{\overline{\tau}_i}{\tau_i}\right) \tag{5.2d}$$

where w_{ij}, w_{ii}, ω_{λ_i} and ω_{τ_i} are weightings expressing the cost of respectively reducing β_{ij}, increasing δ_i and reducing λ_i and τ_i, and can be tuned to indicate areas in the network where it is hard or undesired to apply resources.

The logarithmic resource model for β (5.2a) can be understood as expressing the cost of proportional decrease in spreading rate at a particular node. That is, a reduction in β_{ij} by a certain proportion always takes the same amount of resources.

The design of the weightings w_{ij} is, therefore, easy to understand: e.g. if it takes

ξ_{ij} resources to reduce the spreading rate from i to j to half its original value, then set $w_{ij} = \xi_{ij}/\log(2)$. Note that this implies that it is impossible for β_{ij} to become 0, as this would take infinite resources, which is consistent with many real processes in which it is impossible to completely eliminate the possibility of spread. A similar interpretation holds for the cost of δ (5.2b) except that it is the difference between δ and $\overline{\Delta}$ which is reduced proportionally.

The logarithmic resource model of λ (5.2c) can be understood in a similar way as the resource model of the spreading rate β, i.e. a proportional decrease always has the same cost and it is impossible to reduce the outbreak rate to 0. Finally, for the revisit interval τ (5.2d) this can be thought of as that it is impossible to monitor each node i constantly. Hence, there will always be a non-zero interval rate between measurements. Furthermore, these resource models encourage sparsity as detailed further in Section 5.4.

In Section 5.5.2, in Example 5.3, we will compare the proposed resource model for the spreading rate (5.2a) and recovery rate (5.2b) with the resource model in [132], i.e.

$$f_{ij}\left(\beta_{ij}\right) = \frac{\beta_{ij}^{-1} - \overline{\beta}_{ij}^{-1}}{\underline{\beta}_{ij}^{-1} - \overline{\beta}_{ij}^{-1}}, \tag{5.3a}$$

$$g_i\left(\delta_i\right) = \frac{(1-\delta_i)^{-1} - (1-\underline{\delta}_i)^{-1}}{(1-\overline{\delta}_i)^{-1} - (1-\underline{\delta}_i)^{-1}} \tag{5.3b}$$

as visualized for the spreading rate in Figure 5.1 for $\underline{\beta} = 0.05$ and $\overline{\beta} = 1$. Notice that the proposed model associates higher cost for low resource investments, encouraging sparse allocation.

5.2 Problem Statements

We can study multiple problems, where the goal is to either minimize the risk or keep the risk bounded while minimizing resources. In total there are six different quantities

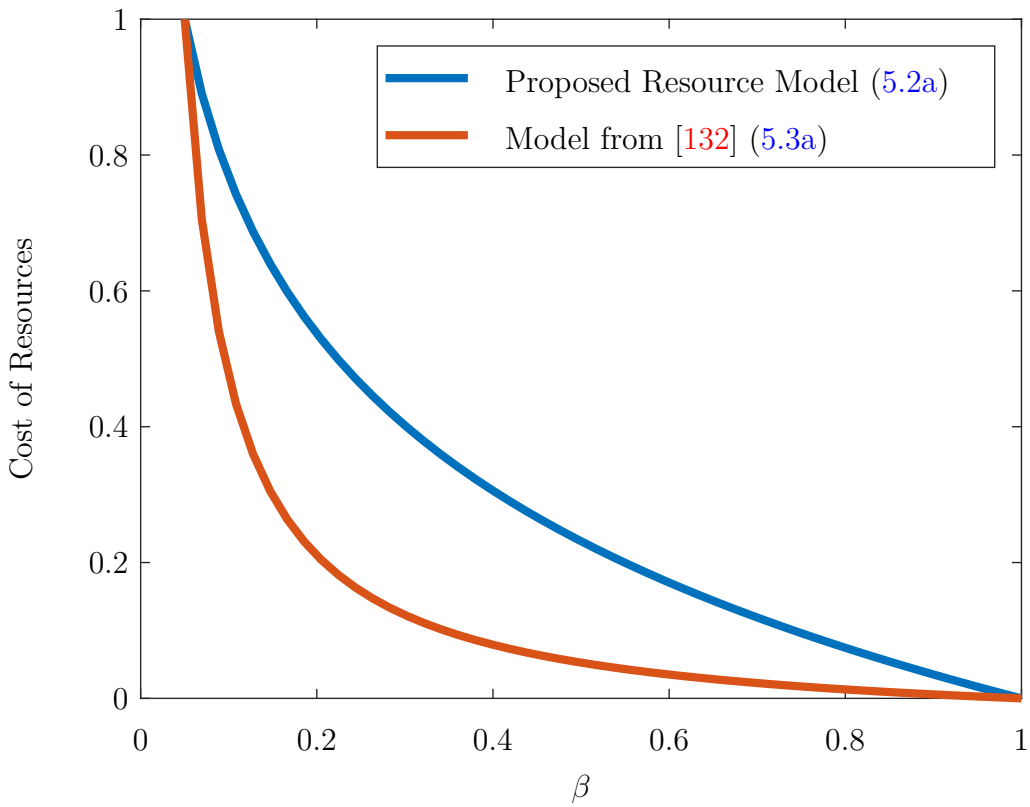

Figure 5.1 – Comparison of resource models (5.2a) and (5.3a) for investment on spreading rate β, with $\underline{\beta} = 0.05$ and $\overline{\beta} = 1$.

we may want to minimize or bound: risk (3.22), resources on spreading rate (5.2a), recovery rate (5.2b) and outbreak rate (5.2c), surveillance workload, i.e. frequency of revisits (5.2d) and discount rate r or the spectral abscissa bound (see Corollary 3.1).

The constraints the optimization will have to adhere to are the dynamic coupling constraint (3.17c), bounds on the spreading rate (5.1a), recovery rate (5.1b), outbreak rate (5.1c), revisit interval (5.1d) and discount rate. We set the bounds on the discount rate as

$$0 \leq r \leq \overline{R} \tag{5.4}$$

where $\overline{R}$ is the maximum discount rate.

The different objectives or costs and constraints are also summarized in respectively Table 5.1 and Table 5.2 including their convex representation, which we discuss in

the next Section 5.3.

Using the above mentioned objectives and constraints, we can now specify the standard set-up of the optimization problem, which is an extension of the LP (3.17).

Problem 5.1 (Intervention Problem)**.** *Minimize the maximum risk bound $R_i = p_i \lambda_i \tau_i$ via sparse resource allocation, given defined resource allocation budgets Γ and a cost c_i associated with each node i. That is, find the optimal state matrix A, discount rate r, outbreak Poisson rate λ_i and revisit interval τ_i that minimizes*

$$\underset{p,r,\beta,\delta,\lambda,\tau}{\text{minimize}} \quad \max_i \left(p_i \lambda_i \tau_i\right) \tag{5.5a}$$

$$\text{such that} \quad p \geq 0, \tag{5.5b}$$

$$p^T A - r p^T \leq -C, \tag{5.5c}$$

$$0 < \underline{\beta}_{ij} \leq \beta_{ij} \leq \overline{\beta}_{ij}, \tag{5.5d}$$

$$0 < \underline{\delta}_i \leq \delta_i \leq \overline{\delta}_i < \overline{\Delta}, \tag{5.5e}$$

$$0 < \underline{\lambda}_i \leq \lambda_i \leq \overline{\lambda}_i, \tag{5.5f}$$

$$0 < \underline{\tau}_i \leq \tau_i \leq \overline{\tau}_i, \tag{5.5g}$$

$$0 \leq r \leq \overline{R}, \tag{5.5h}$$

$$\sum_{ij} f_{ij}\left(\beta_{ij}\right) \leq \Gamma_\beta, \tag{5.5i}$$

$$\sum_i g_i\left(\delta_i\right) \leq \Gamma_\delta, \tag{5.5j}$$

$$\sum_i h_i\left(\lambda_i\right) \leq \Gamma_\lambda, \tag{5.5k}$$

$$\sum_i \psi_i\left(\tau_i\right) \leq \Gamma_\tau. \tag{5.5l}$$

It should be noted that (5.5c) expresses the Hurwitz stability condition (Section 3.3.1) and ensures the optimization is feasible, see Corollary 3.1.

In this thesis we focus on minimizing the maximum risk $\max_i(R_i)$, i.e. we allocate resources to reduce the worst-case expected impact of a localized outbreak. However, the summed risk, i.e. $\sum_i R_i$, can also be used.

Two closely related simplified problems which are often studied in literature [99, 114, 132, 183] are 'resource-constrained risk minimization' and 'risk-constrained risk minimization' where the goal is to keep both the risk and budget allocation small. These problems fall within the presented optimization framework Problem 5.1, but have only resources allocated to spreading and/or recovery rate. That is, compared to Problem 5.1 they have a fixed, given discount rate and outbreak rate and do not consider the joint optimization with surveillance scheduling, i.e. they do not include the interval rate. We will, therefore, use the risk given in (3.23) including the estimated probability $\hat{x}_i(0)$ instead of the probability of an outbreak occurring over a time interval $(\lambda_i \tau_i)$.

Problem 5.2 (Resource-Constrained Risk Minimization)**.** *Given defined resource allocation budget Γ, discount rate r and node dependent cost c_i, find the optimal spreading and recovery rates β_{ij} and δ_i that via sparse resource allocation minimize the maximum risk $\hat{x}(0) \odot p$, i.e. find the updated state matrix A that minimizes*

$$\underset{p,\beta,\delta}{\text{minimize}} \quad \max(\hat{x}(0) \odot p) \tag{5.6a}$$

$$\text{such that} \quad p \geq 0, \tag{5.6b}$$

$$p^T A - r p^T \leq -C, \tag{5.6c}$$

$$0 < \underline{\beta}_{ij} \leq \beta_{ij} \leq \overline{\beta}_{ij}, \tag{5.6d}$$

$$0 < \underline{\delta}_i \leq \delta_i \leq \overline{\delta}_i < \overline{\Delta}, \tag{5.6e}$$

$$\sum_{ij} f_{ij}(\beta_{ij}) + \sum_i g_i(\delta_i) \leq \Gamma. \tag{5.6f}$$

Problem 5.3 (Risk-Constrained Resource Minimization)**.** *Find the optimal spreading and recovery rates β_{ij} and δ_i that via sparse resource allocation minimize the amount of resources required, given an upperbound on the maximum risk γ, discount rate r and node dependent cost c_i, i.e. find the updated state matrix A that minimizes*

$$\underset{p,\beta,\delta}{\text{minimize}} \quad \sum_{ij} f_{ij}(\beta_{ij}) + \sum_i g_i(\delta_i) \tag{5.7a}$$

$$\text{such that} \quad p \geq 0, \tag{5.7b}$$

$$p^T A - rp^T \leq -C, \tag{5.7c}$$

$$0 < \underline{\beta}_{ij} \leq \beta_{ij} \leq \overline{\beta}_{ij}, \tag{5.7d}$$

$$0 < \underline{\delta}_i \leq \delta_i \leq \overline{\delta}_i < \overline{\Delta}, \tag{5.7e}$$

$$p_i \hat{x}_i(0) \leq \gamma. \tag{5.7f}$$

The formulated Problems 5.1, 5.2 and 5.3 are, however, unfortunately not LPs due to the nonlinearity occurring in the dynamic coupling constraint (5.5c) and can, therefore, not easily be optimally solved directly in a scalable way. In the next section, we will, therefore, demonstrate a method to reformulate these problems as convex optimization programs. In Appendix A an alternative resource model and iterative optimization programs to deal with this nonlinearity are explored and discussed as partially published in [153].

Additionally, it should be remarked that the proposed framework is applicable to any linear positive system for which sparse control applications are needed.

Remark 5.2. *The proposed optimization framework is applicable to any linear positive system where sparse changes to the state matrix are required, i.e. for which an integral linear cost function is minimized from the initial condition by changing as few elements of the state matrix as possible. In particular, the framework holds for a system $\dot{x}(t) = Ax(t)$ where A is Metzler, i.e. $a_{ij} \geq 0 \; \forall i \neq j$ similar to (3.9) and a corresponding cost function of the form $J = \int_0^\infty e^{-rt} Cx(t)dt$.*

5.3 Exponentional Cone Programming

This section demonstrates how we can reformulate our constraints and objectives to obtain a convex optimization problem, in particular an exponential cone program (see Section 2.5.4). Our problem formulations as given in the previous section are similar to GPs (Section 2.5.3) in that they are convex after logarithmic transformation.

We define decision variables y_i, v_i, z_i and σ_i for all nodes $i \in \mathcal{V}$, u_{ij} for all pairs $(i, j) \in \mathcal{E}$ and a new variable ρ to obtain a convex spectral abscissa bound. All

Table 5.1 – Spreading process quantities and their convex representation.

Objective	Model Variable	Convex Representation
Risk	$R_i = p_i \lambda_i \tau_i$	$y_i + \log(\overline{\lambda}_i) - \frac{z_i}{\omega_{\lambda_i}} + \log(\overline{\tau}_i) - \frac{\sigma_i}{\omega_{\tau_i}}$
Spreading rate	$\sum_{ij} f_{ij}(\beta_{ij})$	$\sum_{ij} u_{ij}$
Recovery rate	$\sum_i g_i(\delta_i)$	$\sum_i v_i$
Outbreak rate	$\sum_i h_i(\lambda_i)$	$\sum_i z_i$
Surveillance workload	$\sum_i \psi_i(\tau_i)$	$\sum_i \sigma_i$
Spectral abscissa bound	r	$\log(e^{\rho} - \overline{\Delta})$

objectives and constraints can now be reformulated as convex constraints under the following logarithmic transformations;

$$\begin{aligned} y_i &= \log(p_i), \quad u_{ij} = f_{ij}(\beta_{ij}), \quad v_i = g_i(\overline{\Delta} - \delta_i), \\ z_i &= h_i(\lambda_i), \quad \sigma_i = \psi_i(\tau_i), \quad \rho = \log(\overline{\Delta} + r). \end{aligned} \tag{5.8}$$

The objectives and their convex representation are summarized in Table 5.1.

Most convex representations follow directly from the logarithmic transformations given in (5.8), however, we will demonstrate how to obtain the convex logarithmic transformation of the risk R_i, i.e.

$$\log(R_i) = \log(p_i \lambda_i \tau_i) = \log(p_i) + \log(\lambda_i) + \log(\tau_i). \tag{5.9}$$

From (5.8) we can directly see that $\log(p_i) = y_i$, but we will need to rewrite $z_i = h_i(\lambda_i)$ and $\sigma_i = \psi_i(\tau_i)$ to obtain the logarithmic risk equation. We will demonstrate this for z_i. Using (5.2c) we obtain

$$z_i = h_i(\lambda_i) = \omega_{\lambda_i} \log\left(\frac{\overline{\lambda}_i}{\lambda_i}\right) = \omega_{\lambda_i}\left(\log\left(\overline{\lambda}_i\right) - \log\left(\lambda_i\right)\right), \tag{5.10}$$

rearranging we get

$$\frac{z_i}{\omega_{\lambda_i}} = \log\left(\overline{\lambda}_i\right) - \log\left(\lambda_i\right) \tag{5.11}$$

which results in

$$\log(\lambda_i) = \log(\overline{\lambda}_i) - \frac{z_i}{\omega_{\lambda_i}}. \tag{5.12}$$

Table 5.2 – Constraints of the minimization Problem 5.1 and their convex representation.

Name	Model Constraint	Convex Representation
Dynamic coupling constraint	$p^T A - rp^T \leq -C$	$q(y,u,v,\rho) \leq 0$ (5.13)
Spreading rate bounds	$0 < \underline{\beta}_{ij} \leq \beta_{ij} \leq \overline{\beta}_{ij}$	$0 \leq u_{ij} \leq \overline{u}_{ij} = w_{ij}\log\left(\frac{\overline{\beta}_{ij}}{\underline{\beta}_{ij}}\right)$
Recovery rate bounds	$0 < \underline{\delta}_i \leq \delta_i \leq \overline{\delta}_i < \overline{\Delta}$	$0 \leq v_i \leq \overline{v}_i = w_{ii}\log\left(\frac{\overline{\Delta}-\underline{\delta}_i}{\overline{\Delta}-\overline{\delta}_i}\right)$
Outbreak rate bounds	$0 < \underline{\lambda}_i \leq \lambda_i \leq \overline{\lambda}_i$	$0 \leq z_i \leq \overline{z}_i = \omega_{\lambda_i}\log\left(\frac{\overline{\lambda}_i}{\underline{\lambda}_i}\right)$
Revisit interval bounds	$0 < \underline{\tau}_i \leq \tau_i \leq \overline{\tau}_i$	$0 \leq \sigma_i \leq \overline{\sigma}_i = \omega_{\tau_i}\log\left(\frac{\overline{\tau}_i}{\underline{\tau}_i}\right)$
Discount rate bounds	$0 \leq r \leq \overline{R}$	$\log(\overline{\Delta}) \leq \rho \leq \log(\overline{\Delta} + \overline{R})$

In a similar way we can obtain an expression for $\log(\tau_i)$ and finally, we obtain the convex representation of the risk objective as shown in Table 5.1.

The constraints the optimization will have to adhere to are summarized in Table 5.2 and consist of the bounds on the different variables and the dynamic coupling constraint (3.17c), derived from (3.16).

Lemma 5.1. *The dynamic coupling constraint $p^T A - rp^T \leq -C$ is equivalent to the following convex constraint under the transformations* (5.8)

$$q_j(y,u,v,\rho) = \log\Bigg(\sum_{i:(i,j)\in\mathcal{E}} \exp\left(y_i + \log\left(\overline{\beta}_{ij}\right) - \frac{u_{ij}}{w_{ij}} - y_j - \rho\right) + \exp\left(\log\left(\overline{\Delta} - \underline{\delta}_j\right) - \frac{v_j}{w_{jj}} - \rho\right) + \exp\Big(\log\left(c_j\right) - y_j - \rho\Big)\Bigg) \leq 0 \quad \forall j. \tag{5.13}$$

Proof. We obtain (5.13) from (3.16)/(3.17c), which can be rewritten as

$$\sum_{i=1}^{n} p_i A_{ij} - p_j r \leq -c_j \quad \forall j. \tag{5.14}$$

Now using (3.9) we can rewrite this as

$$\sum_{i \neq j} p_i \beta_{ij} - p_j \delta_j - p_j r \leq -c_j \quad \forall j, \tag{5.15}$$

which is equivalent, when introducing $\overline{\Delta} > \overline{\delta_i}$, to

$$\sum_{i \neq j} \frac{p_i \beta_{ij}}{p_j(\overline{\Delta} + r)} + \frac{\overline{\Delta} - \delta_j}{\overline{\Delta} + r} + \frac{c_j}{p_j(\overline{\Delta} + r)} \leq 1 \quad \forall j. \tag{5.16}$$

Taking the log of both sides, using $\rho = \log(\overline{\Delta} + r)$ and rewriting gives (5.13). The convexity follows from the fact that log-sum-exp constraints are convex on $\mathbb{R}^n$ [14]. □

It should be noted that (5.13) can be formulated as a set of exponential cone constraints.

Lemma 5.2. *The bounds on the spreading rates and recovery rates, respectively* $0 < \underline{\beta}_{ij} \leq \beta_{ij} \leq \overline{\beta}_{ij}$ *and* $0 < \underline{\delta}_i \leq \delta_i \leq \overline{\delta}_i < \overline{\Delta}$, *are equivalent to the following equations under convex transformation using* $u_{ij} = f_{ij}(\beta_{ij})$ *and* $v_i = g_i(\overline{\Delta} - \delta_i)$

$$0 \leq u_{ij} \leq w_{ij} \log\left(\frac{\overline{\beta}_{ij}}{\underline{\beta}_{ij}}\right), \tag{5.17a}$$

$$0 \leq v_i \leq w_{ii} \log\left(\frac{\overline{\Delta} - \underline{\delta}_i}{\overline{\Delta} - \overline{\delta}_i}\right). \tag{5.17b}$$

Proof. Rewriting the bounds on β results in

$$0 < \frac{\underline{\beta}_{ij}}{\overline{\beta}_{ij}} \leq \frac{\beta_{ij}}{\overline{\beta}_{ij}} \leq 1 \tag{5.18}$$

which is equivalent to

$$0 \leq \log\left(\frac{\overline{\beta}_{ij}}{\beta_{ij}}\right) \leq \log\left(\frac{\overline{\beta}_{ij}}{\underline{\beta}_{ij}}\right) \tag{5.19}$$

and can be rewritten to (5.17a) using $u_{ij} = w_{ij} \log\left(\frac{\overline{\beta}_{ij}}{\beta_{ij}}\right)$. The bounds on v_i can be found in the same way. □

The bounds on the outbreak rates λ_i and interval rates τ_i can be found following a similar derivation.

Proposition 5.1 (Convex Problem 5.1)**.** *Problem 5.1 is equivalent to the following convex optimization problem, more specifically exponential cone program, under the transformations* $y_i = log\,(p_i)$, $u_{ij} = f_{ij}(\beta_{ij})$, $v_i = g_i(\overline{\Delta} - \delta_i)$, $z_i = h_i(\lambda_i)$, $\sigma_i = \psi_i(\tau_i)$ *and* $\rho = log\left(\overline{\Delta} + r\right)$

$$\underset{y,\rho,u,v,z,\sigma}{\text{minimize}} \quad \max_i \left(y_i + \log\left(\overline{\lambda}_i\right) - \frac{z_i}{\omega_{\lambda_i}} + \log\left(\overline{\tau}_i\right) - \frac{\sigma_i}{\omega_{\tau_i}} \right) \tag{5.20a}$$

$$\text{such that} \quad q(y, u, v, \rho) \leq 0, \tag{5.20b}$$

$$0 \leq u_{ij} \leq \overline{u}_{ij}, \tag{5.20c}$$

$$0 \leq v_i \leq \overline{v}_i, \tag{5.20d}$$

$$0 \leq z_i \leq \overline{z}_i, \tag{5.20e}$$

$$0 \leq \sigma_i \leq \overline{\sigma}_i, \tag{5.20f}$$

$$\log\left(\overline{\Delta}\right) \leq \rho \leq \log\left(\overline{\Delta} + \overline{R}\right), \tag{5.20g}$$

$$\sum_{ij} u_{ij} \leq \Gamma_\beta, \tag{5.20h}$$

$$\sum_i v_i \leq \Gamma_\delta, \tag{5.20i}$$

$$\sum_i z_i \leq \Gamma_\lambda, \tag{5.20j}$$

$$\sum_i \sigma_i \leq \Gamma_\tau. \tag{5.20k}$$

Proof. How to derive the convex objective function (5.20a) from the risk objective (5.11) was demonstrated above in equations (5.10) and (5.11). The dynamic coupling constraint (5.13) equivalence to (5.20b) was proven in Lemma 5.1. The bounds on spreading, recovery, outbreak and interval rate (5.20c) - (5.20f) were derived in Lemma 5.2. (5.20g) follows from (5.5h) by adding $\overline{\Delta}$ and using the transformation $\rho = \log(\overline{\Delta} + r)$. Finally, the resource bounds (5.20h) - (5.20k) follow directly from (5.5i) - (5.5l) and $u_{ij} = f_{ij}(\beta_{ij})$, $v_i = g_i(\overline{\Delta} - \delta_i)$, $z_i = h_i(\lambda_i)$ and $\sigma_i = \psi_i(\tau_i)$. □

Similarly we can derive the equivalent convex optimization problems of Problem 5.2

and 5.3.

Proposition 5.2. *Problem 5.2 is equivalent to the following convex optimization problem under the transformations* $y_i = log\left(p_i\right)$ *and* $u_{ij} = f_{ij}\left(\beta_{ij}\right)$ *and* $v_i = g_i\left(\overline{\Delta} - \delta_i\right)$

$$\underset{y,u,v}{\text{minimize}} \quad \max\left(\log\left(\hat{x}(0)\right) + y\right) \tag{5.21a}$$

$$\begin{aligned}\text{such that} \quad & \log\Bigg(\sum_{i:(i,j)\in\mathcal{E}} \exp\left(y_i + \log\left(\frac{\overline{\beta}_{ij}}{\overline{\Delta}+r}\right) - \frac{u_{ij}}{w_{ij}} - y_j\right) \\ & + \exp\left(\log\left(\frac{\overline{\Delta}-\underline{\delta}_j}{\overline{\Delta}+r}\right) - \frac{v_j}{w_{jj}}\right) + \exp\left(\log\left(\frac{c_j}{\overline{\Delta}+r}\right) - y_j\right)\Bigg) \leq 0 \quad \forall j,\end{aligned} \tag{5.21b}$$

$$0 \leq u_{ij} \leq \overline{u}_{ij}, \tag{5.21c}$$

$$0 \leq v_i \leq \overline{v}_i \tag{5.21d}$$

$$\sum_{ij} u_{ij} + \sum_i v_i \leq \Gamma. \tag{5.21e}$$

Proof. The objective function (5.21a) follows directly from (5.6a) and $y = \log(p)$. We obtain (5.21b) from Lemma 5.1 and taking the assumption that the discount rate r is a fixed parameter instead of a variable. The bounds on spreading rate (5.21c) and recovery rate (5.21d) were derived in Lemma 5.2. Finally, (5.21e) follows directly from (5.6f) and $u_{ij} = f_{ij}\left(\beta_{ij}\right)$ and $v_i = g_i\left(\overline{\Delta} - \delta_i\right)$. □

Proposition 5.3. *Problem 5.3 is equivalent to the following convex optimization problem under the transformations* $y_i = log\left(p_i\right)$ *and* $u_{ij} = f_{ij}\left(\beta_{ij}\right)$ *and* $v_i = g_i\left(\overline{\Delta} - \delta_i\right)$

$$\underset{y,u,v}{\text{minimize}} \quad \sum_{ij} u_{ij} + \sum_i v_i \tag{5.22a}$$

$$\text{such that} \quad \log\Bigg(\sum_{i:(i,j)\in\mathcal{E}} \exp\left(y_i + \log\left(\frac{\overline{\beta}_{ij}}{\overline{\Delta}+r}\right) - \frac{u_{ij}}{w_{ij}} - y_j\right)$$

$$+\exp\left(\log\left(\frac{\overline{\Delta}-\underline{\delta}_j}{\overline{\Delta}+r}\right)-\frac{v_j}{w_{jj}}\right)+\exp\left(\log\left(\frac{c_j}{\overline{\Delta}+r}\right)-y_j\right)\Bigg)\leq 0 \quad \forall j, \tag{5.22b}$$

$$0 \leq u_{ij} \leq \overline{u}_{ij}, \tag{5.22c}$$

$$0 \leq v_i \leq \overline{v}_i \tag{5.22d}$$

$$\log\left(\hat{x}(0)\right)+y \leq \log\left(\gamma\right). \tag{5.22e}$$

Proof. Similar to the proof of Proposition 5.2. □

5.4 Sparsity and Reweighted ℓ_1 minimization

A significant benefit of the exponential cone programming formulation is that it encourages sparse resource allocation. Since the associated variables are non-negative, our resource bounds, formulated as constraints (5.20h) - (5.20k), e.g. $\sum_{ij} u_{ij} \leq \Gamma_\beta$, are ℓ_1 norm constraints and objectives, which are widely used to encourage sparsity [19, 20, 39, 161] as discussed in Section 2.5.5.

If the goal is maximal sparsity, i.e. minimal number of nodes and edges with non-zero resources allocated, then we can use the reweighted ℓ_1 optimization approach of [20] as given in (2.26) in Section 2.5.5. We can adapt this to our problem by iteratively solving the problem, but with a reweighted resource model that approximates the number of nodes and edges with non-zero allocation, e.g.

$$\phi_\beta^k = \sum_{ij} \frac{u_{ij}^k}{u_{ij}^{k-1}+\epsilon} \tag{5.23}$$

where k is the iteration number and ϵ a small positive constant to improve numerical stability.

If we use our resource model as a constraint in the optimization Problem 5.1 we now replace e.g. the constraint (5.20h) with $\phi_\beta^k \leq M$ where M is the bound on the number of edges that can have resources allocated to them. If on the other hand, we want

to minimize the amount of resources used, the objective changes from minimizing the resource model to minimizing ϕ_β^k. We can demonstrate this by having a look at applying reweighted ℓ_1 minimization to Problems 5.2 and 5.3.

We define the iterative reweighted ℓ_1 minimization by

$$\phi_{\beta,\delta}^k = \sum_{ij} \frac{u_{ij}^k}{u_{ij}^{k-1} + \epsilon} + \sum_i \frac{v_i^k}{v_i^{k-1} + \epsilon}. \tag{5.24}$$

For Problem 5.2 we now replace constraint (5.21e) with $\phi_{\beta,\delta}^k \leq M$ where M is the bound on the number of nodes and edges that can have resources allocated to them, similar to the approach for Problem 5.1. For Problem 5.3 the objective changes from minimizing (5.22a) to minimizing $\phi_{\beta,\delta}^k$.

Similarly, we could minimize all resource allocation on nodes and edges for Problem 5.1 together, instead of for separate resource budgets, by defining

$$\phi_{\text{all}}^k = \sum_{ij} \frac{u_{ij}^k}{u_{ij}^{k-1} + \epsilon} + \sum_i \frac{v_i^k}{v_i^{k-1} + \epsilon} + \sum_i \frac{z_i^k}{z_i^{k-1} + \epsilon} + \sum_i \frac{\sigma_i^k}{\sigma_i^{k-1} + \epsilon}. \tag{5.25}$$

The reweighted ℓ_1 iteration approach has no guarantee of convergence or global optimality, nevertheless has been found to be very effective in practice.

5.5 Results

In this section we illustrate how our proposed method can be implemented with multiple examples for two different spreading processes; epidemics and wildfires. First, we discuss a 7 node epidemic example to demonstrate how the optimization framework can be used for identifying critical links and deriving a vaccination strategy. Second, we discuss a larger 359 node epidemic example of a pandemic spreading on the airport transportation network in the United States (US). Third, we demonstrate with a simplified 1000 node wildfire example that our method can provide more targeted resource allocation compared to previous geometric programming approaches. Fourth,

we revisit Example 4.2, i.e. the large wildfire example of 4000 nodes of Section 4.2.2, demonstrating how we can utilize resource allocation and revisit schedules to minimize the risk of an undetected outbreak. Furthermore, we incorporate robot path planning methods for surveillance to show how to bridge the gap between spreading models and path planning. We validate our proposed framework based on the linear model by comparing it to the original stochastic process. Finally, we discuss computation time and scalability.

5.5.1 Epidemics

We discuss two examples involving epidemics in this subsection. A 7 node example to demonstrate first of all simplified resource allocation for the optimal control problem of minimizing risk by modifying the system's dynamics and second a vaccination strategy. Moreover, we discuss the effect of the discount rate in regards to intervention strategies. Finally, we consider a larger air transportation network of 359 nodes to discuss policy making on larger networks in regards to epidemics and how to implement reweighted ℓ_1 minimization if sparsity is the primary goal.

Epidemic Intervention - 7 nodes

To demonstrate how the optimization framework (Problem 5.1 and Proposition 5.1) can be utilized we take an example of an epidemic spreading on a graph $\mathcal{G}(\mathcal{V}, \mathcal{E})$ with $n = 7$ nodes as visualized in Figure 5.2. Here, node color indicates outbreak rate λ_i, weightings w_{ij} are indicated at the edges and node marker size indicates cost c_i. We take homogeneous spreading and recovery rates of $\beta_{ij} = 0.35$ for all $(i, j) \in \mathcal{E}$ and $\delta_i = 0.2$ for all $i \in \mathcal{V}$. In this particular example we have a vulnerable high cost node $i = 7$, which could be an elderly person, which is connected to $i = 6$, which can be thought of as a caretaker or nurse. This link has, therefore, a higher weight $w_{ij} = 10$, hence a larger cost to remove it. Node $i = 6$ is connected to node $i = 1$ who has a high likelihood of getting the disease, e.g. due to their work situation.

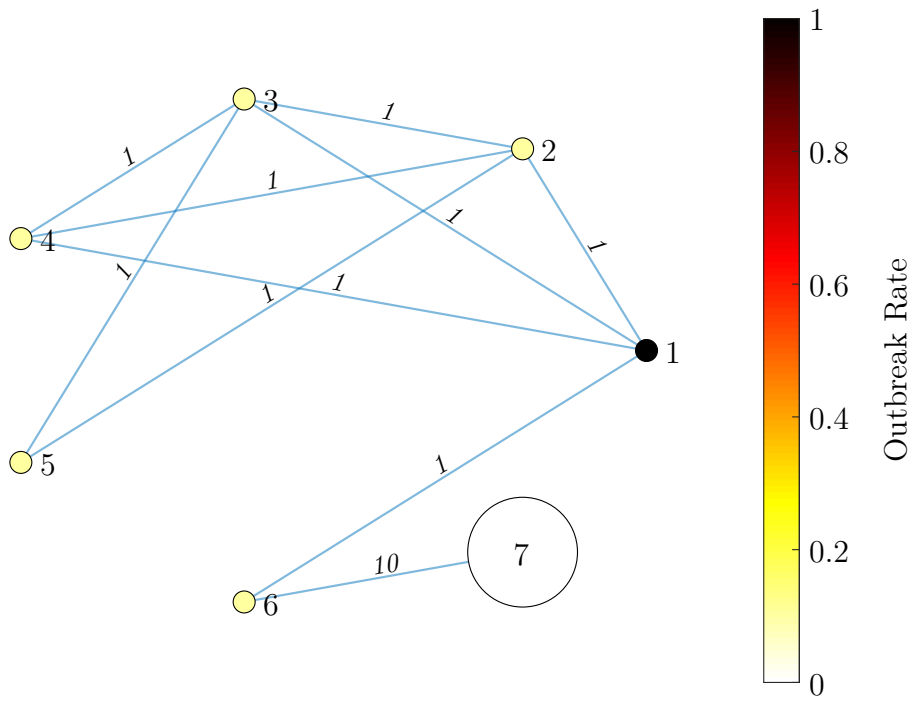

Figure 5.2 – Example 5.1; Epidemic spreading over a graph with $n = 7$ nodes. Node color indicates outbreak rate λ_i, weightings w_{ij} are indicated at the edges, node marker size indicates cost c_i.

We are, first of all, interested to see if our method can indicate the critical link between node 1 and 6. Hence, we take our objective as minimizing the risk (3.22) similar to Problems 5.1 and 5.2, while allocating resources on the links, i.e. spreading rate, take $\Gamma_\beta = 1$ and obtain Figure 5.3. Our method does indeed suggest allocating resources to this particular link, especially considering the larger cost involved in breaking up the link between the nurse and the associated patient.

Next, we compare our method to minimizing the spectral abscissa (3.24), see Figure 5.4. It can be seen, that by only minimizing the spectral abscissa instead of our proposed risk model, the same critical link is not identified, because the spectral abscissa does not take into account node dependent costs and therefore, ignores the importance of node $i = 7$ and only considers reducing overall spreading rate in the network.

Another common scenario in relation to epidemics is vaccination. We model vaccination in such a way that similar to other common methods vaccination of a node

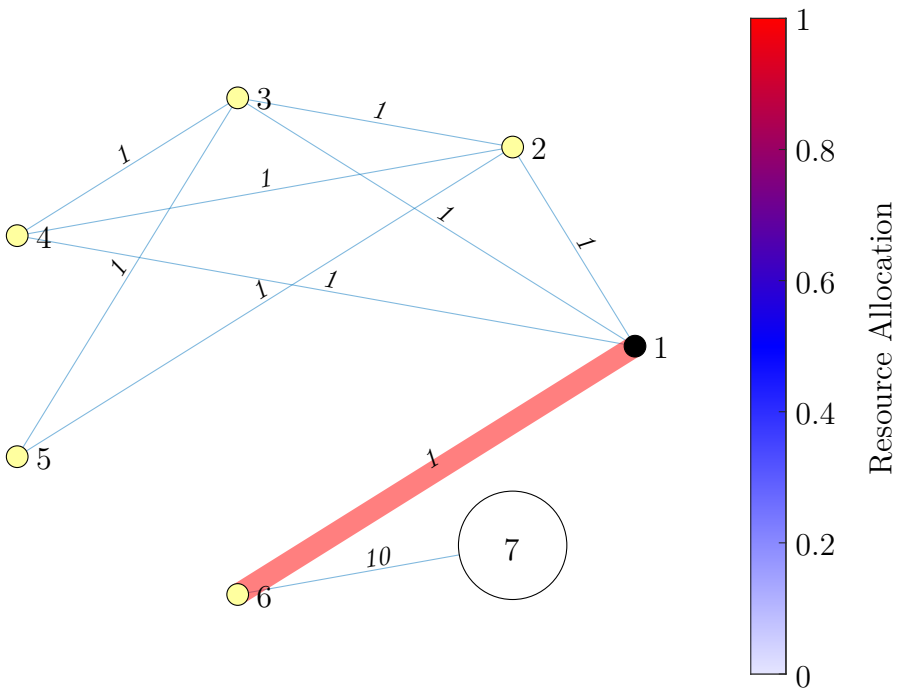

Figure 5.3 – Resource allocation for minimizing the risk (3.22). Node color indicates outbreak rate λ_i, weightings w_{ij} are indicated at the edges, node marker size indicates cost c_i.

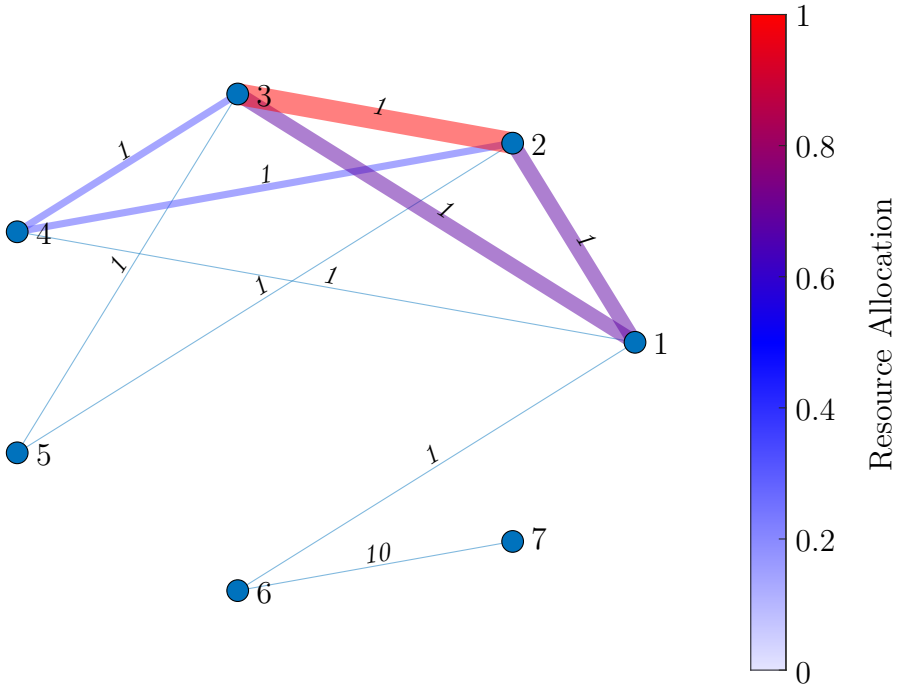

Figure 5.4 – Resource allocation for minimizing the spectral abscissa (3.24).

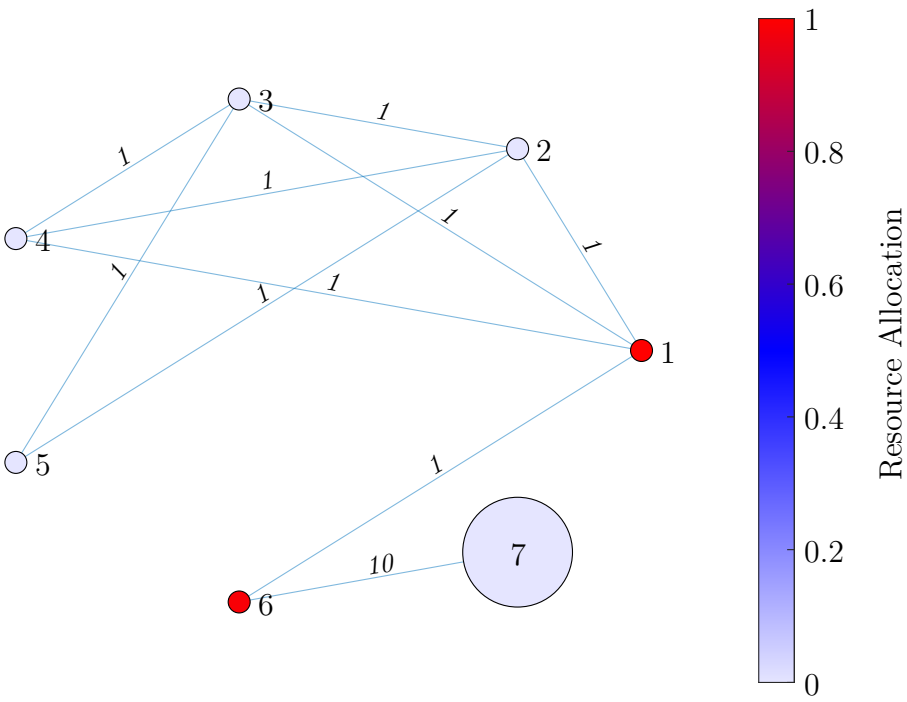

Figure 5.5 – Resource allocation for vaccination scenario. Node color indicates nodes vaccinated, i.e. β_{ij} is reduced and δ_i is increased for nodes $i = 1$ and $i = 6$, $r = 1.3$.

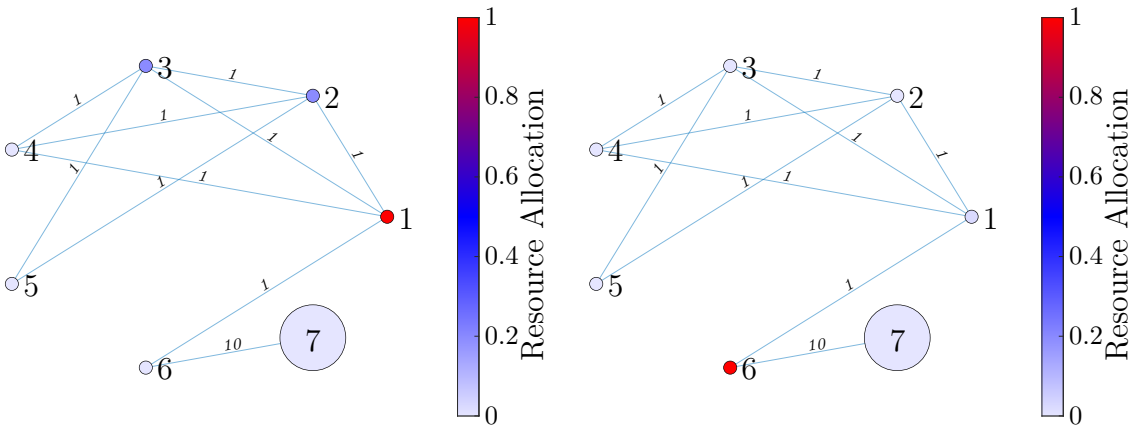

(a) $r = 0.987$ **(b)** $r = 2$

Figure 5.6 – Effect of discount rate r on vaccination strategy compared to Figure 5.5.

both increases its recovery rate [49, 63, 64] and reduces all incoming spreading rates [22, 67, 79, 180]. Setting $\overline{\Delta} = 1$, see Remark 5.1, the obtained resource allocation, or vaccination strategy, is given in Figure 5.5 and Figure 5.6. Here the discount rate r, see Section 3.3.1, determines if we should vaccinate node $i = 1$, i.e. high discount rate prioritizes near future impact, and/or node $i = 6$, i.e. low discount rate prioritizes

long term advantage. The initial zero outbreak rate of node 7 and higher weight on the edge between node 6 and 7, make in this case vaccination of node 7 not relevant.

Note that another common way of modeling vaccination is by including an additional vaccination class into the SIS or SIR model [128, 144, 150]. This, however, goes beyond the scope of this thesis.

Air Transportation Network

We now demonstrate resource allocation and policy making in regards to risk management for a larger network given a spreading process, here an epidemic. We consider the domestic US air transportation network graph based on the number of passengers transported in 2014 [145] consisting of $n = 359$ nodes and 2097 edges as visualized in Figure 5.7. All domestic air traffic within the US excluding Puerto Rico, Virgin Islands and Guam is considered, where multiple airports that serve the same city are combined and routes that have less than 10.000 pax per year are omitted.

Now considering β allocation only and the spread of SARS, we obtain a spreading rate of $\beta = 0.25$ per day, a recovery rate of 0.0352 and a death rate of 0.0279 [24]. For simplicity we consider recovered nodes as removed as well due to (temporary) immunity. For the resource model we now base the weighting w_{ij} on the number of passengers transported, taking the logic that the more flights and passengers, the higher the cost of reducing this traffic. The cost c_i equals the normalized number of passengers served per airport, since this roughly corresponds to the local population and hence, impact of an outbreak.

We now consider two different scenarios with different levels of information. In each case, the objective is to minimize the risk by 50 percent. First, we consider a known outbreak in Philadelphia (PHL) and set $\hat{x}(0)_{PHL} = 1$ and $\hat{x}(0)_i = 0.1$ elsewhere. Note that this corresponds to Problem 5.3, namely 'risk-constrained resource minimization', with spreading rate β allocation only. The resulting resource allocation for $r = 10.7$ is given by Figure 5.8 and reduces passenger numbers on 53 out of 2097 routes.

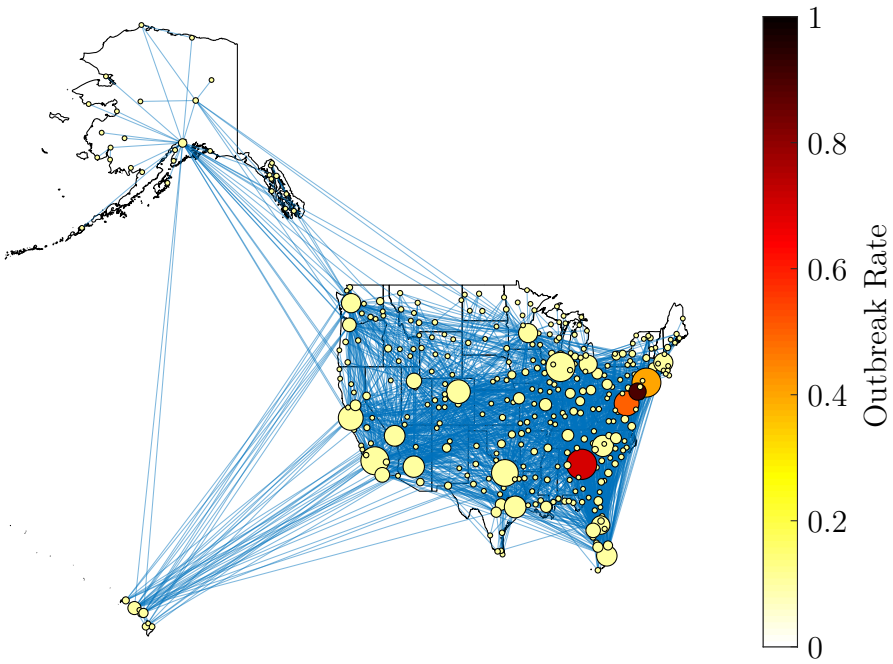

Figure 5.7 – Example 5.2; Epidemic spreading over a graph of the domestic US air transportation network with 359 nodes and 2097 edges based on [145]. Node marker size indicates cost c_i, and the color indicates outbreak rate λ_i for Scenario 2.

We can further improve sparsity by solving the reweighted ℓ_1 minimization as explained in Section 5.4. The resulting allocation is demonstrated in Figure 5.9, here the number of affected routes is reduced to only 11 instead of 53 while achieving the same risk as in Figure 5.8. Hence, by stopping air traffic between Philadelphia and respectively Atlanta, Charlotte, Chicago, Dallas, Denver, Detroit, Houston, Las Vegas, Minneapolis/St. Paul, New York City and Washington DC, risk can be reduced by 50 percent while leaving other busy air routes intact.

Second, we consider the more realistic scenario where the exact outbreak location is not known and take the following estimated outbreak probabilities: Philadelphia (PHL) $\hat{x}(0)_{PHL} = 0.9$, Atlanta (ATL) $\hat{x}(0)_{ATL} = 0.7$, Washington DC (DCA) $\hat{x}(0)_{DCA} = 0.5$, New York City (NYC) $\hat{x}(0)_{NYC} = 0.4$ and $\hat{x}(0)_i = 0.1$ elsewhere. The resulting resource allocation is displayed in Figure 5.10 and for the reweighted ℓ_1 minimization in Figure 5.11. Passenger numbers are reduced on respectively 60 and 13 routes. It can be seen that compared to Figures 5.8 and 5.9 the amount of routes affected has only slightly increased, but the particular routes affected have changed.

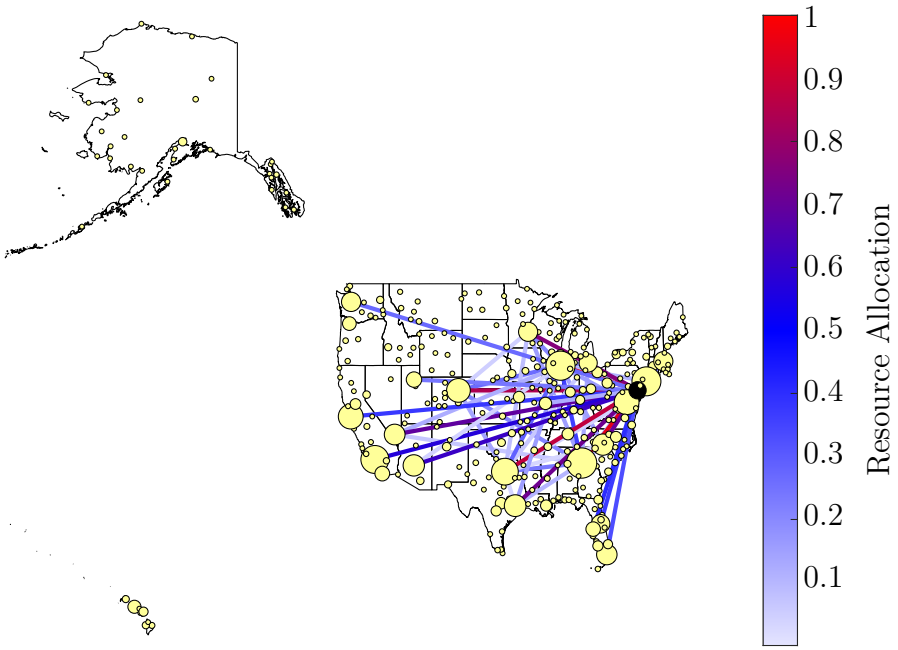

Figure 5.8 – Scenario 1 - Resource allocation given known outbreak in PHL for reducing the risk by 50%. **53** edges have resources allocated. Node marker size indicates cost c_i and the node color indicates outbreak rate λ_i.

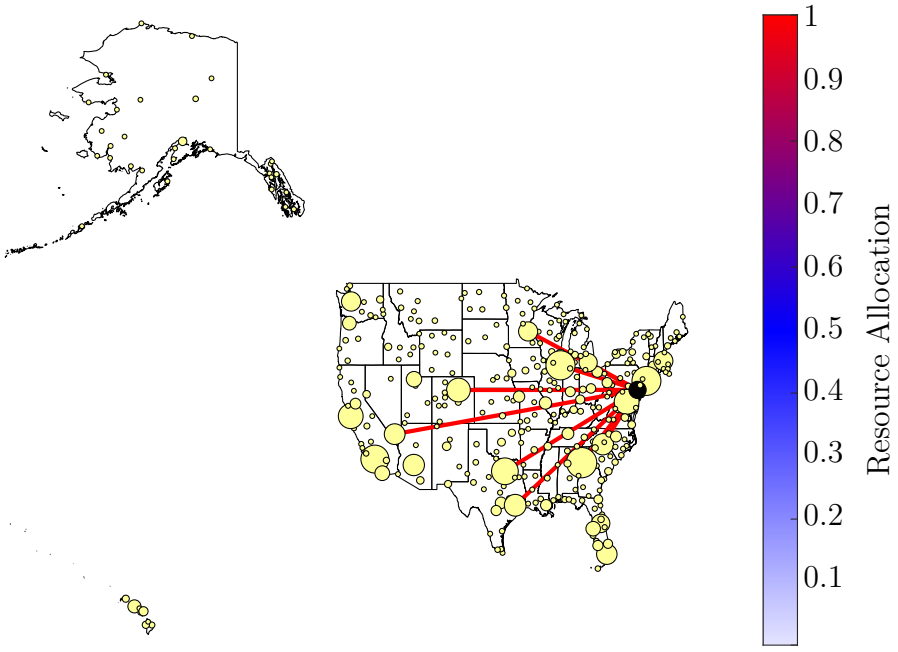

Figure 5.9 – Resource allocation after using reweighted ℓ_1 minimization (5.23) on Figure 5.8. **11** edges have resources allocated.

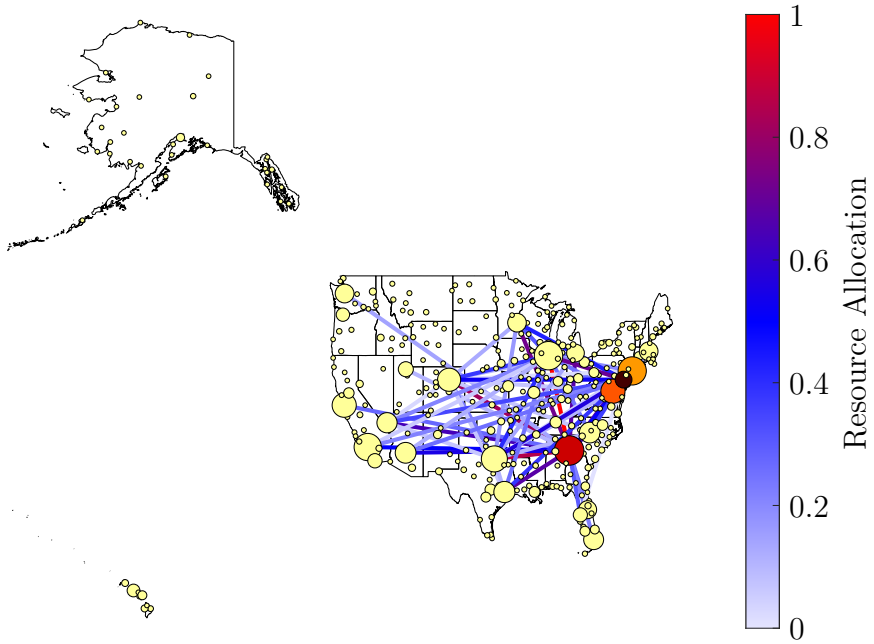

Figure 5.10 – Scenario 2 - Resource allocation reducing the risk by 50% with higher outbreak rates in Philadelphia, Atlanta, Washington DC and New York City. **60** edges have resources allocated. Node marker size indicates cost c_i and the node color indicates outbreak rate λ_i.

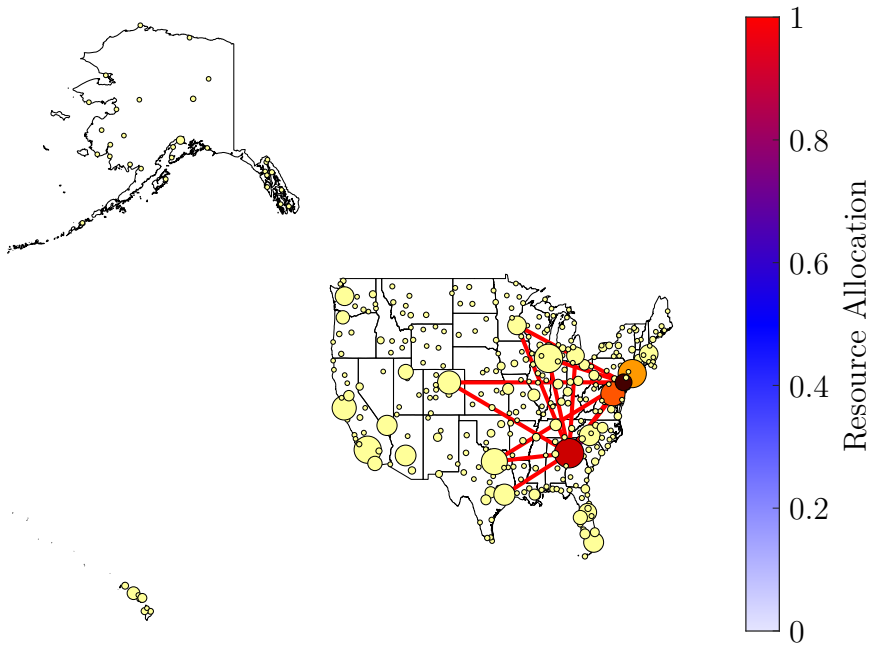

Figure 5.11 – Resource allocation after using reweighted ℓ_1 minimization (5.23) on Figure 5.10. **13** edges have resources allocated.

5.5.2 Wildfires

In the previous subsection, we demonstrated how the optimization framework works with epidemic examples and resource allocation on spreading and recovery rate β and δ. In this subsection, we will make full use of the optimization framework by presenting two wildfire examples consisting of a 1000 and 4000 node graph. We compare the proposed method and resulting resource allocation to other common approaches based on risk and resource model. That is, we particularly investigate if high cost areas are targeted and if the results are sparse. Furthermore, we demonstrate how the joint optimization framework can bridge the gap between spreading models and robotic path planning. Finally, we validate the resulting allocation obtained by using the linearized model to outbreaks of the original underlying stochastic model.

1000 nodes

Let us consider the fictional landscape given in Figure 5.12a consisting of different vegetation types, a city and water. We represent this landscape as a graph with $n = 1000$ nodes, where the edge set $\mathcal{E}$ connects each node to its neighboring 8 nodes, i.e. fire can spread horizontally, vertically and diagonally, see Figure 2.3. Boundary nodes have fewer edges accordingly.

The spreading rates are determined by the vegetation type, wind speed and direction, as per the wildfire models in [3] and [80]. The spreading rate for an edge

$$\beta = \beta_b \beta_{veg} \beta_w \tag{5.26}$$

consists of a baseline spreading rate $\beta_b = 0.5$ and $\beta_{veg} = 0.1, 1$ and 1.4 for respectively desert, grassland and eucalypt forest. Water is considered unburnable and those edges are removed, resulting in a total number of 3486 non-zero edges. β_w is calculated following [3] for a northeasterly wind of $V = 4$ m/s. The spreading rate is corrected for the spread between diagonally connected nodes, following [80]. We set the recovery rate $\delta = 0.5$ for all nodes.

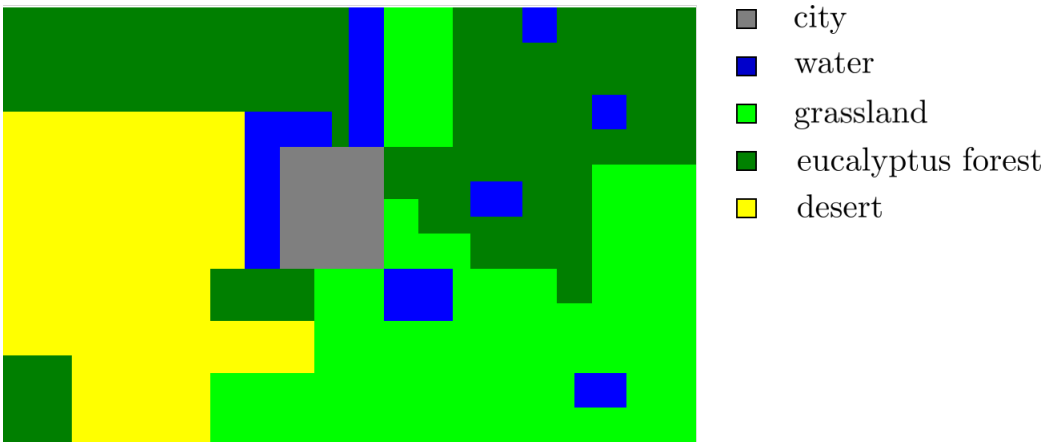

(a) Vegetation Map

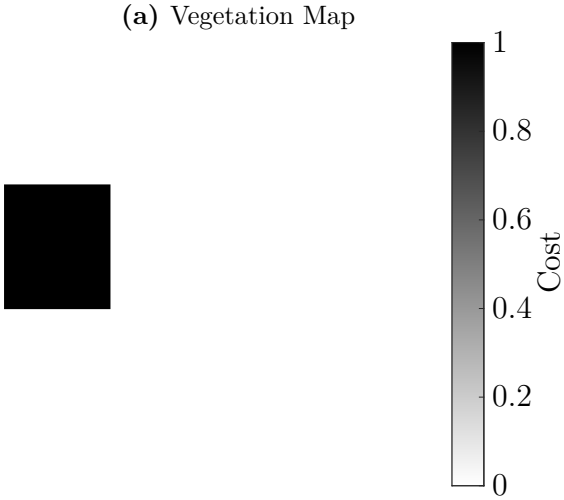

(b) Cost Map

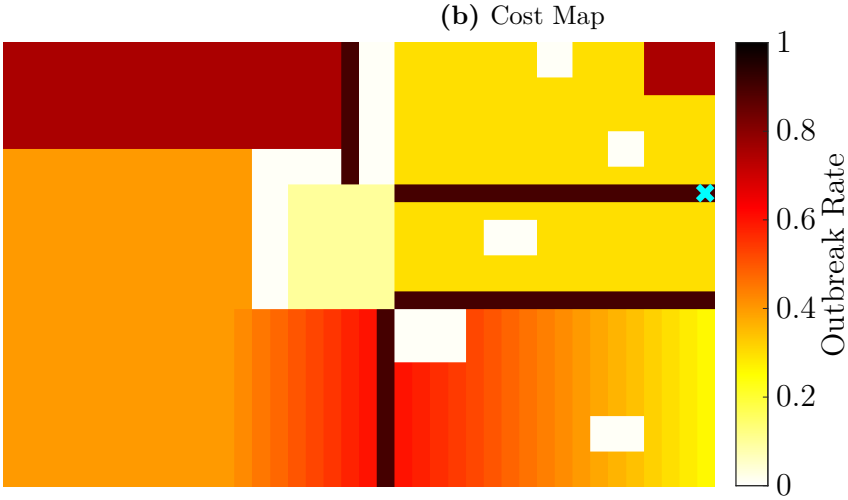

(c) Outbreak Rate

Figure 5.12 – Example 5.3; Fictional landscape with different area types, represented as a grid with $n = 1000$ nodes with its corresponding cost map and outbreak rate. City nodes have a high cost associated with them and the cyan cross indicates the outbreak node for simulations.

We consider resource allocation to reduce the spreading rates β_{ij}, e.g. by digging firelines or controlled burns. We set $w_{ij} = 1$ for all edges (i, j), indicating an equal cost to apply resources to any edge. The cost of the city nodes is taken as $c_i = 1$, whereas $c_i = 0.001$ for all other nodes as illustrated in Figure 5.12b. This could reflect either the higher economic cost of fire reaching a city or the higher risk to human life. The outbreak rate λ_i or outbreak probability $\hat{x}_i(0)$ is depicted in Figure 5.12c, e.g. this could reflect that fires are more likely to start near roads. The discount rate is set to $r = 3.1$.

In this example we consider the simplified optimization framework Problems 5.2 and 5.3. That is, we will not take into account surveillance scheduling, i.e. revisit interval rate τ, nor will we consider resource allocation on the discount rate or outbreak rate.

We compare our proposed objective and resource model with those presented in [132]. Firstly, we compare objectives: our proposed risk model (3.23) and minimizing the spectral abscissa (3.24) as discussed in Section 2.4.1. We do this via Problem 5.2, the budget-constrained resource allocation, using the proposed resource model (5.2a). We take a resource allocation budget of $\Gamma_\beta = 200$ and $\underline{\beta}_{ij} = 1 \times 10^{-8}$ for all edges. The resulting allocations are shown in Figure 5.13, with colored edges indicating resource allocation to reduce β_{ij}, red indicating maximum possible allocation reducing β_{ij} to $\underline{\beta}_{ij}$.

It can be seen in Figure 5.13a that our proposed risk-based objective results in containment lines that protect high cost areas from areas with high risk of spread. In contrast, the spectral abscissa objective (3.24) does not distinguish nodes in terms of cost or likelihood of an outbreak, and containment lines are not obtained (Figure 5.13b).

Note that the same resource allocation maps but with a different colormap can be found in Section B.1. This colormap makes low resource allocation more visible to clearly see the difference in the amount of edges resources are allocated to.

To test the effectiveness of the two approaches, we simulated the stochastic cellular automata (CA) model with a range of resource bounds, with the starting node in-

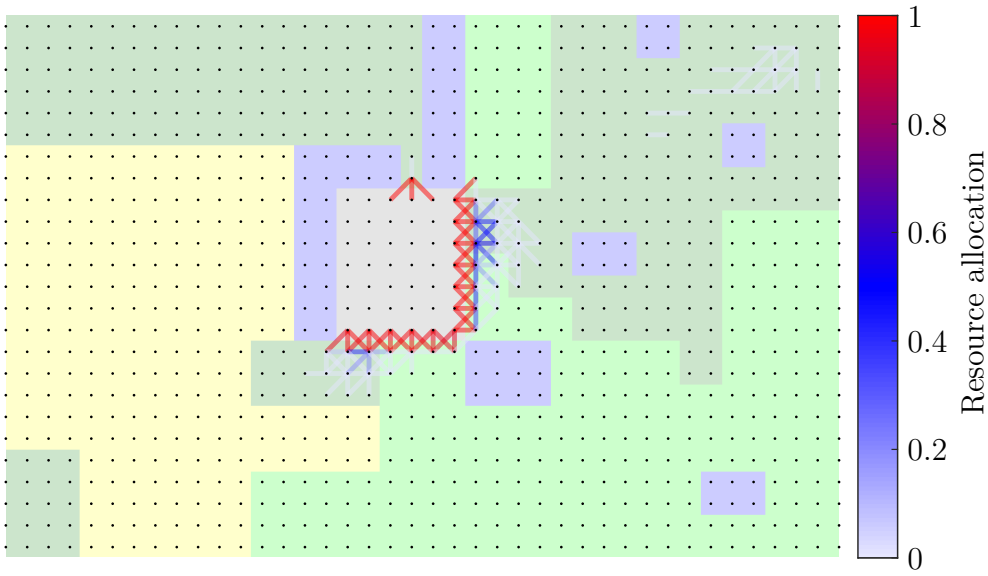

(a) The proposed model: minimize (3.23) subject to constraints on (5.2a). **136** edges have resources allocated.

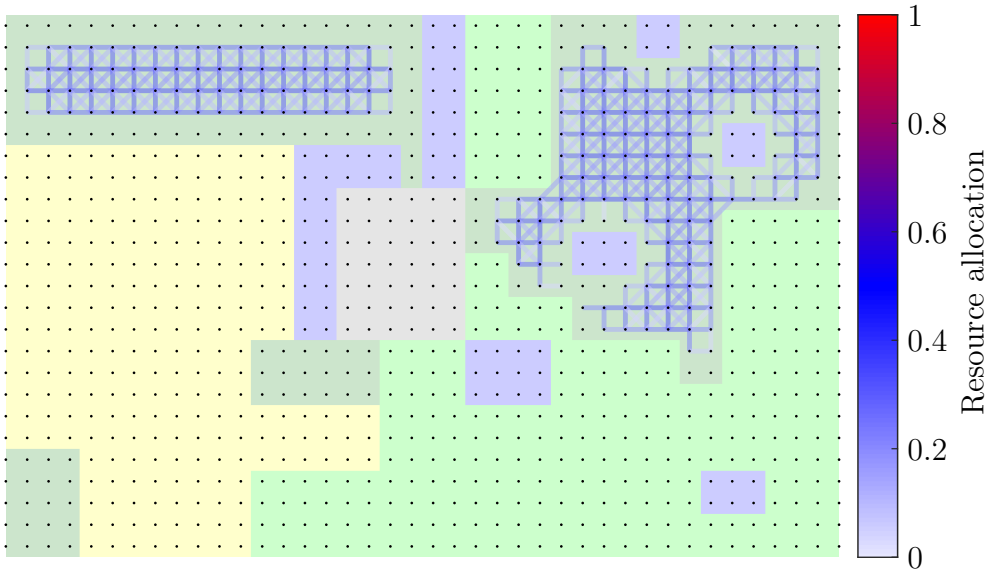

(b) Minimize the spectral abscissa (3.24) subject to constraints on the proposed resource model (5.2a). **611** edges have resources allocated.

Figure 5.13 – Resource allocation for minimizing different risk models for Problem 5.2.

Table 5.3 – Percentage of simulations of stochastic cellular automata model in which the city burns down.

Resource bound Γ_β	0	25	50	100	200
Proposed objective (3.23)	96.10	93.00	81.10	45.50	6.20
Minimizing spectral abscissa (3.24)	96.10	95.00	95.00	94.90	94.70

dicated in Figure 5.12c. Table 5.3 shows the percentage of simulations (over 1000 trials for each scenario) in which the city burns down, defined as $\geq 50\%$ of city nodes burning. It can be seen that with the same resources, the proposed risk model can reduce the impact on the city by nearly 90% whereas the spectral abscissa minimization results in only a slight decrease.

Secondly, we compare resource models via Problem 5.3, i.e. risk-constrained resource minimization. The risk bound that we use is $\gamma = 0.045$, which was the optimal value achieved via Problem 5.2 above, as plotted in Figure 5.13a. Therefore, Figure 5.13a also shows the solution for Problem 5.3 minimizing our proposed resource model (5.2a) subject to the risk constraint $\gamma = 0.045$.

In Figure 5.14 we show the results for minimizing resource model (5.3a) from [132] subject to the maximum risk upperbound $\gamma = 0.045$, and it can be seen that a small investment is made on a large number of nodes, whereas our method finds a much sparser allocation. Out of 3486 total edges, the resource model (5.3a) from [132] allocates resources on 543 edges (Figure 5.14), whereas our proposed method only invests on 136 edges (Figure 5.13a).

To further improve sparsity we solve Problem 5.3 with the reweighted ℓ_1 minimization (5.23) as explained in Section 5.4. The resulting allocation is shown in Figure 5.15. Here, the resource allocation is reduced to only 27 edges while achieving the same risk as the results in Figures 5.13a and 5.14, which allocated to 136 and 543 edges, respectively.

Next, to illustrate the effect of the outbreak rate, we solved Problem 5.2 with $\hat{x}_i(0) = 1$ at the outbreak node and its eight surrounding nodes, and $\hat{x}_i(0) = 0$ for all other

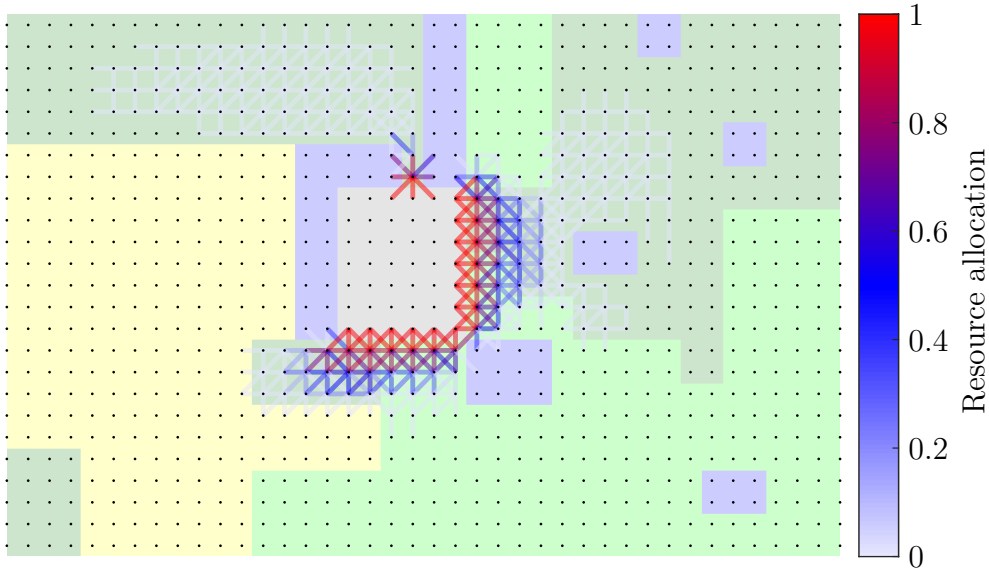

Figure 5.14 – Resource allocation using the resource model from [132] for Problem 5.3: minimize (5.3a) subject to constraints on the proposed risk model (3.23). **543** edges have resources allocated.

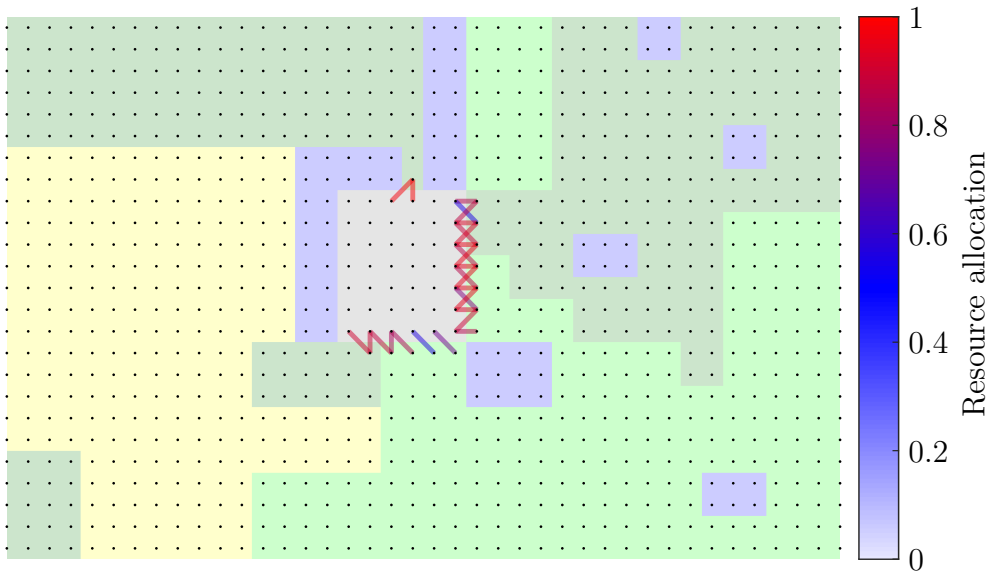

Figure 5.15 – Resource allocation after using reweighted ℓ_1 minimization (5.23) on (5.13a). **27** edges have resources allocated.

nodes, illustrated in Figure 5.16a. This corresponds to precise knowledge of the outbreak location. It can be seen in Figure 5.16b that the outbreak area is aggressively suppressed, while some resources are distributed along the path a fire would take to the city.

It is interesting to contrast Figure 5.13a and Figure 5.16b, the only difference being the outbreak probability $\hat{x}(0)$. If the outbreak location is known precisely (Figure 5.16b) then resources are allocated to suppress the outbreak; if not (Figure 5.13a) then resources are used to protect the high-cost city nodes.

Finally, we look at the effect of the cost map on the resource allocation. If we take a more gradual cost map as displayed in Figure 5.17a, we obtain a resource allocation that is more similar to minimizing the spectral abscissa, i.e. Figure 5.13b, as demonstrated in Figure 5.17b, due to our proposed approach now having to minimize an overall cost over the whole graph. The outbreak rate effect can still be seen, especially on the higher outbreak rate 'road' on the right of the city that is more heavily suppressed. Similarly, the top left and top right corners receive more resources in our method than the spectral abscissa due to the outbreak rate map Figure 5.12c.

Furthermore, we can also model multiple high cost areas in different vegetation instead of one high cost city area, as illustrated in Figure 5.18a. It can be seen in Figure 5.18b that more or less resources are applied to protect these high cost areas depending on the surrounding vegetation and outbreak rate in the area. The high cost eucalyptus patches in the top left and right are most suppressed due to them being surrounded by high spreading edges, the northeasterly wind direction and the higher outbreak rate. Next, the area in the grassland on the bottom still receives some resources due to the medium outbreak and spreading rates, while the high cost area in the desert on the left does not prioritize for resources due to the low spreading rate of the vegetation and lower outbreak rate.

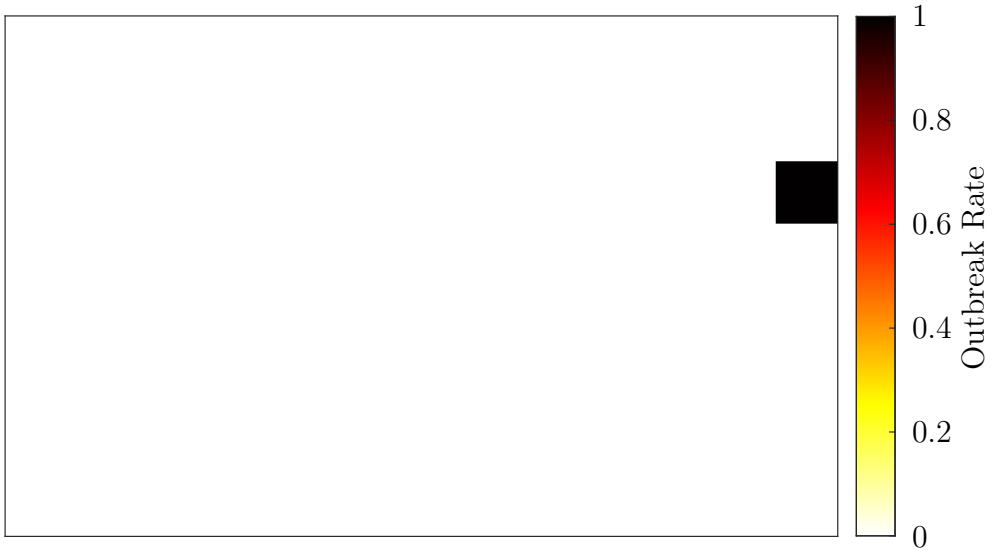

(a) Outbreak Rate

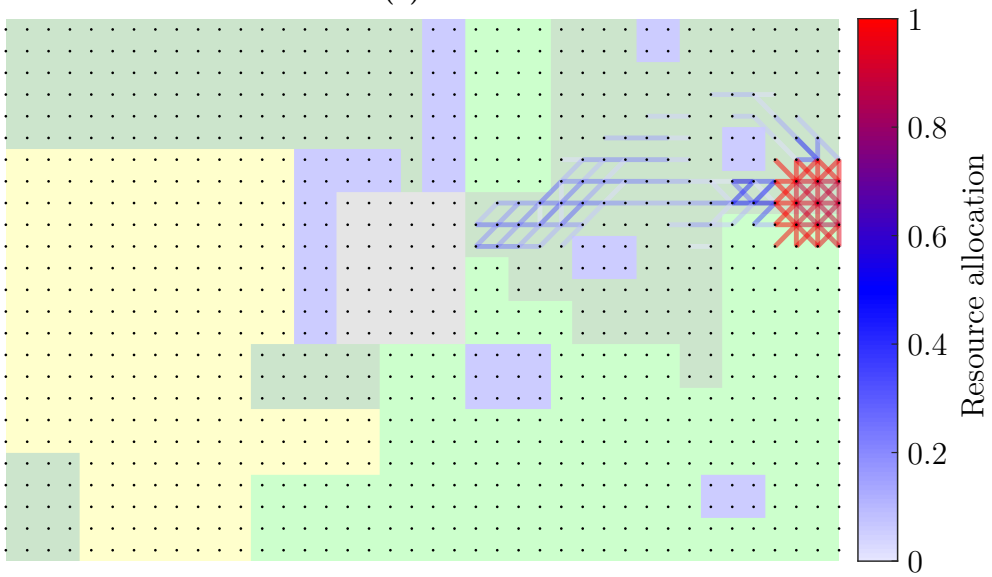

(b) Resource Allocation Map

Figure 5.16 – Resource allocation for the proposed framework with precisely-known initial fire outbreak location. 133 edges have resources allocated.

(a) Cost Map

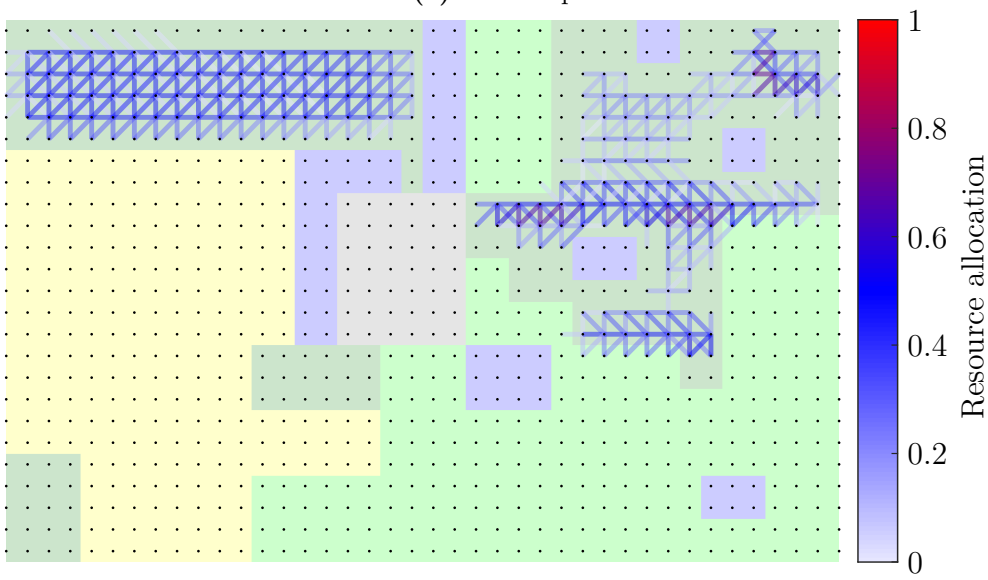

(b) Resource Allocation Map

Figure 5.17 – Resource allocation for the proposed framework with a more gradual cost map. 556 edges have resources allocated.

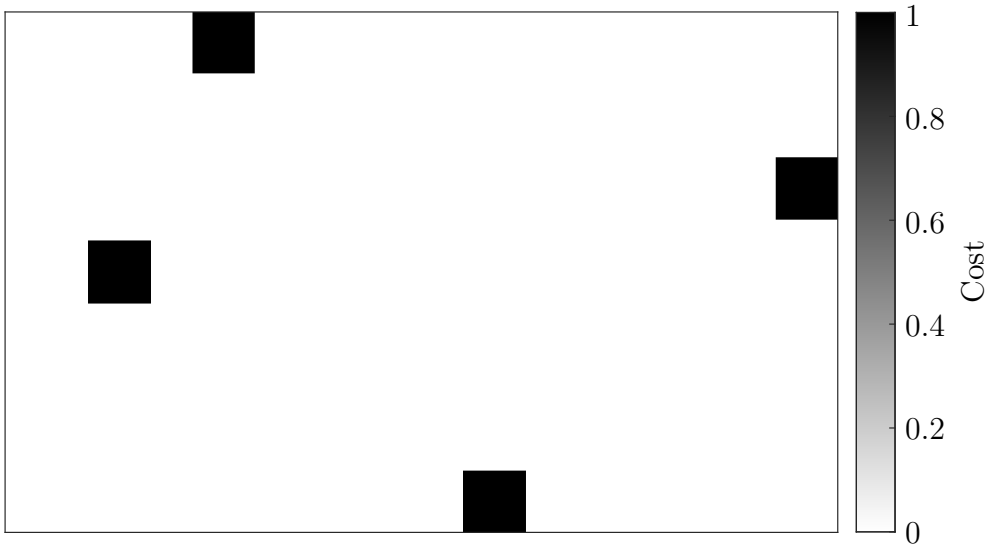

(a) Cost Map

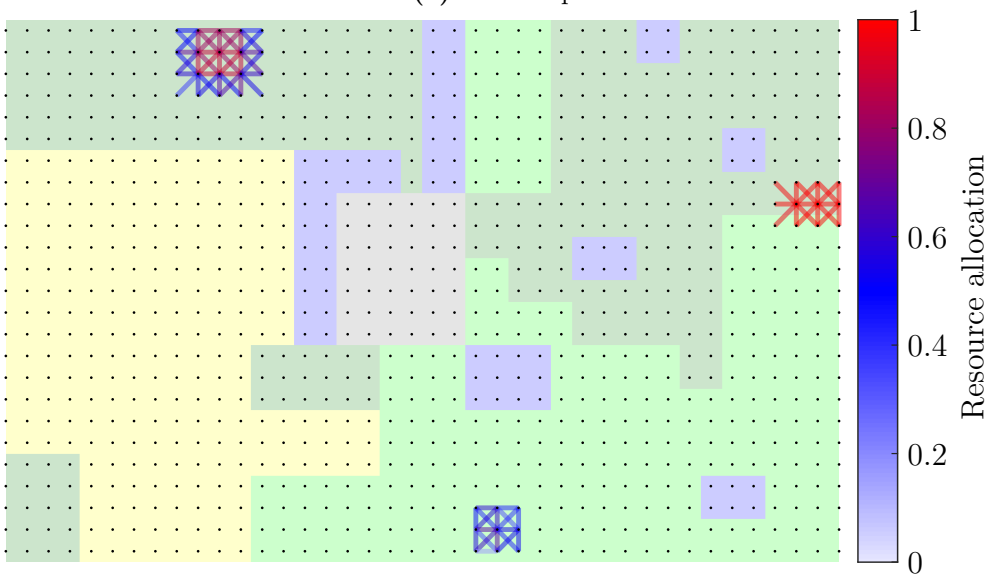

(b) Resource Allocation Map

Figure 5.18 – Resource allocation for the proposed framework with four high cost areas in different vegetation areas. 81 edges have resources allocated.

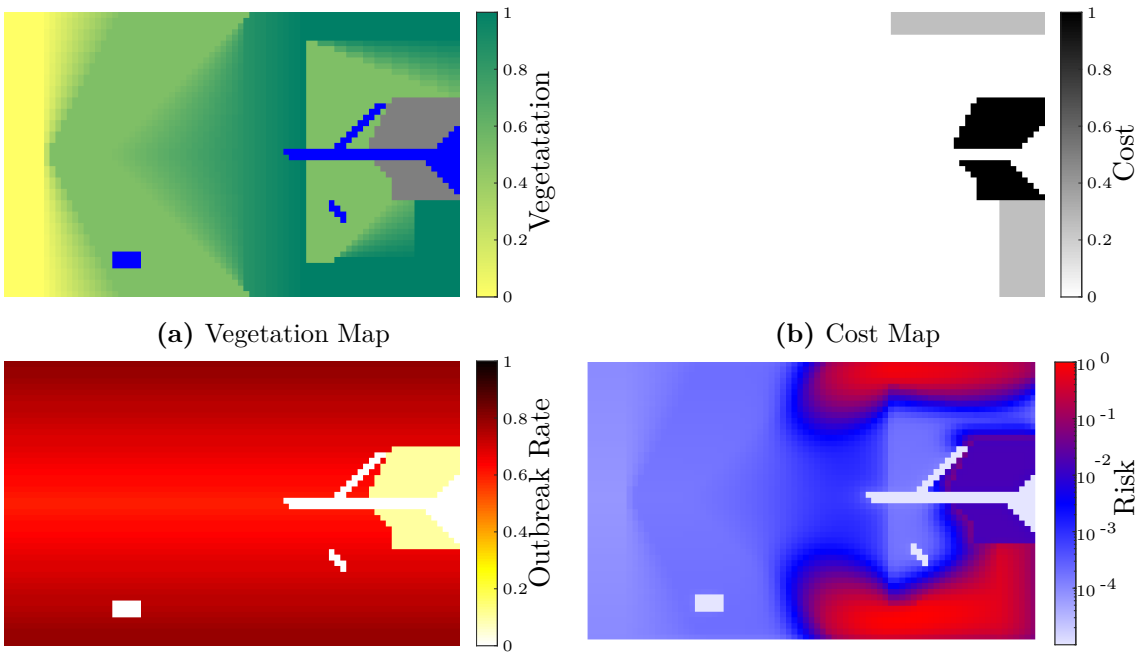

(a) Vegetation Map **(b)** Cost Map

(c) Outbreak Rate **(d)** Risk Map

Figure 5.19 – Example 5.4; Wildfire spreading over a graph with $n = 4000$ nodes representing a simplified landscape with its corresponding cost map, outbreak rate and resulting risk map for a westerly wind of $V = 8$ m/s.

4000 nodes

Finally, we revisit Example 4.2, i.e. the wildfire example of 4000 nodes of Section 4.2.2, here displayed again as Example 5.4 in Figure 5.19, to demonstrate resource allocation in combination with persistent monitoring.

To quickly summarize, this example can be represented as a network graph with $n = 4000$ nodes. The adjacency matrix, i.e. the set of edges $\mathcal{E}$, is set up similar to the previous example. The recovery rate $\delta = 0.5$ for all nodes. For the spreading dynamics $\beta_{veg} = 2 \cdot$Vegetation, where the vegetation value is indicated in Figure 5.19a and $\in [0, 1]$ for respectively minimal and maximal vegetation. For the city $\beta_{veg} = 0.5$ is taken and for the nonburnable water areas $\beta_{veg} = 0$. The cost c_i and outbreak rate λ_i are given in Figure 5.19b and Figure 5.19c, respectively. See Section 4.2.2 for the full details of the parameter setup.

The risk map that we will continue to use in this example from Section 4.2.2 is

illustrated in Figure 5.19d for a westerly wind of $V = 8$ m/s and a discount rate of $r = 4$.

We now consider minimizing the risk of an undetected outbreak by allocating resources and by use of a revisit schedule as proposed in Problem 5.1. Our objective is to minimize the risk (3.22) and we can allocate resources on the spreading rate β, outbreak rate λ and revisit interval τ (5.2). Now taking $\overline{\sigma}_i = \log(8)$, $\Gamma_\beta = 2000, \Gamma_\lambda = 500$ and $\Gamma_\tau = 1500$, we obtain the allocation in Figure 5.20. It can be seen that resources are mainly allocated to high spreading areas that also have higher cost.

If we want to increase sparsity further, we can use the reweighted ℓ_1 minimization as explained in Section 5.4. Increasing the upperbound for σ_i to $\log(16)$, the resulting allocation is visualized in Figure 5.21. The amount of edges with resources allocated is reduced from 1273 to 289 while achieving the same risk bound.

To demonstrate how the proposed optimization framework can connect spreading models to path planning, we give an example of integrating the obtained revisit rate with an algorithm for persistent monitoring similar to Section 4.2.2. We will again take the minimum maximum latency walk from [2] to find the path (see Section 2.3.3 for details) and assume that the UAV is able to monitor a 4x4 square of nodes at the same time.

We use the revisit map given in Figure 5.20c as input, where we take the maximum revisit rate of the 4x4 square of nodes rounded to the nearest integer. The minimum maximum latency walk for persistent monitoring as visualized in Figure 5.22 is obtained. The eight corresponding subwalks of Figure 5.22 can be found in Appendix B and are depicted in Figure B.3.

We compare our proposed resource allocation, as shown in Figure 5.20, with minimizing the spectral abscissa (3.24), depicted in Figure 5.23, taking the same resource allocation budget. It can be seen that the spectral abscissa invests in reducing high spreading rates, but it is unable to take into account the node dependent cost c_i.

Finally, to validate our proposed method, which is based on various bounds and approximations, we simulate the original stochastic model (3.4) a 1000 times and

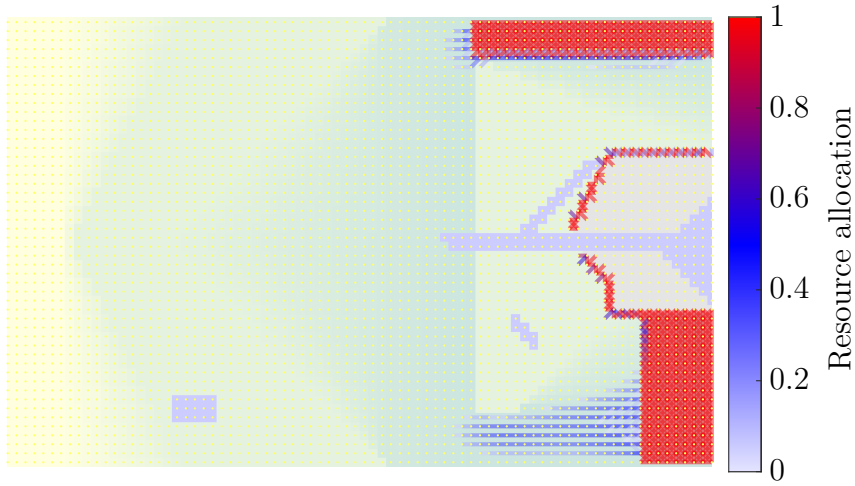

(a) Resource allocation on spreading rate β

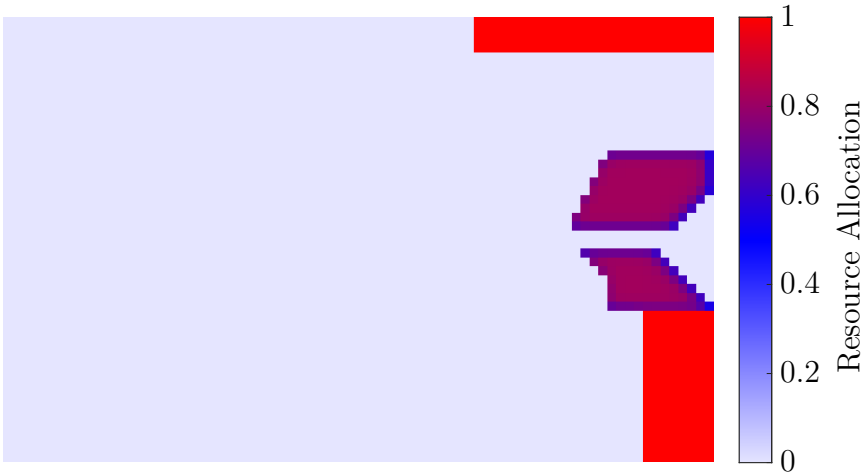

(b) Resource allocation on outbreak rate λ

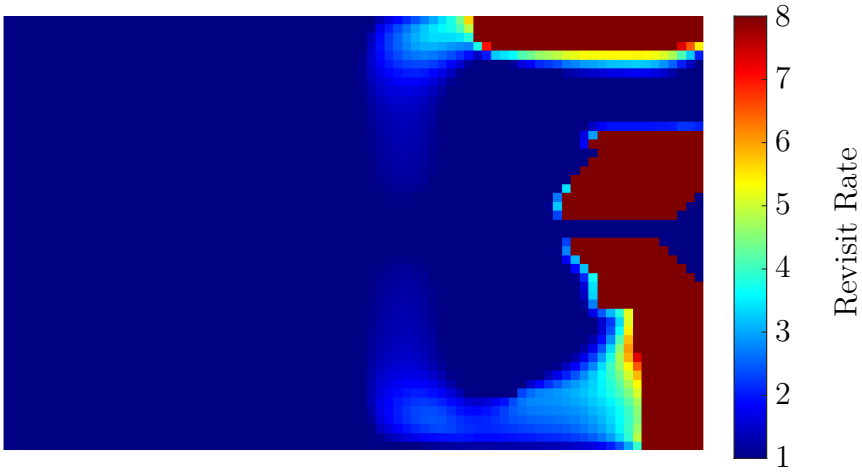

(c) Proposed revisit rate $\frac{1}{\tau}$

Figure 5.20 – Resource allocation for the proposed Problem 5.1: minimize the risk (3.22) with resource budgets $\Gamma_\beta = 2000, \Gamma_\lambda = 500$ and $\Gamma_\tau = 1500$.

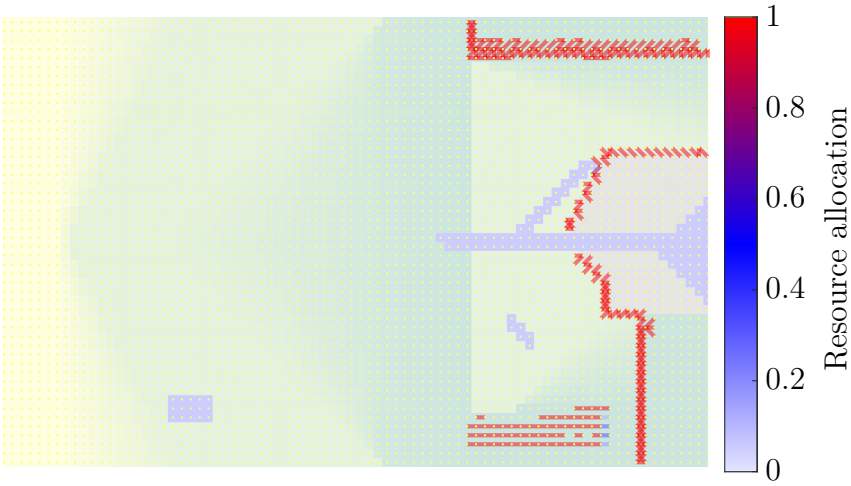

(a) Resource allocation on spreading rate β

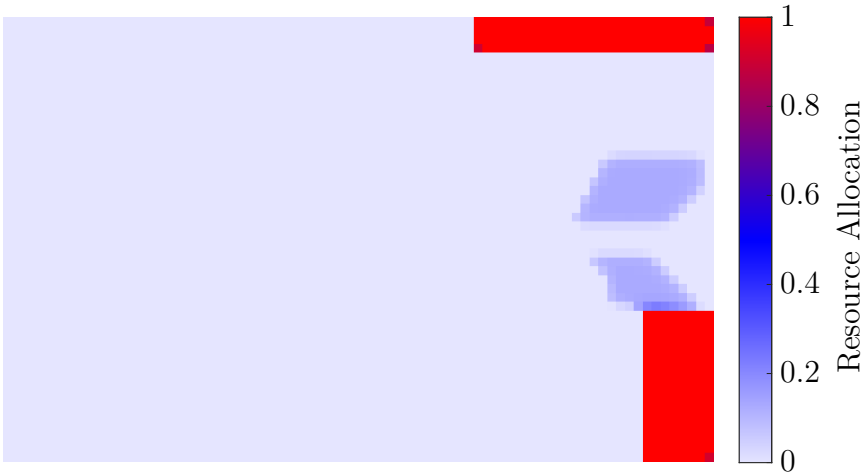

(b) Resource allocation on outbreak rate λ

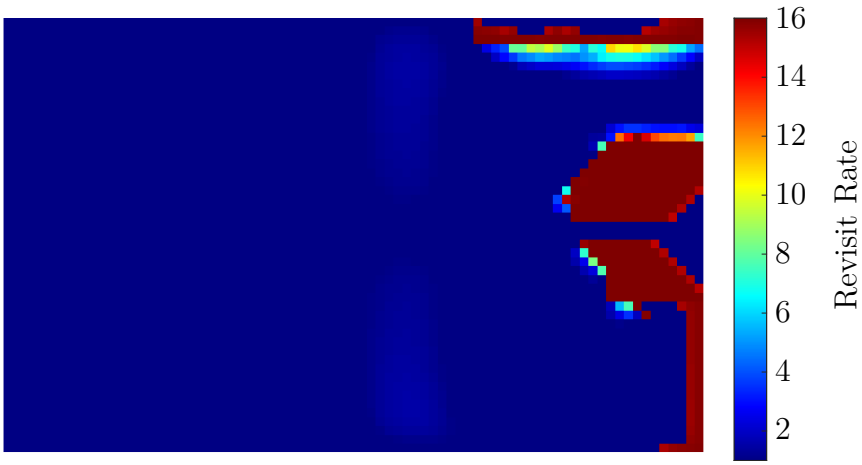

(c) Proposed revisit rate $\frac{1}{\tau}$

Figure 5.21 – Resource allocation after using reweighted ℓ_1 minimization (5.25) on Figure 5.20.

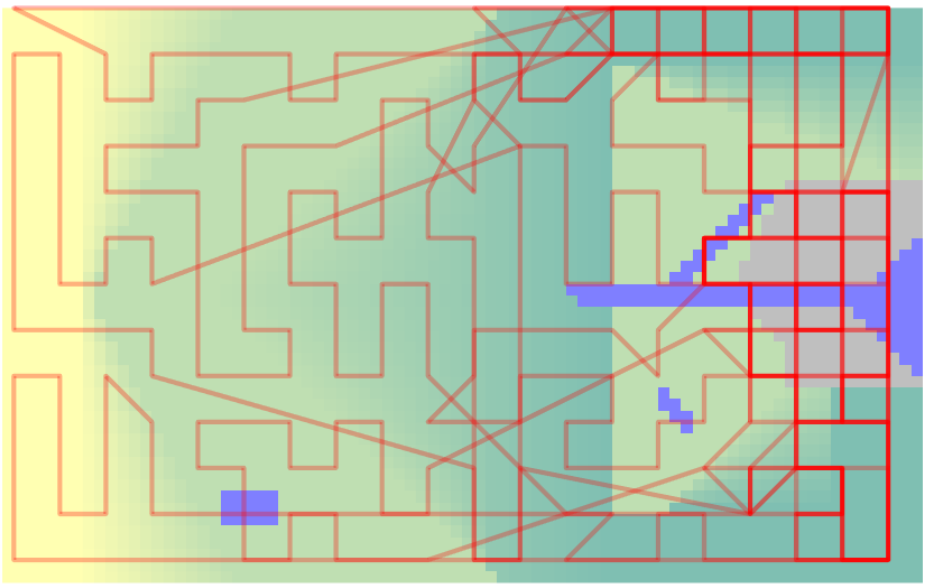

Figure 5.22 – Persistent monitoring path consisting of 8 subwalks based on the revisit map in Figure 5.20c. Darker lines indicate multiple subwalks.

compare our proposed resource allocation, Figure 5.20, to minimizing the spectral abscissa (3.24), Figure 5.23, based on total cost and warning time.

Warning time is taken as time between fire detection and reaching a high cost node (i.e. $c_i \geq 0.25$). Fire detection is obtained by simulating an UAV flying along the path as shown in Figure 5.22 starting at a randomized location, whereas for the comparison model, the path is taken as a standard lawnmower pattern. A positive warning time implies the outbreak is detected before it reaches a high cost node, negative warning time indicates it is detected after. The fire outbreak node is randomly chosen for each run based on the outbreak rate probabilities. We assume that the UAV flies 24 times faster than the fire spreads, based on average fire spread rate [3, 29] and taking an average UAV speed of 20 m/s [119].

In Figure 5.24, we show a scatter plot showing the resulting costs and warning times for the randomized fire outbreak scenarios. It can be seen that the proposed method overall has a higher reduction in cost and a longer warning time for higher cost runs,

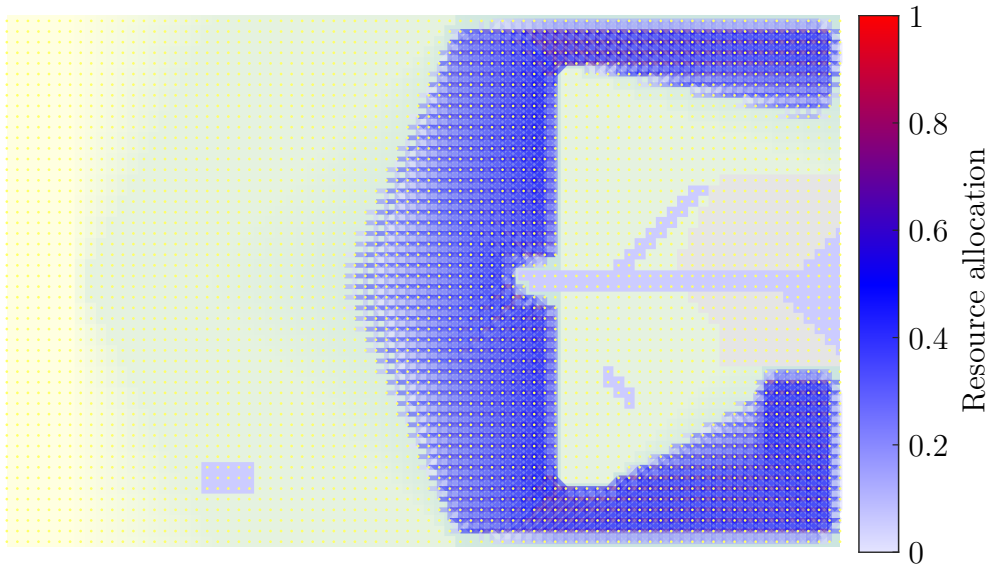

Figure 5.23 – Resource allocation on spreading rate β for minimizing the spectral abscissa (3.24) using the same resource allocation budget as Figure 5.20.

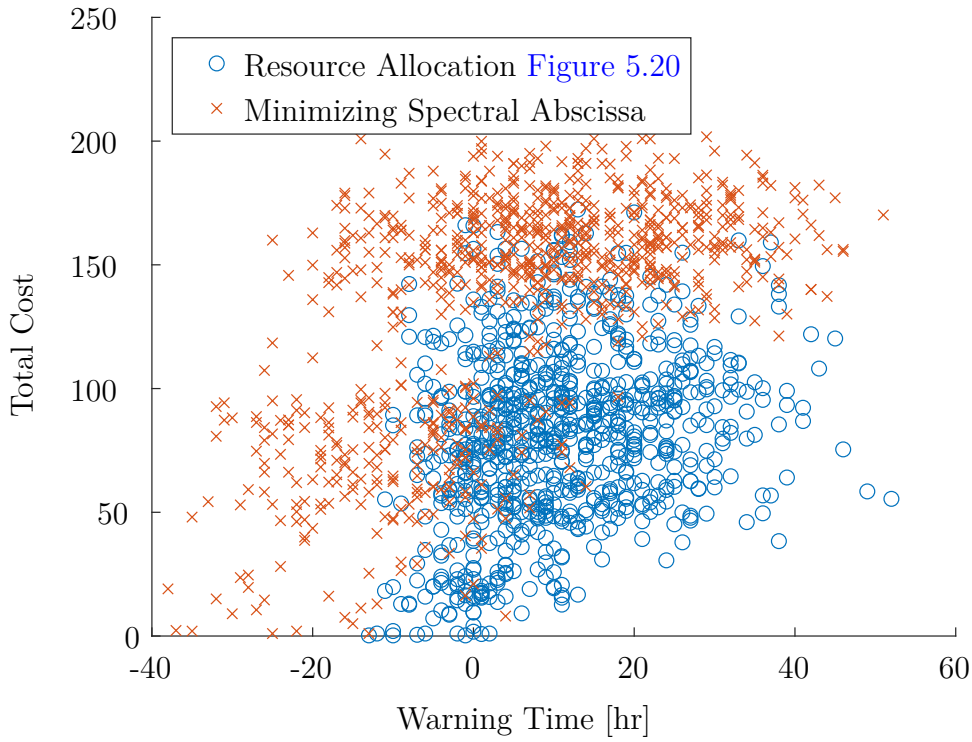

Figure 5.24 – Comparing total cost and warning time of the stochastic model for our proposed resource allocation, Figure 5.20, versus minimizing the spectral abscissa, Figure 5.23.

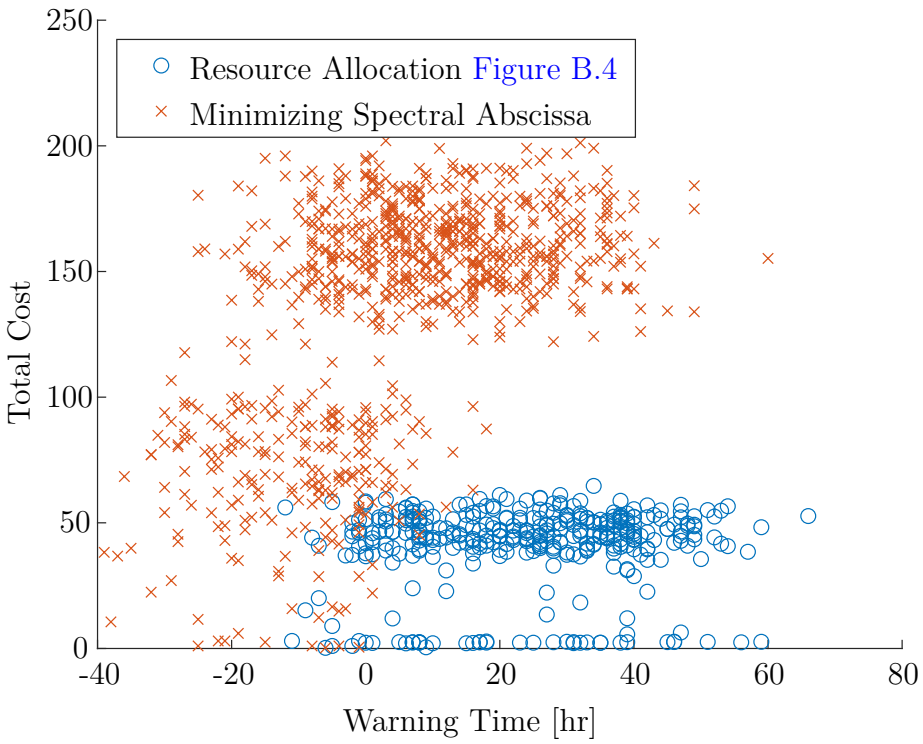

Figure 5.25 – Comparing total cost and warning time of the stochastic model for our proposed resource allocation, Figure B.4, versus minimizing the spectral abscissa, Figure B.5.

compared to the baseline method of minimizing the spectral abscissa and performing a lawnmower surveillance pattern.

Example simulations of runs with the stochastic SIR model for Figure 5.24 can be found in Appendix B, Section B.2, in Figures B.7-B.12.

Besides the discussed proposed resource allocation, different allocation budgets result in more or less suppression of the stochastic fire outbreak. An example is given in Figure 5.25 for $\Gamma_\beta = 1500$, $\Gamma_\lambda = 500$ and $\Gamma_\tau = 1000$. The corresponding resource allocation for both our method as well as minimizing the spectral abscissa with the same budget can be found in Appendix B, Section B.2, in respectively Figure B.4 and Figure B.5.

In this scenario due to the lower revisit rates and budget, i.e. shorter warning times, resources are used for more direct suppression to protect the city. Furthermore, 63.9%

Table 5.4 – Run time for the proposed method in seconds.

	State dimension n	60	240	1000	4000	16000
Figure 5.13a	β allocation time	0.34	0.57	2.15	17.98	53.83
	β & δ allocation time	0.34	0.59	4.17	8.27	48.85
Figure 5.20	β, λ & τ allocation time	0.42	0.70	3.20	11.59	46.16

of runs had no cost at all compared to 14% of the spectral abscissa runs. These runs are due to the corresponding infinite warning time not shown in Figure 5.25. It can be seen that overall the total obtained stochastic cost is significantly lower when again run for a 1000 times compared to Figure 5.24 and compared to minimizing the spectral abscissa with the same resource allocation budget.

5.5.3 Computation and Scalability

In this subsection we examine scalability of the proposed method. We recorded the run time for Example 5.3 for allocation of resources on β alone, as well as on β and δ, for networks of various sizes obtained by downsampling or interpolating the landscape in Figure 5.12a. Similarly, we recorded the run time for β, λ and τ resource allocation of various sizes for Example 5.4 as depicted in Figure 5.19.

The intervention optimization problems were formulated using Julia [11] and solved with MOSEK v9.2 on an Intel i7, 2.6GHz, 8GB RAM. The results are shown in Table 5.4 and Figures 5.26 and 5.27. For the presented examples up to 4000 nodes this is in the order of seconds. Furthermore, the run time grows linearly in the number of nodes, which suggests that the method is scalable to very large networks.

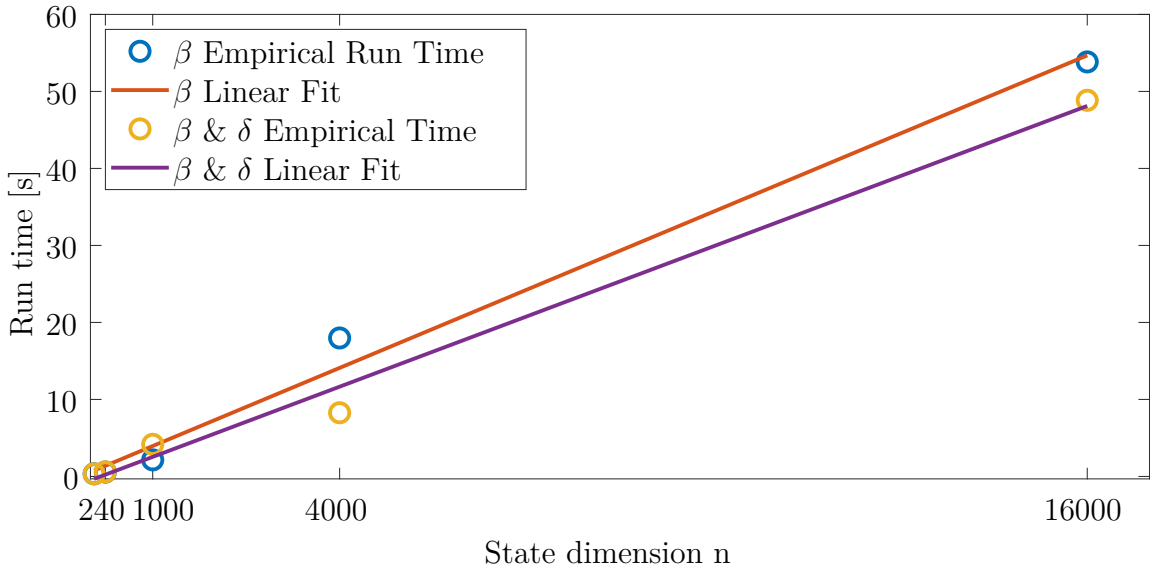

Figure 5.26 – Run time for Example 5.3 for different resource allocations, e.g. see Figure 5.13a for β allocation for $n = 1000$, and different dimensions in seconds. Empirical run time values can be found in Table 5.4.

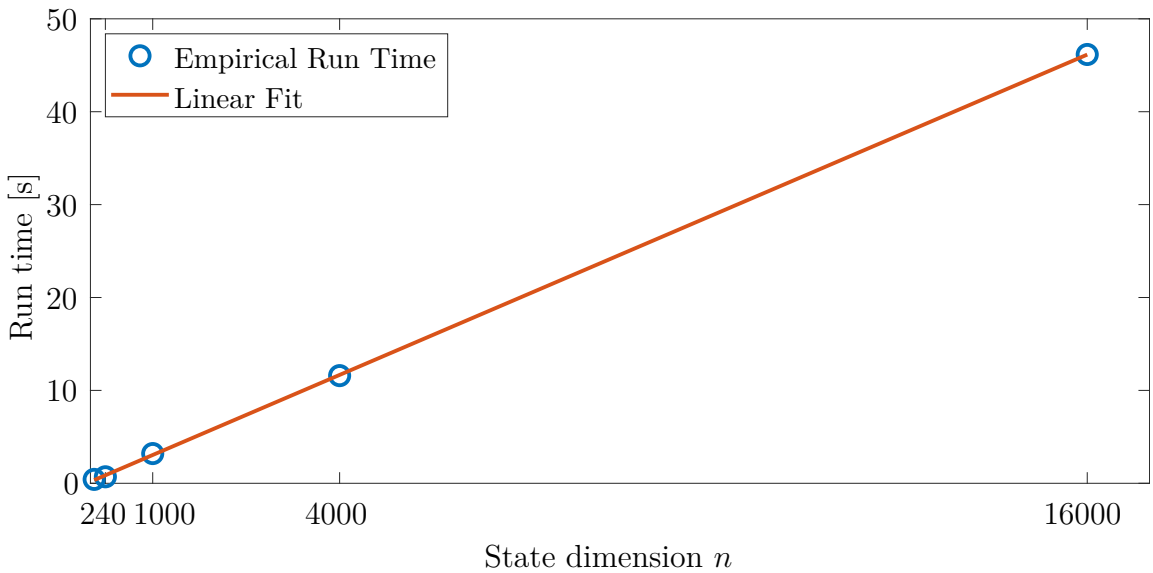

Figure 5.27 – Run time for Example 5.4, β, λ and τ resource allocation depicted in Figure 5.20, in different dimensions in seconds. Empirical run time values can be found in Table 5.4.

5.6 Conclusions

In this chapter we presented a flexible convex optimization framework that minimizes the risk of spreading processes by integrating surveillance schedules and sparse control. We demonstrated how our logarithmic resource models for spreading, recovery and outbreak rate led to sparse resource allocation and discussed how ℓ_1 minimization could be utilized if sparse outcomes are the main goal. By reformulating our constraints and objectives as convex constraints using logarithmic transformation, we obtained a convex optimization program or more specifically an exponential cone program. With multiple examples of spreading processes, i.e. epidemics and wildfires, we conveyed the use and scalability of the presented framework. We found that the proposed model outperforms standard methods such as minimizing the spectral abscissa and that the results obtained with the linear model minimize and bound the risk of the original stochastic process.

Chapter 6

Conclusion

In this thesis we developed a flexible optimization framework to bound and minimize the risk of spreading processes, such as epidemics and wildfires, by use of both surveillance schedules and sparse control. In particular, we focused on the joint optimization of surveillance and intervention, providing targeted, sparse resource allocation and developing scalable algorithms. For wildfires specifically, we also bridged the gap between spreading models and remote sensing.

In this concluding chapter, we provide a summary of the thesis, state the main contributions, address the research objective and discuss open problems and potential directions for future work.

6.1 Summary

Epidemics and wildfires can be thought of as spreading processes in which an initial localized outbreak spreads rapidly to neighboring nodes and throughout a network. The real-world risks associated with such events have stressed the importance and current shortcoming of both being able to quickly map and monitor the spread of infection and being able to get an accurate risk estimate to plan appropriate intervention strategies. When setting up an optimization framework to tackle this problem, four

other aspects have been found to be of importance. First of all, being able to provide targeted risk estimation and minimization for more vulnerable or high cost areas. Second, due to the large network structures, scalability of algorithms and third, sparsity of resource allocation. Finally, for wildfires specifically there is a gap between fire spreading models and persistent monitoring algorithms for remote sensing.

In order to address this problem we defined our **research objective** as *'develop a joint optimization framework for both surveillance and intervention purposes that is 1) based on a risk model with node dependent costs for targeted risk minimization, 2) results in sparse outcomes, 3) is scalable to large network sizes and 4) can be connected to persistent monitoring algorithms for robot path planning'*.

Chapter 2 has presented background literature on modeling spreading processes and discussed different theories and approaches that can be used for surveillance and intervention of them. It was found that spreading models are commonly modeled as Markov processes. The most well-known and documented models are the Susceptible-Infected-Susceptible (SIS) and Susceptible-Infected-Removed (SIR) models, coming from the epidemics literature. Similar for wildfires, cellular automata (CA) models are most suitable, since they have a low computational cost and deal well with heterogeneous data. However, for surveillance and intervention purposes the stochastic model is not directly suitable. It is, therefore, common that stochastic models are approximated as ODE models, which in turn can be approximated by linear models, which are proven to provide an upperbound on expected values and therefore, usually the object of study.

We found that existing methods to indicate influential nodes in a network cannot take into account node dependent cost. Moreover, surveillance scheduling literature is still limited for spreading processes, in particular for epidemics. For wildfires persistent monitoring is more an active area of research, however, limited to either fire perimeter estimation or optimal path planning. For intervention, a suitable approach that results in scalable algorithms includes regulating spreading and recovery rate of the process via convex optimization, in particular geometric programming. However, these approaches do not necessarily provide sparse control for targeted intervention

in large networks. We, therefore, looked into sparsity inducing methods for convex optimization. More specifically, ℓ_1 norm constraints and objectives are known to encourage sparsity. Furthermore, convex optimization problems are preferred, because they can be solved reliably and numerically very efficient.

In Chapter 3 we defined a risk model based on the product of the probability of an undetected outbreak in a given time interval and the impact of that outbreak. That is, risk was defined as the product of the outbreak rate, revisit time interval and impact of the outbreak. We proposed to model the outbreak rate as a Poisson process, where we take the linear upperbound of at least one event occurring within a time interval. Next, we discussed why the linear spreading model is a suitably proxy for studying the underlying stochastic model. Moreover, we defined a cost function, where we found that the cost function associated with the linear model upperbounds the cost function associated with the stochastic model. We used the properties of positive systems to find the linear cost-to-go or node impact vector, which we discussed further by giving examples of a 'priority map' that shows the node impact or cost-to-go for different cost and spreading parameters and we discussed the effect of the discount rate. Finally, we presented our proposed risk model, discussed feasibility in regards to the Hurwitz assumption and mean-field estimation and how it differs from other risk models, such as the spectral abscissa, by taking into account node dependent costs.

With the defined risk model, we formulated the surveillance problem in Chapter 4. In the surveillance problem, the dynamics of the spreading process are fixed and the aim is to identify and bound the future cost of an undetected outbreak spreading from each node. This could be done by finding the largest revisit interval for each node that we can use in surveillance schedules. We analyzed the risk model and results of the surveillance problem by first showing the effect of different parameters and discount rate on the risk map, afterwards we discussed a larger realistic wildfire example and demonstrated how to implement persistent monitoring path planning to bound the risk.

In the next Chapter 5 we extended this problem by including resource allocation for risk minimization. We, finally, arrived at our complete proposed approach of a flexi-

ble convex optimization framework that minimizes the risk of spreading processes by integrating surveillance schedules and sparse control. We first demonstrated how our logarithmic resource models for spreading, recovery and outbreak rate can be understood as a proportional decrease and lead to sparse resource allocation. Later on we discussed how reweighted ℓ_1 minimization could be utilized if sparse outcomes are the primary goal. Next, we formulated our main optimization problem and discussed problems such as 'resource-constrained risk minimization' and 'risk-constrained resource minimization' that fall within this proposed framework. We obtained a convex optimization program, or more specifically exponential cone program, by reformulating our constraints and objectives to convex constraints and objectives by using logarithmic transformations.

With multiple examples of spreading processes we conveyed the use and scalability of the presented optimization framework. We demonstrated how the framework could be used for identifying critical links in different epidemic and wildfire scenarios. Furthermore, we found that the proposed model outperforms previous approaches, such as minimizing the spectral abscissa, by providing more targeted, sparse resource allocation. With a large wildfire example we demonstrated how we could utilize resource allocation and revisit schedules to minimize the risk of an undetected outbreak and incorporated robot path planning methods for surveillance. Finally, we validated that the results obtained with the linear model reduced and bounded the risk of the original stochastic process.

In this final Chapter 6, we will first demonstrate how we addressed our research objective by stating our main contributions in Section 6.1.1. Next, in Section 6.2 open problems and potential directions for future work will be discussed. This includes time dependent intervention, time-varying networks, more realistic propagation models and sensing assumptions, more elaborate UAV path planning scenarios and real-world implementation.

6.1.1 Contributions and Research Objective

Summarized, the goal of this thesis was to bound and minimize the risk of spreading processes such as epidemics and wildfires via surveillance schedules and sparse resource allocation. The main contributions of this thesis that address this objective and the research objective stated at the beginning of this section can be summarized as follows.

We developed a flexible optimization framework that stands out and distinguishes itself from previous literature, because it provides and includes:

- the joint optimization of both surveillance and intervention via sensor scheduling and sparse control **(main research objective)**,
- a risk model based on the product of the probability of an undetected outbreak with its discounted future cost with node dependent weightings **(research objective part 1)**,
- sparsity inducing resource models for spreading, recovery and outbreak rate **(research objective part 2)**,
- scalability due to the use of convex programming, in particular exponential cone programming **(research objective part 3)**, and
- for wildfires specific; we bridged the gap between spreading models and robotic path planning by developing revisit maps based on the risk **(research objective part 4)**.

We demonstrated the use and flexibility of the proposed framework by providing examples and results for epidemic and wildfire scenarios. It is illustrated how the proposed risk model provides targeted risk estimation and minimization and is based on richer information than network topology alone and can deal with regular network structures such as a grid. Furthermore, we showed and discussed how our method leads to sparse resource allocation and achieved scalable algorithms.

6.2 Future Work

The optimization framework for risk minimization of spreading processes presented in this thesis offers a static control solution for time-invariant networks based on the linearized model of the Markov process. Therefore, different areas to extend this research for future work can be established and will be discussed in this section. Potential directions include dynamic control of static networks, i.e. time dependent intervention, control of dynamic networks, i.e. time-varying networks, more realistic propagation models and sensing assumptions beyond the mean-field estimation and Markov model, more elaborate UAV planning scenarios and real-world implementation.

6.2.1 Time Dependent Intervention

A drawback of the current presented joint optimization framework is that is offers a static control or static intervention solution only. That is, the resource allocation and surveillance schedule is determined once based on the current state instead of allocated over time. A more realistic assumption would be to have dynamic control and hence, time dependent intervention.

Dynamic resource allocation for epidemics is studied in [40, 147]. Here network properties are identified to respectively identify limitations on and derive upper and lower bounds for epidemic extinction time. More recently, dynamic programming (DP) [10] and in particular, model predictive control (MPC) has been proposed for time dependent intervention [87, 173, 183].

These approaches, however, do not provide targeted, sparse resource allocation and that is where our proposed risk model and resource model could be integrated.

Model Predictive Control

Model Predictive Control (MPC) is a robust feedback strategy for solving optimal control problems that can deal with a variety of different models. For spreading models, MPC has been proposed for dynamic resource allocation for both deterministic epidemic models [87] and stochastic models [173].

Köhler et al. [88] extend their work in [87] by investigating MPC approaches to optimally control the COVID-19 outbreak in Germany. Here 'resource allocation' is considered social distancing measures and the goal is to minimize the number of fatalities. In [149] nonlinear MPC is applied to an SIS model. Similar to our approach the state matrix or 'contact network' is altered to reduce the spread. Furthermore, critical control bounds are determined to investigate controllability.

In particular, the MPC approach proposed in [87, 88] is very interesting, because a similar spreading model as presented in this thesis is used and our proposed risk model falls within the category of cost functions that work within their framework. However, their current approach does not necessarily lead to sparse and targeted results, hence leaves room for future work. Compared to our current framework, the main difference would be that the parameters are updated per time step and hence, additional constraints on the budget per time step are needed, including updates on the bounds of the parameters. The downside of such an iterative approach, however, is the longer solving time.

6.2.2 Time-varying Networks

A second opportunity for future work is extending our work to time-varying networks. Time-varying networks are often more realistic and appropriate, particularly for spreading processes such as epidemics and social networks, where interactions and hence, the connectivity of the network, change over time. Similarly, it would also be interesting to examine the time-varying nature of the spreading and recovery variables. For wildfires these could capture the changing wind and temperature patterns, and for epidemics the varying spreading and recovery rates as different variants

emerge or new treatments are developed. Time-varying networks are, however, more challenging and complex to analyze [113, 183].

An interesting starting point and example of control of time-varying network is given in [112], where geometric programming techniques are used to find the solution. Hence, this could be extended to include our current framework and proposed risk and resource model. Their proposed approach includes a weighted time-varying adjacency matrix, i.e. the B matrix consisting of spreading rates β_{ij} changes over time, and the optimization is solved for an updated geometric program.

In [120, 121] stability analysis of heterogeneous epidemic processes on time-varying networks is investigated. Conditions for global exponential stability and convergence to the disease-free equilibrium are provided where the Hurwitz assumption of the linearized system can be relaxed due to the time-varying nature of the system. Furthermore, quarantine control by decreasing the value of the connectivity matrix is discussed. Gracy et al. [56] provide a distributed control strategy involving increasing the recovery rate by defining conditions for stability and exponential convergence to the disease-free equilibrium in terms of the joint spectral radius of defined matrices. A different approach is taken in Paré et al. [123], where the authors utilize the reweighted ℓ_1 optimization approach (see Section 5.4) to solve an antidote problem for a multi-competitive virus model.

In general, there appear to be four different ways of dealing with time-varying networks. First of all, time-scale separation, where the assumption is made that the spreading process and the network dynamics evolve on a different time-scale. Second, temporal-switching networks, where a switching network is created based on a sequence of static networks. Third, activity-driven networks, where the network changes are based on 'actions' taken by the nodes and finally, edge-Markovian dynamic graphs, where each edge has a Markov process associated with it. For more in-depth discussion and analysis, we refer to [183].

6.2.3 Different spreading models

In Chapter 3 we use the mean-field estimation to obtain the set of nonlinear equations, which upperbounds the assumed underlying Markov process. Based on the linearized version of these equations we obtained the presented convex optimization framework. A more accurate model would be to use the stochastic model directly instead of the deterministic approximation. This would result in more accurate control. There is, however, no guarantee that a similar easy to solve convex optimization can be obtained by using the stochastic model. Similarly, this will most likely result in a reduction in scalability and increase in computational cost.

Furthermore, we model spreading processes similar to most existing literature [113, 183] assuming an underlying stochastic Markov process in which both transmission and recovery time, i.e. time it takes for a node to respectively become infected or recover, follow exponential trajectories. However, empirical studies have shown that in many real scenarios, this distribution is not necessarily exponential [116, 183] and the non-Markovianity of the spreading system may have a large impact on the actual real-life spread [45, 156].

A step towards a proposed approach that does not rely on the mean-field approximation is given in [116]. Here the lower bound on the exponential decay rate to the infection-free equilibrium is found without relying on the mean-field approximation. However, as highlighted and emphasized in [45, 156], there is still a lot to be explored and established and this could be an important area of future research. There will, however, always be a trade-off between accuracy of the model and complexity and computation time.

Another option that would be interesting to look at are stochastic agent based models, which provide a different approach to modeling the individual connections and interactions compared to deterministic network models.

Agent based models rely on data involving human behavior and individual interaction, which can make them very accurate depending on data availability, but, therefore, also very complex to analyze and use [13]. Therefore, because both agent based and

deterministic models have their advantages and disadvantages, a hybrid of them has been proposed in [1, 13] and might be an interesting direction for future work.

6.2.4 Parameter estimation and sensing assumptions

In Chapters 4 and 5 we considered and explored the surveillance problem and intervention problem. A third problem that is often considered is parameter estimation. Currently, full knowledge of the outbreak likelihood and parameters of the system is required and assumed, which is often unrealistic and therefore, a disadvantage of our current approach.

A more realistic assumption is that parameters are not necessarily exactly known nor perfectly measurable. An interesting extension of our current work would, therefore, be to consider a model that can deal with this uncertainty in parameters.

An example of how to deal with these challenges for monitoring epidemics is given in [169]. Here, the spreading model is extended by not only including a model of measurement, i.e. testing, but more importantly including the problems and possibilities of false positives and negatives.

The work by Köhler et al. [88] already highlighted earlier for their MPC approach, uses interval arithmetic that can also take unknown and uncertain parameters into account if exact measurements of the state are not available.

Similarly, for wildfires, imperfect observations could also be integrated with path planning for persistent monitoring.

Finally, it would be interesting to look into the dual problem of state estimation and sparse sensor placement. Instead of resource allocation, we could optimize and obtain observer gains or sparse sensor locations to estimate the state of the system. That is, minimize the state estimation error to obtain the minimum number of sensors required or the observer gains.

6.2.5 UAV path planning

One of our thesis objectives was to bridge the gap between fire propagation models and UAV path planning algorithms for remote sensing. In this thesis, we presented a solution using the algorithm from [2]. However, path planning for remote sensing is well advanced (e.g. [129, 152, 179]). Therefore, many more extensions can be made, such as multi-UAV approaches or implementing path planning algorithms, such as the orienteering problem (OP), that make a trade-off between which nodes to visit instead of visiting all nodes in different cycles.

Multi-UAV path planning

Wildfires often occur on very large areas and networks, therefore, it makes sense that the area would be surveilled with multiple UAVs. To define the multi-UAV path planning approach, the most simple approach would be to split the area using weighted Voronoi subspaces based on the revisit rate [6, 43].

Another way to approach the problem of dividing the area is to consider it as a p-median problem [106]. The p-median problem is defined as optimally placing p facilities to minimize the demand weighted average distance between demand nodes and facilities. Instead of facilities we would allocate UAVs and demand can be interpreted as the revisit rate required to bound the risk.

However, many more approaches exist and a complete survey of current state-of-the-art and challenges can be found in [111].

Path planning trade-off algorithms

In Chapters 4 and 5 we demonstrated connecting fire propagation models to path planning models for remote sensing by giving an example of a persistent monitoring algorithm in which all nodes have to be monitored given a certain schedule. However, if time is limited, trade-off path planning algorithms might be more relevant.

An example of a routing problem in which a trade-off is made on which nodes to visit is the orienteering problem (OP). Here, the goal is to find a path that visits a subset of nodes that maximizes the total collected sum, where each node has a weight associated with it [59]. This weight could be the revisit rate or risk.

Fuel and turn limitations can also be considered, such as in the DOP discussed in [129], where the proposed solution is based on the variable neighborhood search. Another common nonlinear extension to the OP is called the correlated orienteering problem [179].

It should be noted that in the case of the OP the risk map could also be taken directly as input when no additional time or resources can be allocated to monitoring the nodes.

6.2.6 Real-world Implementation

The work presented in this thesis is, foremost, theoretical in nature and not meant as an experimental set up that can directly be applied to the real-world. However, for future work it would be interesting to look into and go towards real-world implementation.

For both wildfires and epidemics, the underlying models are quite well evaluated and the spreading parameters based and evaluated on real-world data [3, 24, 28, 80, 81, 133]. The next step to go towards real-world implementation would be to tune and evaluate the cost and resource parameters to get an idea of how the different resources and measures such as waterbombing, lockdowns and vaccination affect the spreading and recovery rates.

For wildfires, Mutthulakshmi et al. [110] look into the effect of fire containment lines on the spreading rate, both in regards to constructed physical fire lines and temporary fire lines such as waterbombing. In [27] on the other hand, the effect of fuel treatment methods, such as thinning and backburning, is investigated.

For epidemics, each disease will be different, hence different measurements might

have to be taken with different results. For example, outbreak control for SARS is investigated in [24]. For COVID-19 examples of models for the efficiency of facemasks and lockdowns are given in [158] and for vaccination in [134]. Unfortunately, due to the inherent different nature of different types of diseases, new or updated models for each new disease and vaccine will have to developed as new outbreaks or diseases emerge to obtain the most accurate predictions for real-world implementation.

How to model and implement surveillance in real-world scenarios is quite different in regards to wildfires and epidemics. For wildfires, surveillance is quite straightforward in regards to robotic path planning, with different approaches being discussed in the previous Section 6.2.5. It is also easier to monitor or 'test' large areas of the network. Whereas for epidemics on the other hand, it can be more restrictive what or whom can be tested and how to incorporate and interpret the results. Furthermore, false negatives and positives depend on the testing abilities available, which will vary depending on the type of disease and epidemic, where for wildfires they will depend on sensors on e.g. the UAV.

Similarly, for wildfires the area network and structure is very well-known, whereas for epidemics the network is a lot harder to map and changing social and contact networks pose another modeling challenge. Finally, resources in regards to fire management are often easier to control and implement than measures such as vaccination, which are a socio-political issue.

6.3 Conclusion

This final chapter concluded this thesis on 'Risk Minimization for Spreading Processes over Networks via Surveillance Scheduling and Sparse Control'. A summary of the thesis and main contributions was provided and suggestions for directions of future work were established and discussed. These include extending the proposed work to dynamic intervention and time-varying networks. In particular model predictive control is suitable for extending the current proposed framework to time dependent intervention and time-varying networks. Next, we looked into models that go beyond

the mean-field approximation such as stochastic agent based models. Moreover, we discussed including constraints or functions to the framework to include unknown state parameters and more realistic sensing assumptions. Furthermore, the connection to UAV path planning can be extended by implementing multi-UAV approaches or path planning trade-off algorithms such as the Dubins orienteering problem. Finally, we discussed real-world implementation challenges of the proposed optimization framework for both wildfires and epidemics.

List of References

[1] Ajelli, M., Gonçalves, B., Balcan, D., Colizza, V., Hu, H., Ramasco, J. J., Merler, S., and Vespignani, A. Comparing large-scale computational approaches to epidemic modeling: agent-based versus structured metapopulation models. *BMC Infectious Diseases*, 10(1):1–13, 2010.

[2] Alamdari, S., Fata, E., and Smith, S. L. Persistent monitoring in discrete environments: Minimizing the maximum weighted latency between observations. *The International Journal of Robotics Research*, 33(1):138–154, 2014.

[3] Alexandridis, A., Vakalis, D., Siettos, C. I., and Bafas, G. V. A cellular automata model for forest fire spread prediction: The case of the wildfire that swept through Spetses Island in 1990. *Applied Mathematics and Computation*, 204(1):191–201, 2008.

[4] Andersen, H.-E., McGaughey, R. J., and Reutebuch, S. E. Estimating forest canopy fuel parameters using LIDAR data. *Remote Sensing of Environment*, 94(4):441–449, feb 2005.

[5] Anderson, D. H., Catchpole, E. A., De Mestre, N. J., and Parkes, T. Modelling the spread of grass fires. *The ANZIAM Journal*, 23(4):451–466, 1982.

[6] Aurenhammer, F. and Edelsbrunner, H. An optimal algorithm for constructing the weighted voronoi diagram in the plane. *Pattern Recognition*, 17(2):251–257, 1984.

[7] Bailey, N. T. J. *The mathematical theory of epidemics*. Charles Griffin, London, 1957.

[8] Berman, A. and Plemmons, R. J. *Nonnegative matrices in the mathematical sciences*, volume 9. SIAM, 1994.

[9] Bertsekas, D. P. *Convex optimization theory*. Athena Scientific, Belmont, Massachusetts, 2009.

[10] Bertsekas, D. P. et al. *Dynamic programming and optimal control: Vol. 1*. Athena Scientific, Belmont, Massachusetts, 2000.

[11] Bezanson, J., Edelman, A., Karpinski, S., and Shah, V. B. Julia: A fresh approach to numerical computing. *SIAM Review*, 59(1):65–98, 2017.

[12] Bloem, M., Alpcan, T., and Başar, T. Optimal and robust epidemic response for multiple networks. *Control Engineering Practice*, 17(5):525–533, 2009.

[13] Bobashev, G. V., Goedecke, D. M., Yu, F., and Epstein, J. M. A hybrid epidemic model: combining the advantages of agent-based and equation-based approaches. In *Proceedings of the 2007 Winter Simulation Conference*, pages 1532–1537. IEEE, 2007.

[14] Boyd, S. and Vandenberghe, L. *Convex optimization*. Cambridge university press, 2004.

[15] Boyd, S., Kim, S. J., Vandenberghe, L., and Hassibi, A. A tutorial on geometric programming. *Optimization and Engineering*, 8(1):67–127, 2007.

[16] Briat, C. Robust stability and stabilization of uncertain linear positive systems via integral linear constraints: L_1-gain and L_∞-gain characterization. *International Journal of Robust and Nonlinear Control*, 23(17):1932–1954, 2013.

[17] Bullo, F., Frazzoli, E., Pavone, M., Savla, K., and Smith, S. L. Dynamic vehicle routing for robotic systems. *Proceedings of the IEEE*, 99(9):1482 – 1504, 2011.

[18] Burrows, N. Lessons and Insights From Significant Bushfires in Australia and Overseas. Technical Report May, Bushfire and Natural Hazards CRC, 2019.

[19] Candès, E. J., Romberg, J., and Tao, T. Robust uncertainty principles: Exact signal reconstruction from highly incomplete frequency information. *IEEE Transactions on Information Theory*, 52(2):489–509, 2006.

[20] Candès, E. J., Wakin, M. B., and Boyd, S. P. Enhancing sparsity by reweighted ℓ_1 minimization. *Journal of Fourier Analysis and Applications*, 14 (5-6):877–905, 2008.

[21] Chandrasekaran, V. and Shah, P. Relative entropy optimization and its applications. *Mathematical Programming Series A*, 161:1–32, 2016.

[22] Chen, F. H. A susceptible-infected epidemic model with voluntary vaccinations. *Journal of Mathematical Biology*, 53(2):253–272, 2006.

[23] Choset, H. and Pignon, P. Coverage path planning: The boustrophedon cellular decomposition. In Zelinsky, A., editor, *Field and Service Robotics*, pages 203–209. Springer, London, 1998.

[24] Chowell, G., Castillo-Chavez, C., Fenimore, P. W., Kribs-Zaleta, C. M., Arriola, L., and Hyman, J. M. Model parameters and outbreak control for SARS. *Emerging Infectious Diseases*, 10(7):1258, 2004.

[25] Chung, F., Horn, P., and Tsiatas, A. Distributing antidote using pagerank vectors. *Internet Mathematics*, 6(2):237–254, 2009.

[26] Chuvieco, E. and Congalton, R. G. Application of remote sensing and geographic information systems to forest fire hazard mapping. *Remote Sensing of Environment*, 29(2):147–159, 1989.

[27] Cochrane, M. A., Moran, C. J., Wimberly, M. C., Baer, A. D., Finney, M. A., Beckendorf, K. L., Eidenshink, J., and Zhu, Z. Estimation of wildfire size and risk changes due to fuels treatments. *International Journal of Wildland Fire*, 21(4):357–367, 2012.

[28] Colizza, V., Barrat, A., Barthélemy, M., and Vespignani, A. Predictability and epidemic pathways in global outbreaks of infectious diseases: the SARS case study. *BMC Medicine*, 5(1):1–13, 2007.

[29] Cruz, M. G. and Alexander, M. E. The 10% wind speed rule of thumb for estimating a wildfire's forward rate of spread in forests and shrublands. *Annals of Forest Science*, 76(2):1–11, 2019.

[30] Dahl, J. and Andersen, E. D. A primal-dual interior-point algorithm for nonsymmetric exponential-cone optimization. *Mathematical Programming*, 2021.

[31] Dangerfield, C. E., Vyska, M., and Gilligan, C. A. Resource allocation for epidemic control across multiple sub-populations. *Bulletin of Mathematical Biology*, 81(6):1731–1759, 2019.

[32] Dantzig, G. B. and Thapa, M. N. *Linear programming 1: introduction*. Springer, 1997.

[33] Davies, A. Record Covid cases in NSW overshadow other statistics which reveal the outbreak will inevitably get worse. http://www.theguardian.com/world/2021/aug/18/record-covid-cases-in-nsw-overshadowed-other-statistics-which-reveal-the-outbreak-will-inevitably-get-worse. 2021. Accessed: 18-08-2021.

[34] Dhingra, N. K., Colombino, M., and Jovanović, M. Structured decentralized control of positive systems with applications to combination drug therapy and leader selection in directed networks. *IEEE Transactions on Control of Network Systems*, 6(1):352–362, 2019.

[35] Di Giamberardino, P. and Iacoviello, D. Optimal control of SIR epidemic model with state dependent switching cost index. *Biomedical Signal Processing and Control*, 31:377–380, 2017.

[36] Di Giamberardino, P. and Iacoviello, D. Optimal resource allocation to reduce an epidemic spread and its complication. *Information*, 10(6):213, 2019.

[37] Dinh, Q. T. and Diehl, M. Local convergence of sequential convex programming for nonconvex optimization. In Moritz, D., Glineur, F., Jarlebring, E., and Michiels, W., editors, *Recent Advances in Optimization and its Applications in Engineering*, pages 93–102. Springer, Berlin, Heidelberg, 2010.

[38] Dirr, G., Ito, H., Rantzer, A., and Rüffer, B. S. Separable lyapunov functions for monotone systems: Constructions and limitations. *Discrete & Continuous Dynamical Systems-B*, 20(8):2497, 2015.

[39] Donoho, D. L. Compressed sensing. *IEEE Transactions on Information Theory*, 52(4):1289–1306, 2006.

[40] Drakopoulos, K., Ozdaglar, A., and Tsitsiklis, J. N. When is a network epidemic hard to eliminate? *Mathematics of Operations Research*, 42(1):1–14, 2017.

[41] Dutta, R., Das, A., and Aryal, J. Big data integration shows australian bush-fire frequency is increasing significantly. *Royal Society Open Science*, 3 (2):150241, 2016.

[42] Enns, E. A., Mounzer, J. J., and Brandeau, M. L. Optimal link removal for epidemic mitigation: A two-way partitioning approach. *Mathematical Biosciences*, 235(2):138–147, 2012.

[43] Erwig, M. The graph voronoi diagram with applications. *Networks: An International Journal*, 36(3):156–163, 2000.

[44] Eshghi, S., Khouzani, M. H. R., Sarkar, S., and Venkatesh, S. S. Optimal patching in clustered epidemics of malware. *IEEE Transactions Network*, 24 (1):283–298, 2015.

[45] Feng, M., Cai, S.-M., Tang, M., and Lai, Y.-C. Equivalence and its invalidation between non-Markovian and Markovian spreading dynamics on complex networks. *Nature Communications*, 10(1):1–10, 2019.

[46] Fiedler, M. and Ptak, V. On matrices with non-positive off-diagonal elements and positive principal minors. *Czechoslovak Mathematical Journal*, 12(3): 382–400, 1962.

[47] Finney, M. A. FARSITE, Fire Area Simulator–model development and evaluation. Research Paper RMRS-RP-4, Ogden, UT: US Department of Agriculture, Forest Service, Rocky Mountain Research Station, 1998.

[48] Flood, M. M. The traveling-salesman problem. *Operations Research*, 4(1): 61–75, 1956.

[49] Forster, G. A. and Gilligan, C. A. Optimizing the control of disease infestations at the landscape scale. *Proceedings of the National Academy of Sciences*, 104(12):4984–4989, 2007.

[50] Freeman, L. C. Centrality in social networks conceptual clarification. *Social Networks*, 1(3):215–239, 1978.

[51] Ganesh, A., Massoulié, L., and Towsley, D. The effect of network topology on the spread of epidemics. In *Proceedings of the 24th Annual Joint Conference of the IEEE Computer and Communications Societies*, volume 2, pages 1455–1466. IEEE, 2005.

[52] Gasmi, A., Noor, S., Tippairote, T., Dadar, M., Menzel, A., and Bjørklund, G. Individual risk management strategy and potential therapeutic options for the COVID-19 pandemic. *Clinical Immunology*, 215:108409, 2020.

[53] Ghorbanzadeh, O., Blaschke, T., Gholamnia, K., and Aryal, J. Forest Fire Susceptibility and Risk Mapping Using Social/Infrastructural Vulnerability and Environmental Variables. *Fire*, 2(3):50, 2019.

[54] Gillen, C. P., Matsypura, D., and Prokopyev, O. A. Operations research techniques in wildfire fuel management. In Butenko, S., Pardalos, P. M., and Shylo, V., editors, *Optimization Methods and Applications. Springer Optimization and Its Applications*, volume 130, pages 119–135. Springer, Cham, 2017.

[55] Glineur, F. An extended conic formulation for geometric optimization. *Foundations of Computing and Decision Sciences*, 25(3):161–174, 2000.

[56] Gracy, S., Paré, P. E., Sandberg, H., and Johansson, K. H. Analysis and distributed control of periodic epidemic processes. *IEEE Transactions on Control of Network Systems*, 8(1):123–134, 2020.

[57] Graml, R. and Wigley, G. Bushfire hotspot detection through uninhabited aerial vehicles and reconfigurable computing. In *Proceedings of the 2008 IEEE Aerospace Conference*, pages 1–13. IEEE, 2008.

[58] Griffith, J. D., Kochenderfer, M. J., Moss, R. J., Mišić, V. V., Gupta, V., and Bertsimas, D. Automated Dynamic Resource Allocation for Wildfire Suppression. *Lincoln Laboratory Journal*, 22(2):38–59, 2017.

[59] Gunawan, A., Lau, H. C., and Vansteenwegen, P. Orienteering problem: A survey of recent variants, solution approaches and applications. *European Journal of Operational Research*, 255(2):315–332, 2016.

[60] Gutin, G. and Punnen, A. P. *The traveling salesman problem and its variations*, volume 12. Springer Science & Business Media, 2006.

[61] Ha, J. S. and Choi, H. L. On periodic optimal solutions of persistent sensor planning for continuous-time linear systems. *Automatica*, 99:138–148, 2019.

[62] Hadjichrysanthou, C. and Sharkey, K. J. Epidemic control analysis: Designing targeted intervention strategies against epidemics propagated on contact networks. *Journal of Theoretical Biology*, 365:84–95, 2015.

[63] Han, S., Preciado, V. M., Nowzari, C., and Pappas, G. J. Data-driven network resource allocation for controlling spreading processes. *IEEE Transactions on Network Science and Engineering*, 2(4):127–138, 2015.

[64] Hansen, E. and Day, T. Optimal control of epidemics with limited resources. *Journal of Mathematical Biology*, 62(3):423–451, 2011.

[65] Hernández Encinas, L., Hoya White, S., Martín del Rey, A., and Rodríguez Sánchez, G. Modelling forest fire spread using hexagonal cellular automata. *Applied Mathematical Modelling*, 31(6):1213–1227, 2007.

[66] Hethcote, H. W. Qualitative analyses of communicable disease models. *Mathematical Biosciences*, 28(3-4):335–356, 1976.

[67] Hethcote, H. W. The mathematics of infectious diseases. *SIAM Review*, 42(4): 599–653, 2000.

[68] Holko, A., Edrek, M., Pastuszak, Z., and Phusavat, K. Epidemiological modeling with a population density map-based cellular automata simulation system. *Expert Systems With Applications*, 48:1–8, 2015.

[69] Holme, P., Kim, B. J., Yoon, C. N., and Han, S. K. Attack vulnerability of complex networks. *Physical Review E*, 65(5):056109, 2002.

[70] Howden, D. and Hendtlass, T. Collective intelligence and bush fire spotting. In *Proceedings of the 10th annual conference on Genetic and evolutionary computation*, pages 41–48, 2008.

[71] Huber, M. F. and Hanebeck, U. D. Priority list sensor scheduling using optimal pruning. In *Proceedings of the 11th International Conference on Information Fusion*, pages 1–8. IEEE, 2008.

[72] Hughes, L. and Steffan, W. Be Prepared: Climate Change and the Australian bushfire threat. Technical report, Climate Council of Australia, 2016.

[73] Hung, N. M., Van Tran, Q., Liu, J., and Ahn, H.-S. Resource allocation for epidemic network under complications. In *Proceedings of the 19th International Conference on Control, Automation and Systems*, pages 1512–1516. IEEE, 2019.

[74] Jaafari, A., Mafi-Gholami, D., Thai Pham, B., and Tien Bui, D. Wildfire Probability Mapping: Bivariate vs. Multivariate Statistics. *Remote Sensing*, 11(6):618, 2019.

[75] Jawaid, S. T. and Smith, S. L. Submodularity and greedy algorithms in sensor scheduling for linear dynamical systems. *Automatica*, 61:282–288, 2015.

[76] Johnston, P., Milne, G., and Kelso, J. A heat transfer simulation model for wildfire spread. *Forest Ecology and Management*, 234:S78, 2006.

[77] Jolly, W. M., Cochrane, M. A., Freeborn, P. H., Holden, Z. A., Brown, T. J., Williamson, G. J., and Bowman, D. M. J. S. Climate-induced variations in global wildfire danger from 1979 to 2013. *Nature Communications*, 6:7537, 2015.

[78] Julian, K. D. and Kochenderfer, M. J. Distributed wildfire surveillance with autonomous aircraft using deep reinforcement learning. *Journal of Guidance, Control, and Dynamics*, 42(8):1768–1778, 2019.

[79] Kar, T. K. and Batabyal, A. Stability analysis and optimal control of an SIR epidemic model with vaccination. *Biosystems*, 104(2-3):127–135, 2011.

[80] Karafyllidis, I. and Thanailakis, A. A model for predicting forest fire spreading using cellular automata. *Ecological Modelling*, 99(1):87–97, 1997.

[81] Kelso, J. K., Mellor, D., Murphy, M. E., and Milne, G. J. Techniques for evaluating wildfire simulators via the simulation of historical fires using the AUSTRALIS simulator. *International Journal of Wildland Fire*, 24(6): 784–797, 2015.

[82] Kelso, J. K., Mellor, D., and Milne, G. J. The Australis Wildfire Simulator. http://smr.csse.uwa.edu.au/australis.html. 2018. Accessed: 09-05-2018.

[83] Kermark, M. and Mckendrick, A. Contributions to the mathematical theory of epidemics. Part I. *Proceedings of the Royal Society A*, 115(5):700–721, 1927.

[84] Khanafer, A. and Başar, T. An Optimal Control Problem Over Infected Networks. *Proceedings of the International Conference of Control, Dynamic Systems, and Robotics*, (125):1–6, 2014.

[85] Khanafer, A., Başar, T., and Gharesifard, B. Stability of epidemic models over directed graphs: A positive systems approach. *Automatica*, 74:126–134, 2016.

[86] Kitsak, M., Gallos, L. K., Havlin, S., Liljeros, F., Muchnik, L., Stanley, H. E., and Makse, H. A. Identification of influential spreaders in complex networks. *Nature Physics*, 6(11):888–893, 2010.

[87] Köhler, J., Enyioha, C., and Allgöwer, F. Dynamic resource allocation to control epidemic outbreaks a model predictive control approach. In *Proceedings of the 2018 American Control Conference*, pages 1546–1551. IEEE, 2018.

[88] Köhler, J., Schwenkel, L., Koch, A., Berberich, J., Pauli, P., and Allgöwer, F. Robust and optimal predictive control of the COVID-19 outbreak. *Annual Reviews in Control*, 51:525–539, 2021.

[89] Leuenberger, M., Parente, J., Tonini, M., Pereira, M. G., and Kanevski, M. Wildfire susceptibility mapping: Deterministic vs. stochastic approaches. *Environmental Modelling and Software*, 101:194–203, 2018.

[90] Li, C., Van De Bovenkamp, R., and Van Mieghem, P. Susceptible-infected-susceptible model: A comparison of N-intertwined and heterogeneous mean-field approximations. *Physical Review E*, 86(2):026116, 2012.

[91] Liberatore, F., León, J., Hearne, J., and Vitoriano, B. Fuel management operations planning in fire management: A bilevel optimisation approach. *Safety Science*, 137:105181, 2021.

[92] Lin, F., Fardad, M., and Jovanović, M. Design of optimal sparse feedback gains via the alternating direction method of multipliers. *IEEE Transactions on Automatic Control*, 58(9):2426–2431, 2013.

[93] Lin, S. Computer solutions of the traveling salesman problem. *Bell System Technical Journal*, 44(10):2245–2269, 1965.

[94] Lindmark, G. and Altafini, C. Minimum energy control for complex networks. *Scientific Reports*, 8:3188, 2018.

[95] Little, J. D. C., Murty, K. G., Sweeney, D. W., and Karel, C. An algorithm for the traveling salesman problem. *Operations Research*, 11(6):972–989, 1963.

[96] Liu, J., Paré, P. E., Nedich, A., Tang, C. Y., Beck, C. L., and Başar, T. Analysis and control of a continuous-time bi-virus model. *IEEE Transactions on Automatic Control*, 64(12):4891–4906, 2019.

[97] Liu, J. G., Lin, J. H., Guo, Q., and Zhou, T. Locating influential nodes via dynamics-sensitive centrality. *Scientific Reports*, 6:21380, 2016.

[98] Madar, N., Kalisky, T., Cohen, R., Ben-Avraham, D., and Havlin, S. Immunization and epidemic dynamics in complex networks. *The European Physical Journal B - Condensed Matter and Complex Systems*, 38(2):269–276, 2004.

[99] Mai, V. S., Battou, A., and Mills, K. Distributed Algorithm for Suppressing Epidemic Spread in Networks. *IEEE Control Systems Letters*, 2(3):555–560, 2018.

[100] Manchester, I. R. and Slotine, J.-J. E. On existence of separable contraction metrics for monotone nonlinear systems. In *Proceedings of the 20th IFAC World Congress*, volume 50, issue 1, pages 8226–8231, 2017.

[101] Matsypura, D., Prokopyev, O. A., and Zahar, A. Wildfire fuel management: network-based models and optimization of prescribed burning. *European Journal of Operational Research*, 264(2):774–796, 2018.

[102] McVernon, J. How low do we have to go? http://www.doherty.edu.au/news-events/news/how-low-do-we-have-to-go. 2021. Accessed: 25-08-2021.

[103] Miller, J. C. and Hyman, J. M. Effective vaccination strategies for realistic social networks. *Physica A: Statistical Mechanics and its Applications*, 386(2): 780–785, 2007.

[104] Minas, J. P., Hearne, J. W., and Handmer, J. W. A review of operations research methods applicable to wildfire management. *International Journal of Wildland Fire*, 21(3):189–196, 2012.

[105] Minas, J. P., Hearne, J. W., and Martell, D. L. A spatial optimisation model for multi-period landscape level fuel management to mitigate wildfire impacts. *European Journal of Operational Research*, 232(2):412–422, 2014.

[106] Mladenović, N., Brimberg, J., Hansen, P., and Moreno-Pérez, J. A. The p-median problem: A survey of metaheuristic approaches. *European Journal of Operational Research*, 179(3):927–939, 2007.

[107] Morton, R. and Wickwire, K. H. On the optimal control of a deterministic epidemic. *Advances in Applied Probability*, 6(4):622–635, 1974.

[108] MOSEK. MOSEK Modeling Cookbook 3.2.3. 2021.

[109] Mutlu, M., Popescu, S. C., and Zhao, K. Sensitivity analysis of fire behavior modeling with LIDAR-derived surface fuel maps. *Forest Ecology and Management*, 256(3):289–294, 2008.

[110] Mutthulakshmi, K., Wee, M. R. E., Wong, Y. C. K., Lai, J. W., Koh, J. M., Acharya, U. R., and Cheong, K. H. Simulating forest fire spread and fire-fighting using cellular automata. *Chinese Journal of Physics*, 65:642–650, 2020.

[111] Nigam, N. The Multiple Unmanned Air Vehicle Persistent Surveillance Problem: A Review. *Machines*, 2(1):13–72, 2014.

[112] Nowzari, C., Ogura, M., Preciado, V. M., and Pappas, G. J. Optimal resource allocation for containing epidemics on time-varying networks. In *Proceedings of the 49th Asilomar Conference on Signals, Systems and Computers*, pages 1333–1337. IEEE, 2015.

[113] Nowzari, C., Preciado, V. M., and Pappas, G. J. Analysis and Control of Epidemics: A Survey of Spreading Processes on Complex Networks. *IEEE Control Systems Magazine*, 36(1):26–46, 2016.

[114] Nowzari, C., Preciado, V. M., and Pappas, G. J. Optimal resource allocation for control of networked epidemic models. *IEEE Transactions on Control of Network Systems*, 4(2):159–169, 2017.

[115] Ogura, M. and Preciado, V. M. Efficient containment of exact SIR Markovian processes on networks. In *Proceedings of the 55th IEEE Conference on Decision and Control*, pages 967–972. IEEE, 2016.

[116] Ogura, M. and Preciado, V. M. Stability of SIS spreading processes in networks with non-Markovian transmission and recovery. *IEEE Transactions on Control of Network Systems*, 7(1):349–359, 2019.

[117] Ogura, M., Kishida, M., and Lam, J. Geometric programming for optimal positive linear systems. *IEEE Transactions on Automatic Control*, 65(11): 4648–4663, 2019.

[118] Page, L., Brin, S., Motwani, R., and Winograd, T. The pagerank citation ranking: Bringing order to the web. Technical Report 1999-66, Stanford InfoLab, November 1999.

[119] Pan, Q., Wen, X., Lu, Z., Li, L., and Jing, W. Dynamic speed control of unmanned aerial vehicles for data collection under internet of things. *Sensors*, 18(11):3951, 2018.

[120] Paré, P. E., Beck, C. L., and Nedić, A. Stability analysis and control of virus spread over time-varying networks. In *Proceedings of the 54th IEEE Conference on Decision and Control*, pages 3554–3559. IEEE, 2015.

[121] Paré, P. E., Beck, C. L., and Nedić, A. Epidemic processes over time-varying networks. *IEEE Transactions on Control of Network Systems*, 5(3):1322–1334, 2018.

[122] Paré, P. E., Beck, C. L., and Başar, T. Modeling, estimation, and analysis of epidemics over networks: An overview. *Annual Reviews in Control*, 20: 345–360, 2020.

[123] Paré, P. E., Liu, J., Beck, C. L., Nedić, A., and Başar, T. Multi-competitive viruses over time-varying networks with mutations and human awareness. *Automatica*, 123:109330, 2021.

[124] Pasqualetti, F., Durham, J. W., and Bullo, F. Cooperative patrolling via weighted tours: Performance analysis and distributed algorithms. *IEEE Transactions on Robotics*, 28(5):1181–1188, 2012.

[125] Pastor-Satorras, R. and Vespignani, A. Immunization of complex networks. *Physical Review E*, 65(3):036104, 2002.

[126] Pastor-Satorras, R., Castellano, C., Van Mieghem, P., and Vespignani, A. Epidemic processes in complex networks. *Reviews of Modern Physics*, 87(3): 925, 2015.

[127] Peeri, N. C., Shrestha, N., Rahman, M. S., Zaki, R., Tan, Z., Bibi, S., Baghbanzadeh, M., Aghamohammadi, N., Zhang, W., and Haque, U. The SARS, MERS and novel coronavirus (COVID-19) epidemics, the newest and biggest global health threats: what lessons have we learned? *International Journal of Epidemiology*, 49(3):717–726, 2020.

[128] Peng, X.-L., Xu, X.-J., Fu, X., and Zhou, T. Vaccination intervention on epidemic dynamics in networks. *Physical Review E*, 87(2):022813, 2013.

[129] Penicka, R., Faigl, J., Vána, P., and Saska, M. Dubins orienteering problem. *IEEE Robotics and Automation Letters*, 2(2):1210–1217, 2017.

[130] Pezzutto, M., Rosselló, N. B., Schenato, L., and Garone, E. Smart testing and selective quarantine for the control of epidemics. *Annual Reviews in Control*, 51:540–550, 2021.

[131] Preciado, V. M., Zargham, M., Enyioha, C., Jadbabaie, A., and Pappas, G. Optimal vaccine allocation to control epidemic outbreaks in arbitrary networks. In *Proceedings of the 52nd IEEE Conference on Decision and Control*, pages 7486–7491. IEEE, 2013.

[132] Preciado, V. M., Zargham, M., Enyioha, C., Jadbabaie, A., and Pappas, G. J. Optimal resource allocation for network protection against spreading

processes. *IEEE Transactions on Control of Network Systems*, 1(1):99–108, 2014.

[133] Preisler, H. K., Brillinger, D. R., Burgan, R. E., and Benoit, J. Probability based models for estimation of wildfire risk. *International Journal of wildland fire*, 13(2):133–142, 2004.

[134] Pritchard, E., Matthews, P. C., Stoesser, N., Eyre, D. W., Gethings, O., Vihta, K.-D., Jones, J., House, T., VanSteenHouse, H., Bell, I., Bell, J. I., Newton, J. N., Farrar, J., Diamond, I., Rourke, E., Studley, R., Crook, D., Peto, T. E. A., Walker, A. S., and Pouwels, K. B. Impact of vaccination on new SARS-CoV-2 infections in the United Kingdom. *Nature Medicine*, 27: 1370 – 1378, 2021.

[135] Qu, B., Li, C., Van Mieghem, P., and Wang, H. Ranking of nodal infection probability in susceptible-infected-susceptible epidemic. *Scientific Reports*, 7: 9233, 2017.

[136] Rabinovich, S., Curry, R. E., and Elkaim, G. H. Toward dynamic monitoring and suppressing uncertainty in wildfire by multiple unmanned air vehicle system. *Journal of Robotics*, 2018:6892153, 2018.

[137] Ramírez-Llanos, E. and Martínez, S. Distributed discrete-time optimization algorithms with applications to resource allocation in epidemics control. *Optimal Control Applications and Methods*, 39(1):160–180, 2018.

[138] Rantzer, A. Scalable control of positive systems. *European Journal of Control*, 24:72–80, 2015.

[139] Robinson, S. M. Strongly regular generalized equations. *Mathematics of Operations Research*, 5(1):43–62, 1980.

[140] Ross, S. M. *Stochastic processes*. New York: Wiley, 2nd edition, 1996.

[141] Rothermel, R. C. A mathematical model for predicting fire spread in wildland fuels. Research Paper INT-115, Ogden, UT: US Department of Agriculture, Forest Service, Intermountain Forest and Range Experiment Station, Oregon, 1972.

[142] Rothermel, R. C. How to predict the spread and intensity of forest and range fires. General Technical Report INT-143, Ogden, UT: US Department of Agriculture, Forest Service, Intermountain Forest and Range Experiment Station, 1983.

[143] Rothermel, R. C. Predicting behavior and size of crown fires in the northern rocky mountains. Research Paper INT-438, Ogden, UT: US Department of Agriculture, Forest Service, Intermountain Research Station, 1991.

[144] Ruan, Z., Tang, M., and Liu, Z. Epidemic spreading with information-driven vaccination. *Physical Review E*, 86(3):036117, 2012.

[145] Santos, B. F., Sa, C., and Clarke, J. Data underlying the research on portfolio-based airline fleet planning. TU Delft - 4TU.Centre for Research Data. 2019.

[146] Savla, K., Frazzoli, E., and Bullo, F. Traveling salesperson problems for the dubins vehicle. *IEEE Transactions on Automatic Control*, 53(6):1378–1391, 2008.

[147] Scaman, K., Kalogeratos, A., and Vayatis, N. Suppressing epidemics in networks using priority planning. *IEEE Transactions on Network Science and Engineering*, 3(4):271–285, 2016.

[148] Schneider, C. M., Mihaljev, T., Havlin, S., and Herrmann, H. J. Suppressing epidemics with a limited amount of immunization units. *Physical Review E*, 84(6):061911, 2011.

[149] Sélley, F., Besenyei, Á., Kiss, I. Z., and Simon, P. L. Dynamic control of modern, network-based epidemic models. *SIAM Journal on Applied Dynamical Systems*, 14(1):168–187, 2015.

[150] Shaw, L. B. and Schwartz, I. B. Enhanced vaccine control of epidemics in adaptive networks. *Physical Review E*, 81(4):046120, 2010.

[151] Skeele, R. C. and Hollinger, G. A. Aerial vehicle path planning for monitoring wildfire frontiers. In Wettergreen, D. S. and Barfoot, T. D., editors, *Field and Service Robotics. Springer Tracts in Advanced Robotics*, volume 113, pages 455–467. Springer, Cham, 2016.

[152] Smith, S. L., Schwager, M., and Rus, D. Persistent robotic tasks: Monitoring and sweeping in changing environments. *IEEE Transactions on Robotics*, 28 (2):410–426, 2012.

[153] Somers, V. L. J. and Manchester, I. R. Priority maps for surveillance and intervention of wildfires and other spreading processes. In *Proceedings of the 2019 International Conference on Robotics and Automation*, pages 739–745. IEEE, 2019.

[154] Somers, V. L. J. and Manchester, I. R. Sparse Resource Allocation for Control of Spreading Processes via Convex Optimization. *IEEE Control Systems Letters*, 5(2):547–552, 2021.

[155] Somers, V. L. J. and Manchester, I. R. Minimizing the Risk of Spreading Processes via Surveillance Schedules and Sparse Control. *IEEE Transactions on Control of Network Systems*, Under review.

[156] Starnini, M., Gleeson, J. P., and Boguñá, M. Equivalence between non-Markovian and Markovian dynamics in epidemic spreading processes. *Physical Review Letters*, 118(12):128301, 2017.

[157] Stepanov, A. and Smith, J. M. G. Modeling wildfire propagation with Delaunay triangulation and shortest path algorithms. *European Journal of Operational Research*, 218(3):775–788, 2012.

[158] Stutt, R. O. J. H., Retkute, R., Bradley, M., Gilligan, C. A., and Colvin, J. A modelling framework to assess the likely effectiveness of facemasks in combination with 'lock-down' in managing the COVID-19 pandemic. *Proceedings of the Royal Society A*, 476(2238):20200376, 2020.

[159] Sullivan, A. L. Wildland surface fire spread modelling, 1990–2007. 3: Simulation and mathematical analogue models. *International Journal of Wildland Fire*, 18(4):387–403, 2009.

[160] Summers, T. H., Cortesi, F. L., and Lygeros, J. On Submodularity and Controllability in Complex Dynamical Networks. *IEEE Transactions on Control of Network Systems*, 3(1):91–101, 2016.

[161] Tibshirani, R. Regression shrinkage and selection via the lasso. *Journal of the Royal Statistical Society: Series B (Methodological)*, 58(1):267–288, 1996.

[162] Torres, J. A., Roy, S., and Wan, Y. Sparse resource allocation for linear network spread dynamics. *IEEE Transactions on Automatic Control*, 62(4): 1714–1728, 2017.

[163] Umenberger, J. and Manchester, I. R. Scalable identification of stable positive systems. In *Proceedings of the 55th IEEE Conference on Decision and Control*, pages 4630–4635. IEEE, 2016.

[164] Van Mieghem, P. and van de Bovenkamp, R. Accuracy criterion for the mean-field approximation in susceptible-infected-susceptible epidemics on networks. *Physical Review E*, 91(3):032812, 2015.

[165] Van Mieghem, P. The N-intertwined SIS epidemic network model. *Computing*, 93:147–169, 2011.

[166] Van Mieghem, P. *Performance analysis of complex networks and systems.* Cambridge University Press, 2014.

[167] Van Mieghem, P., Omic, J., and Kooij, R. Virus spread in networks. *IEEE/ACM Transactions on Networking*, 17(1):1–14, 2009.

[168] Van Mieghem, P., Stevanović, D., Kuipers, F., Li, C., Van De Bovenkamp, R., Liu, D., and Wang, H. Decreasing the spectral radius of a graph by link removals. *Physical Review E*, 84(1):016101, 2011.

[169] Vasiliauskaite, V., Antulov-Fantulin, N., and Helbing, D. On some fundamental challenges in monitoring epidemics. *Philosophical Transactions of the Royal Society A*, 380(2214):20210117, 2022.

[170] Vitus, M. P., Zhang, W., Abate, A., Hu, J., and Tomlin, C. J. On efficient sensor scheduling for linear dynamical systems. *Automatica*, 48(10):2482–2493, 2012.

[171] Wan, Y., Roy, S., and Saberi, A. Network design problems for controlling virus spread. In *Proceedings of the 46th IEEE Conference on Decision and Control*, pages 3925–3932. IEEE, 2007.

[172] Wan, Y., Roy, S., and Saberi, A. Designing spatially heterogeneous strategies for control of virus spread. *IET Systems Biology*, 2(4):184–201, 2008.

[173] Watkins, N. J., Nowzari, C., and Pappas, G. J. Robust economic model predictive control of continuous-time epidemic processes. *IEEE Transactions on Automatic Control*, 65(3):1116–1131, 2019.

[174] Wei, Y., Rideout, D., and Kirsch, A. An optimization model for locating fuel treatments across a landscape to reduce expected fire losses. *Canadian Journal of Forest Research*, 38(4):868–877, 2008.

[175] Ye, M., Liu, J., Anderson, B. D. O., and Cao, M. Distributed Feedback Control on the SIS Network Model: An Impossibility Result. In *Proceedings of the 21st IFAC World Congress*, volume 53, issue 2, pages 10955–10962, 2020.

[176] Ye, M., Liu, J., Anderson, B. D. O., and Cao, M. Applications of the poincare-hopf theorem: Epidemic models and lotka-volterra systems. *IEEE Transactions on Automatic Control*, 2021.

[177] Yebra, M., Dijk, A. V., and Cary, G. Mapping Bushfire Hazards and Impacts. Technical Report 462.2019, Australian National University & Bushfire and Natural Hazards CRC, 2019.

[178] Youssef, M. and Scoglio, C. An individual-based approach to SIR epidemics in contact networks. *Journal of Theoretical Biology*, 283(1):136–144, 2011.

[179] Yu, J., Schwager, M., and Rus, D. Correlated orienteering problem and its application to persistent monitoring tasks. *IEEE Transactions on Robotics*, 32 (5):1106–1118, 2016.

[180] Zaman, G., Kang, Y. H., and Jung, I. H. Stability analysis and optimal vaccination of an SIR epidemic model. *BioSystems*, 93(3):240–249, 2008.

[181] Zarghamy, M. and Preciadoy, V. Worst-case scenarios for greedy, centrality-based network protection strategies. In *Proceedings of the 48th Annual Conference on Information Sciences and Systems*, pages 1–6. IEEE, 2014.

[182] Zhang, W., Lu, S., and Pei, Y. A geometric programming approach for optimal resource allocation to control epidemic outbreaks in arbitrary networks. *Communications in Mathematical Biology and Neuroscience*, 2018: 1–17, 2018.

[183] Zino, L. and Cao, M. Analysis, prediction, and control of epidemics: A survey from scalar to dynamic network models. *IEEE Circuits and Systems Magazine*, 21(4):4–23, 2021.

Appendix A

Nonlinear Intervention Approach

In Chapter 5 we looked into the intervention problem by considering resource allocation to minimize the risk. We proposed logarithmic resource models and demonstrated how to reformulate the resulting problem as an exponential cone program. We did, however, also explore other methods for resource allocation to minimize the risk.

For example in [153] we proposed the following framework, where we include a new resource allocation or 'control' matrix K to alter the original system dynamics and state matrix (3.8). The task is again to reduce the discounted cost-to-go by finding a sparse set of locations for intervention within a budgeted constraint.

The new closed loop system is given by

$$\dot{x}(t) = (A - K)x(t) \tag{A.1}$$

where K is the control matrix and restricted to the total resource constraint $\sum k_{ij} \leq \Gamma$, where Γ is the maximum budget available. Note that this imposes an ℓ_1-type constraint on the elements of K and hence, encourages sparsity similar to the resource model constraints in Section 5.1.

We can now extend the LP (3.17) from Chapter 3 to obtain the problem formulation;

$$\begin{aligned}
\underset{p,K}{\text{minimize}} \quad & |p|_1 && \text{(A.2a)}\\
\text{such that} \quad & p \geq 0, && \text{(A.2b)}\\
& p^T A - rp^T - p^T K \leq -C, && \text{(A.2c)}\\
& \sum_{ij} K \leq \Gamma, && \text{(A.2d)}\\
& K \geq 0, && \text{(A.2e)}\\
& K \leq A, && \text{(A.2f)}\\
& k_{ij} = 0 \quad \forall (i,j) \notin \mathcal{E}. && \text{(A.2g)}
\end{aligned}$$

However, the multiplication of decision variables $p^T K$ means this is not a linear program (LP). Furthermore, note that we can also take $\max(p_i \lambda_i \tau_i)$ as the objective to minimize, similar to Problem 5.1, instead of the direct extension of (3.17), i.e. (A.2a). Moreover, for simplicity we do not consider resource allocation on the outbreak rate λ_i, the revisit interval τ_i nor discount rate r similar to Problem 5.2.

To solve this nonlinear program different iterative solving approaches have been explored that we will summarize and discuss in the following sections. Although all of these proposed approaches have been shown to give good results in practice and do also include sparse resource models, global optimality could not be proven and for all methods exceptions have been found in which cyclic behavior of the results occurred instead of convergence to an optimum. Furthermore, due to the iterative approach of these methods, they are also not as scalable as the method proposed in Chapter 5.

A.1 Iterative Linear Program

To deal with the nonlinearity we define an iterative linear program where we introduce p_0 as the initial guess of p, which can be obtained by solving either (3.16) or (3.17).

We will minimize the maximum risk bound $R(t) = \hat{x}(0) \odot p$ (3.23) from Chapter 3,

similar to Problem 5.2 and therefore, define the following optimization program

$$\begin{aligned}
\underset{p,K}{\text{minimize}} \quad & \max(\hat{x}(0) \odot p) && \text{(A.3a)}\\
\text{such that} \quad & p \geq 0, && \text{(A.3b)}\\
& p^T A - rp^T - p_0^T K \leq -C, && \text{(A.3c)}\\
& \sum_{ij} K \leq \Gamma, && \text{(A.3d)}\\
& K \geq 0, && \text{(A.3e)}\\
& K \leq A, && \text{(A.3f)}\\
& k_{ij} = 0 \quad \forall (i,j) \notin \mathcal{E} && \text{(A.3g)}
\end{aligned}$$

where K is the control matrix.

We now solve this optimization iteratively, while updating p_0 in (A.3c) in the next iteration with the obtained p from the previous iteration till the outcome converges, i.e. $p_0 = p$. Hence, the dynamic coupling constraint (A.3c) is an approximation and not necessarily accurately solved in the earlier iterations due to the inclusion of the approximation of p to minimize the cost of the system. The optimization can be extended by including nodes as possible control resource options by changing the constraints on k_{ij} to $k_{ij} \geq 0 \forall i = j$, i.e. the equivalence of allocation of resources on the recovery rate δ_i as explained in Chapter 5.

A.1.1 Change of variables

A similar but slightly different approach was taken in [153] by proposing a change of variables. The approximation of each iteration then moves from the dynamic coupling constraint to the resource allocation matrix.

Following [138] a new variable $q = p^T K$ is introduced, resulting in the updated constraint $p^T A - rp^T - q \leq -C$. However, to take into account the restriction imposed upon the control matrix K by the total resource constraint Γ and the adjacency matrix, we take $P = \text{diag}(p)$ and $Q = PK$ to preserve the specified structure of K.

This implies $\vec{1}P = p^T$ and $\vec{1}Q = q$, where $\vec{1}$ is the row vector with all ones of the appropriate dimension and the problem can be reformulated as

$$\begin{aligned}
\underset{P,Q}{\text{minimize}} \quad & \max\left(P\hat{x}(0)\right) && \text{(A.4a)}\\
\text{such that} \quad & P \geq 0, && \text{(A.4b)}\\
& Q \geq 0, && \text{(A.4c)}\\
& \vec{1}(PA - rP - Q) \leq -C, && \text{(A.4d)}\\
& \sum_{ij} P_0^{-1}Q \leq \Gamma, && \text{(A.4e)}\\
& P_0^{-1}Q \leq A, && \text{(A.4f)}\\
& q_{ij} = 0 \quad \forall (i,j) \notin \mathcal{E} && \text{(A.4g)}
\end{aligned}$$

where $\sum_{ij} |P_0^{-1}Q| \approx \sum_{ij} |K_{ij}| \leq \Gamma$ and P_0 is the initial guess of P taken as the solution of (3.16).

The optimization problem now consists of minimizing the maximum risk (A.4a) or the trace of P, i.e. $\sum_i^n P_{ii}$, while updating P_0 to the obtained P till the outcome converges, i.e. $P_0 = P$. Afterwards, the final control matrix $K = P^{-1}Q$.

A.1.2 Linearization

Finally, another approach is to take the linearization of the problem and optimize for dP and dK. That is (A.2) is reformulated as

$$\begin{aligned}
\underset{dP,dK}{\text{minimize}} \quad & \max\left((P_0 + dP)\,\hat{x}(0)\right) && \text{(A.5a)}\\
\text{such that} \quad & P_0 + dP \geq 0, && \text{(A.5b)}\\
& \vec{1}((P_0 + dP)A - r(P_0 + dP) - P_0K_0 - P_0dK - dPK_0) \leq -C, && \text{(A.5c)}\\
& \sum_{ij}(K_0 + dK) \leq \Gamma, \quad (K_0 + dK) \geq 0, \quad (K_0 + dK) \leq A, && \text{(A.5d)}\\
& dk_{ij} = 0 \quad \forall (i,j) \notin \mathcal{E} && \text{(A.5e)}
\end{aligned}$$

where $P = \text{diag}(p)$ similar to (A.4).

A.1.3 Computation and Convergence

These different approaches were tested for different scenarios up to $n = 1000$ nodes. Different iterative approaches converged quicker for different scenarios, but overall convergence generally occurred within 5 to 10 iterations.

Global optimality of these approaches, however, could not be proven and run time is depended on the number of iterations needed. Furthermore, exceptions were found for all discussed formulations where cyclic behavior of the result was obtained and convergence was not obtained for one or both of the parameters.

An approach could be to reformulate our problem similar to [37]. Here local convergence is proven for sequential convex programming for non-convex optimization of the form

$$\underset{p}{\text{minimize}} \quad c^T p \tag{A.6a}$$

$$\text{such that} \quad g(p) = 0, \quad p \in \Omega, \tag{A.6b}$$

where $c \in \mathbb{R}^n$, $g : \mathbb{R}^n \to \mathbb{R}^m$ is nonlinear and smooth on its domain, and Ω is a nonempty closed convex subset in $\mathbb{R}^n$, given that the optimization problem satisfies the following conditions:

1. The set of Karush-Kuhn-Tucker (KKT) points of the non-convex problem is nonempty,
2. The strong regularity condition as defined by [139] should hold,
3. The nonlinear constraint, $g(p) = 0$, should be weakly nonlinear, i.e. have small second derivatives, in a neighborhood of a stationary point or the corresponding Lagrange multipliers are sufficiently small in the neighborhood of the Lagrange multiplier of the KKT point.

We refer to [37] for more details.

Appendix B

Additional Figures Chapter 5

In this appendix additional figures are presented for the two wildfire examples in Section 5.5.2. In Section B.1 the same resource allocation maps as already presented for the 1000 node Example 5.3, are given but illustrated with a different colormap to emphasize low resource allocation edges.

In Section B.2 additional figures for the 4000 node Example 5.4 are presented. First, the eight subwalks belonging to Figure 5.22 are illustrated. Next, the resource allocations used to make the scatter plot Figure 5.25 are depicted. Finally, example simulation runs with the stochastic model for scatter plots Figure 5.24 and Figure 5.25 are presented.

B.1 1000 node Wildfire Example

In this appendix section, we show the same resource allocation maps already depicted in Figures 5.13 and 5.14, but with a colormap that visualizes lower resource allocations to emphasize how our method provides more sparse results compared to minimizing other resource models, see Figure B.1 and Figure B.2.

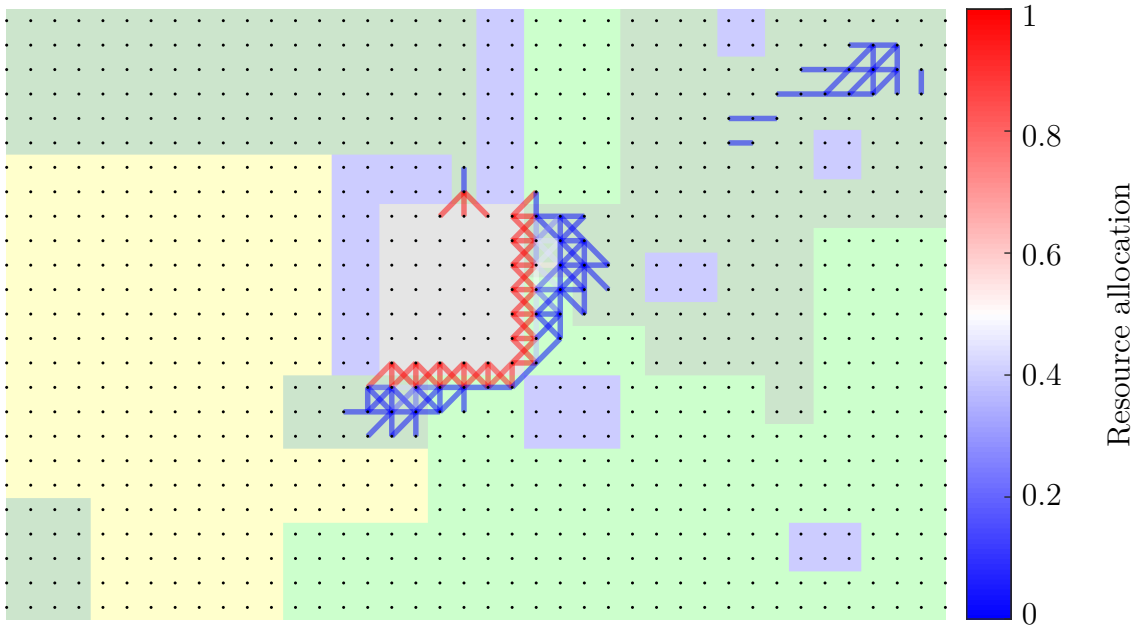

(a) The proposed model: minimize (3.23) subject to constraints on (5.2a). **136** edges have resources allocated.

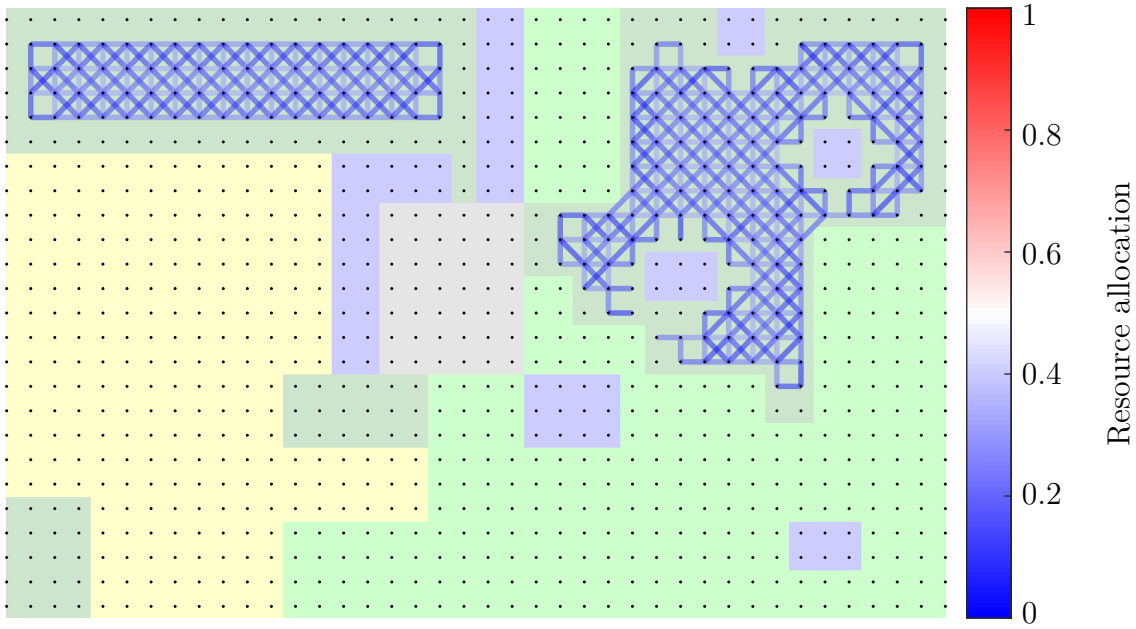

(b) Minimize the spectral abscissa (3.24) subject to constraints on the proposed resource model (5.2a). **611** edges have resources allocated.

Figure B.1 – Resource allocation for minimizing different risk models for Problem 5.2.

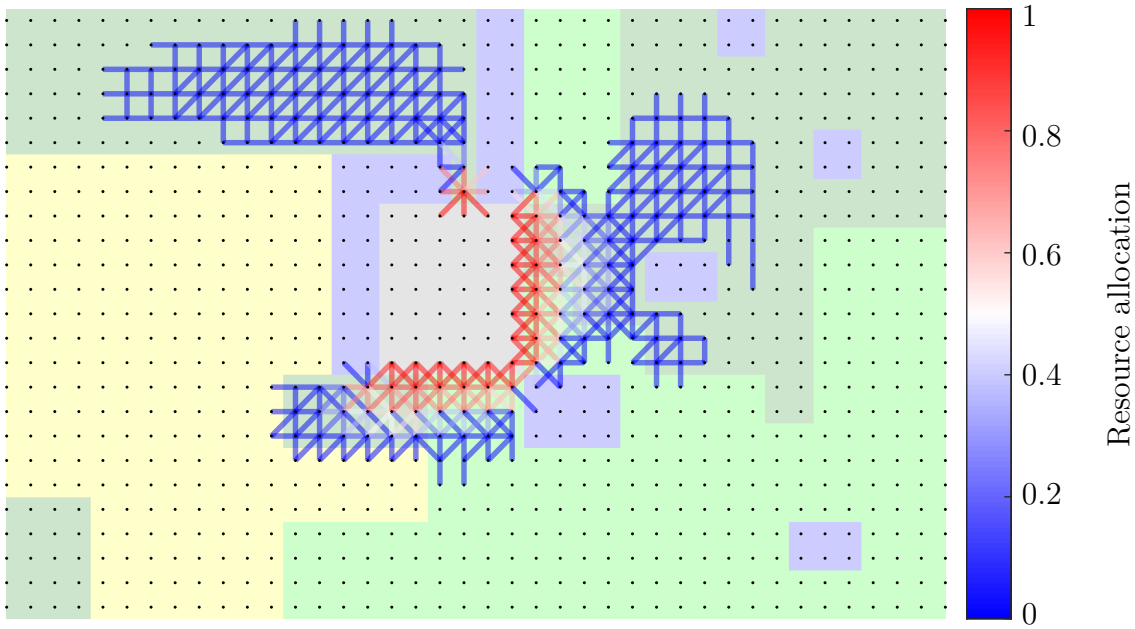

Figure B.2 – Resource allocation using the resource model from [132] for Problem 5.3: minimize (5.3a) subject to constraints on the proposed risk model (3.23). **543** edges have resources allocated.

B.2 4000 node Wildfire Example

In this appendix section, we give additional figures for Example 5.4. First, the eight subwalks of the minimum maximum latency persistent monitoring path in Figure 5.22 are given in Figure B.3.

Next, the resource allocations used to generate the scatter plot Figure 5.25 are presented in respectively Figure B.4 and Figure B.5 for minimizing our proposed risk model (3.22) for $\Gamma_\beta = 1500$, $\Gamma_\lambda = 500$ and $\Gamma_\tau = 1000$ and for minimizing the spectral abscissa with the same allocation budget.

Finally, examples of simulation runs with the stochastic SIR model for scatter plot Figure 5.24 are presented in Figures B.7-B.12. Examples for a fire starting in two different locations, as illustrated in Figure B.6, are given for the proposed resource allocation (Figure 5.20), for the resource allocation obtained by minimizing the spectral abscissa (Figure 5.23) and for not applying any resource allocation. Table B.1 indicates which scenario and resource allocation can be found in which figure.

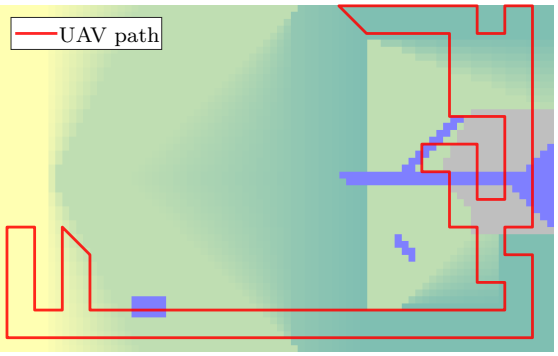

(a) Sub Walk 1

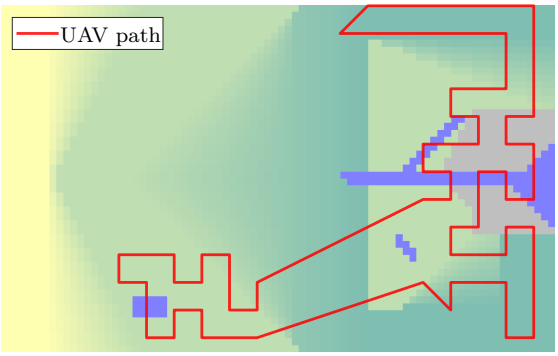

(b) Sub Walk 2

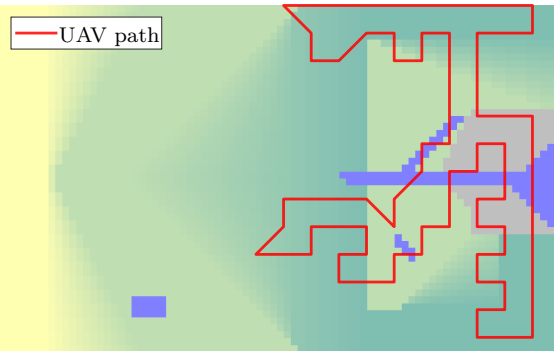

(c) Sub Walk 3

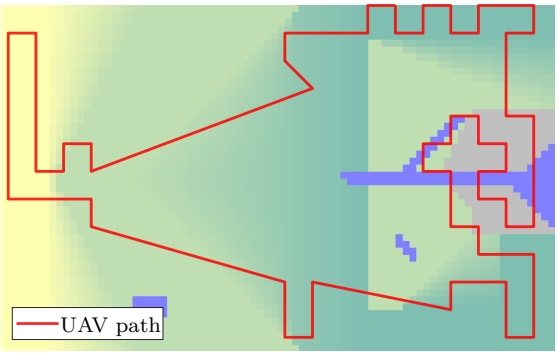

(d) Sub Walk 4

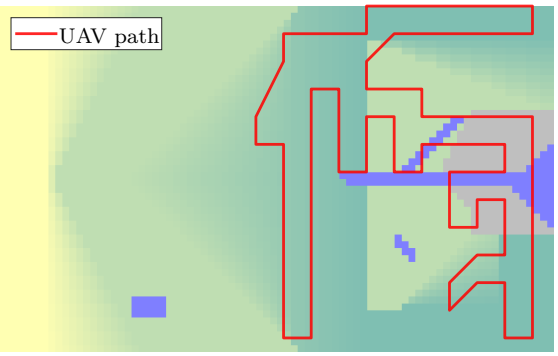

(e) Sub Walk 5

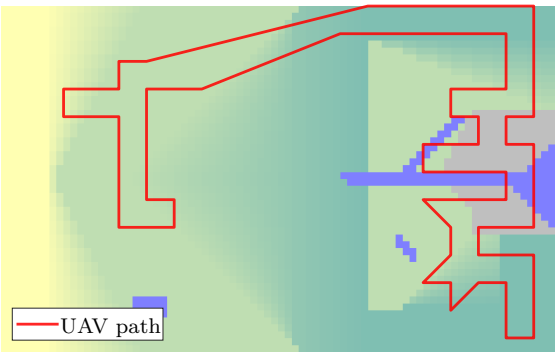

(f) Sub Walk 6

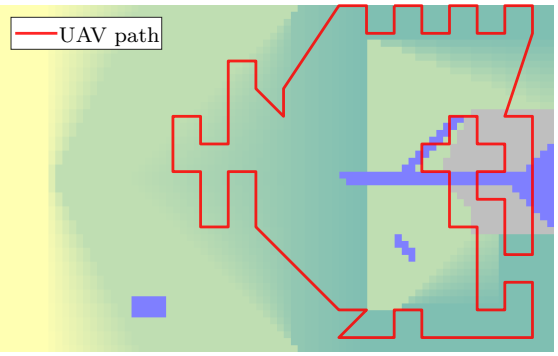

(g) Sub Walk 7

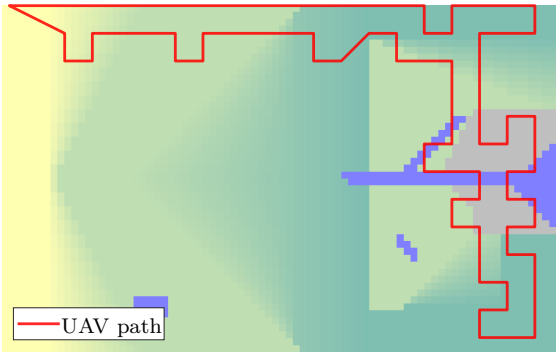

(h) Sub Walk 8

Figure B.3 – The eight subwalks corresponding to Figure 5.22.

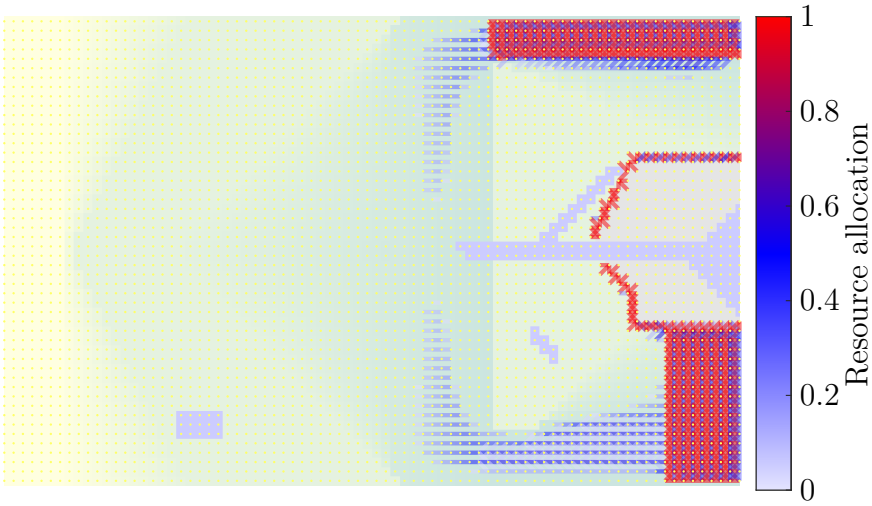

(a) Resource allocation on spreading rate β

(b) Resource allocation on outbreak rate λ

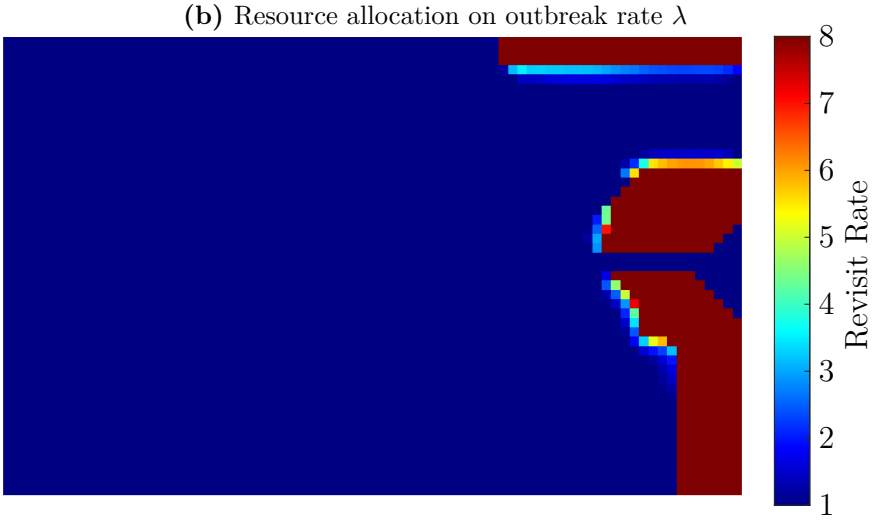

(c) Proposed revisit rate $\frac{1}{\tau}$

Figure B.4 – Resource allocation for the proposed Problem 5.1: minimize the risk (3.22) with resource budgets $\Gamma_\beta = 1500, \Gamma_\lambda = 500$ and $\Gamma_\tau = 1000$.

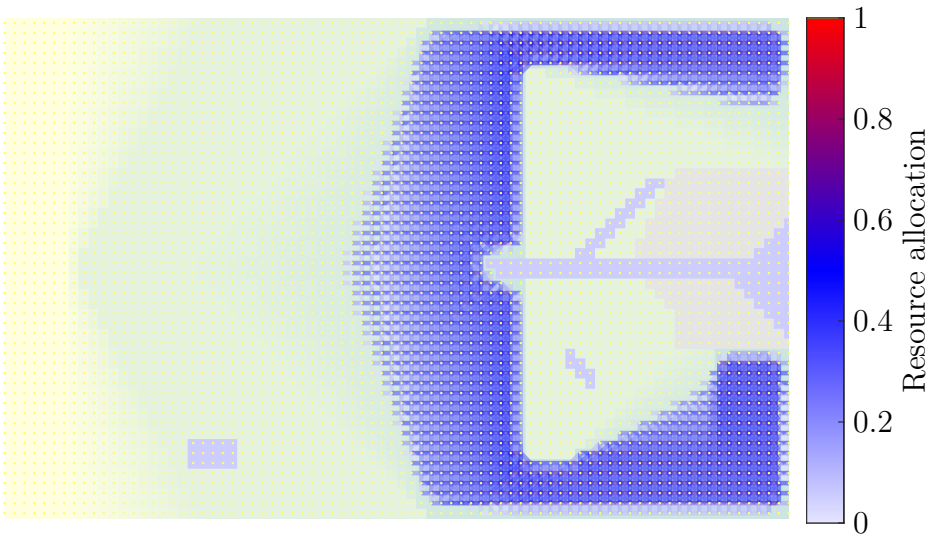

Figure B.5 – Resource allocation on spreading rate β for minimizing the spectral abscissa (3.24). The same resource allocation budget compared to B.4 is used.

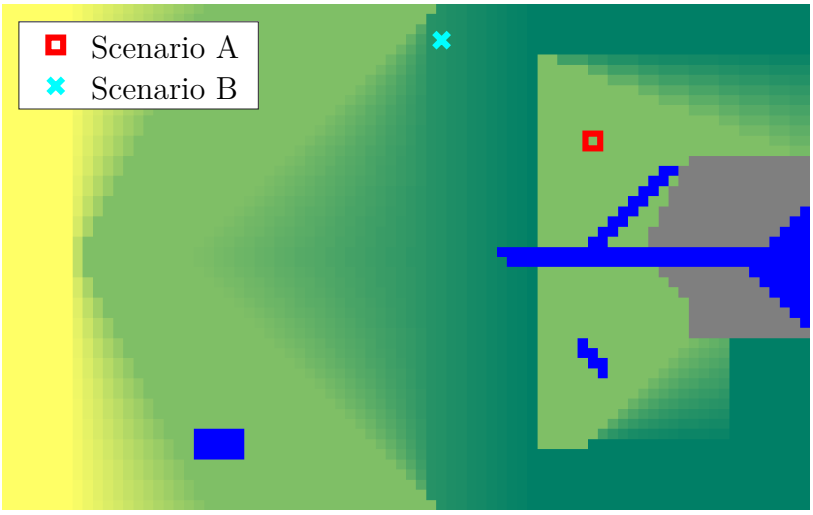

Figure B.6 – Fire start locations for scenario A and B for the stochastic simulation runs displayed in Figures B.7-B.12.

Table B.1 – Figure indicator for the example stochastic simulation runs for different scenarios as indicated in Figure B.6 for the proposed resource allocation, minimizing spectral abscissa and no resource allocation.

	Proposed	Spectral Abscissa	None
Scenario A	Figure B.7	Figure B.8	Figure B.9
Scenario B	Figure B.10	Figure B.11	Figure B.12

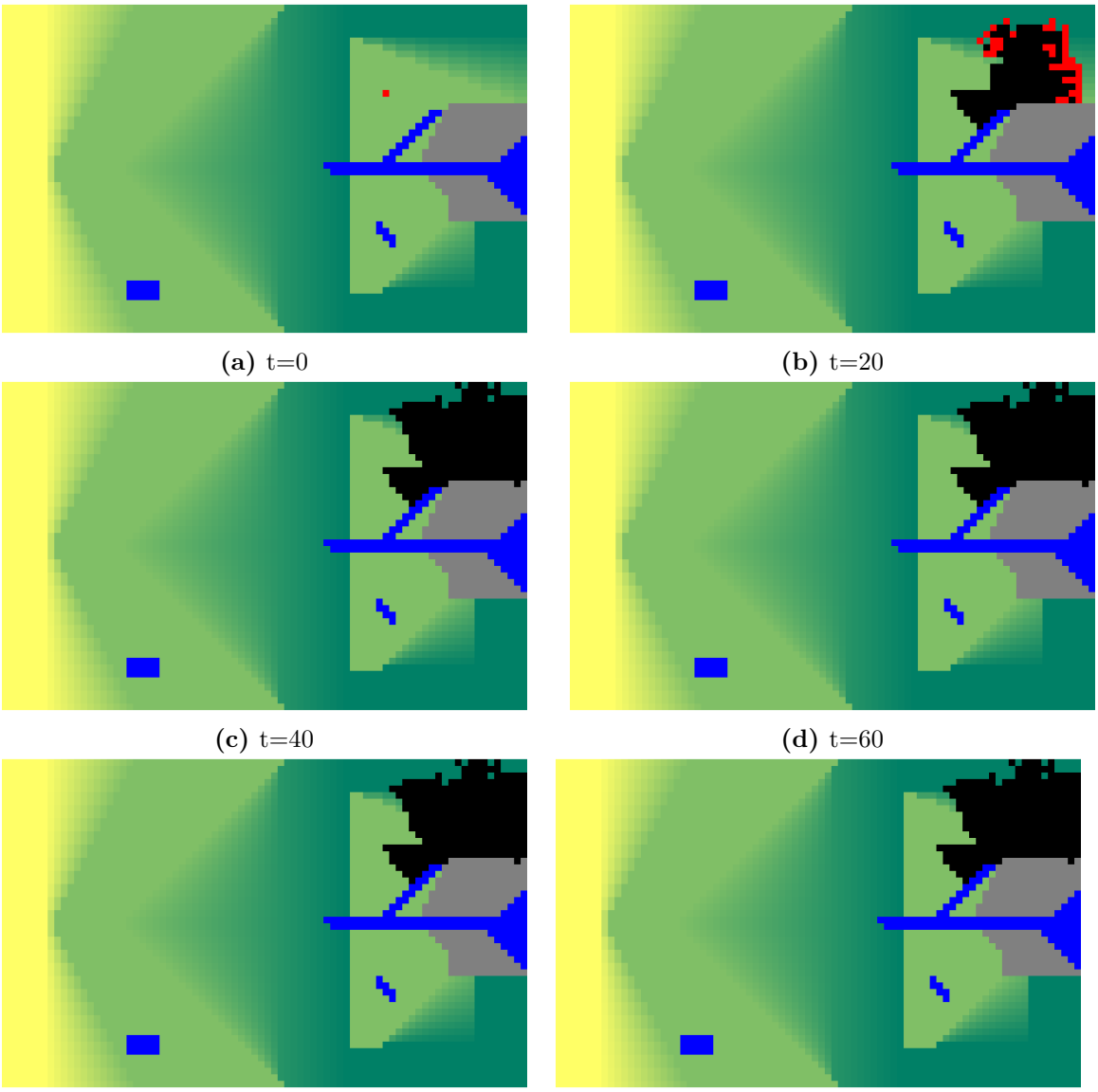

(a) t=0 **(b)** t=20 **(c)** t=40 **(d)** t=60 **(e)** t=80 **(f)** t=100

Figure B.7 – Scenario A - Proposed resource allocation. Stochastic SIR simulation with our proposed resource allocation, Figure 5.20, as part of scatter plot Figure 5.24. Total cost equals 10.98 and the warning time is 6 hours. Red indicates 'on fire' and black 'burned'. Time t is displayed in hours.

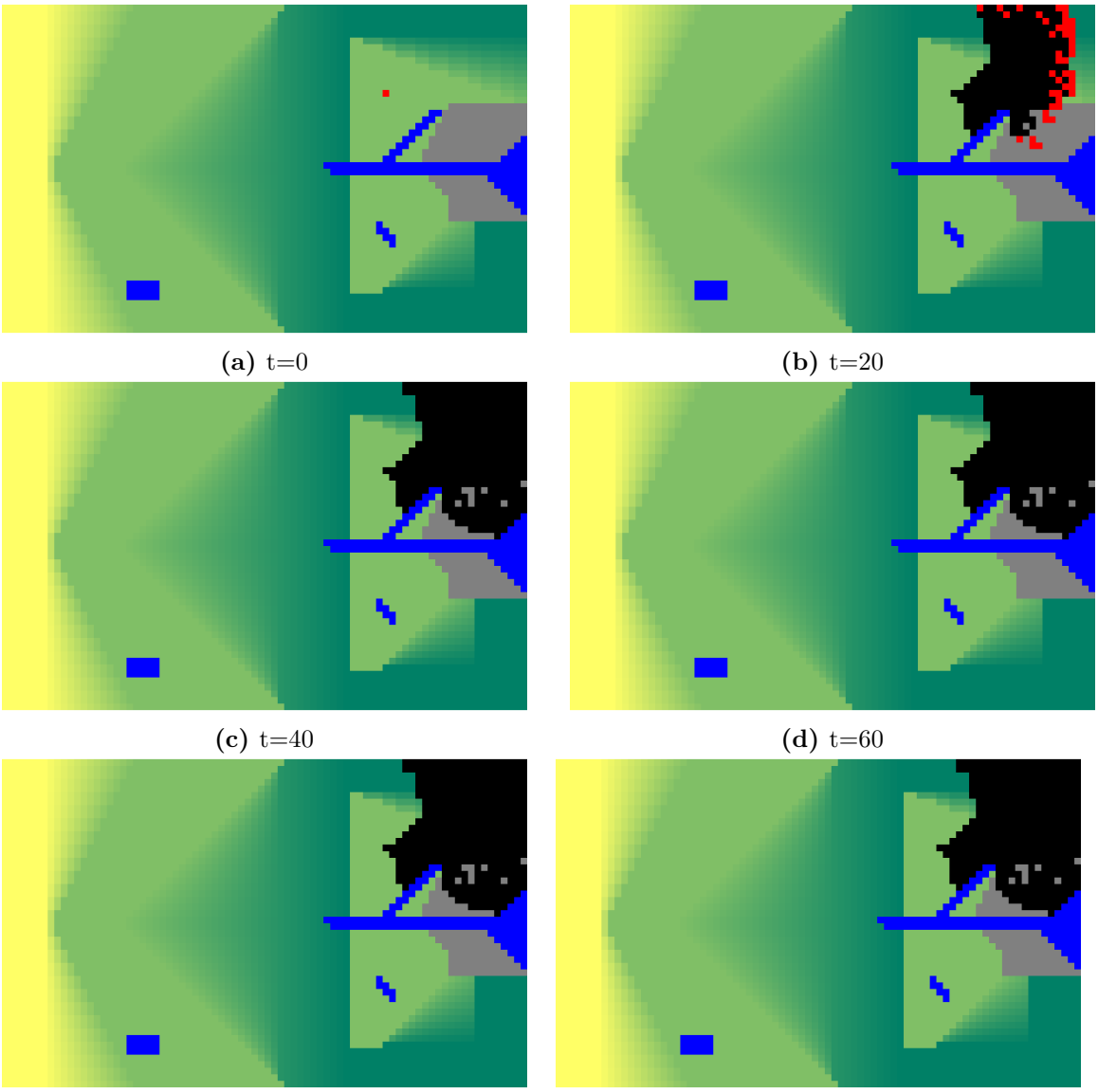

(a) t=0 **(b)** t=20 **(c)** t=40 **(d)** t=60 **(e)** t=80 **(f)** t=100

Figure B.8 – Scenario A - Spectral abscissa resource allocation. Stochastic SIR simulation with resource allocation obtained by minimized the spectral abscissa, Figure 5.23, as part of scatter plot Figure 5.24. Total cost equals 101.22 and the warning time is minus 21 hours. Red indicates 'on fire' and black 'burned'. Time t is displayed in hours.

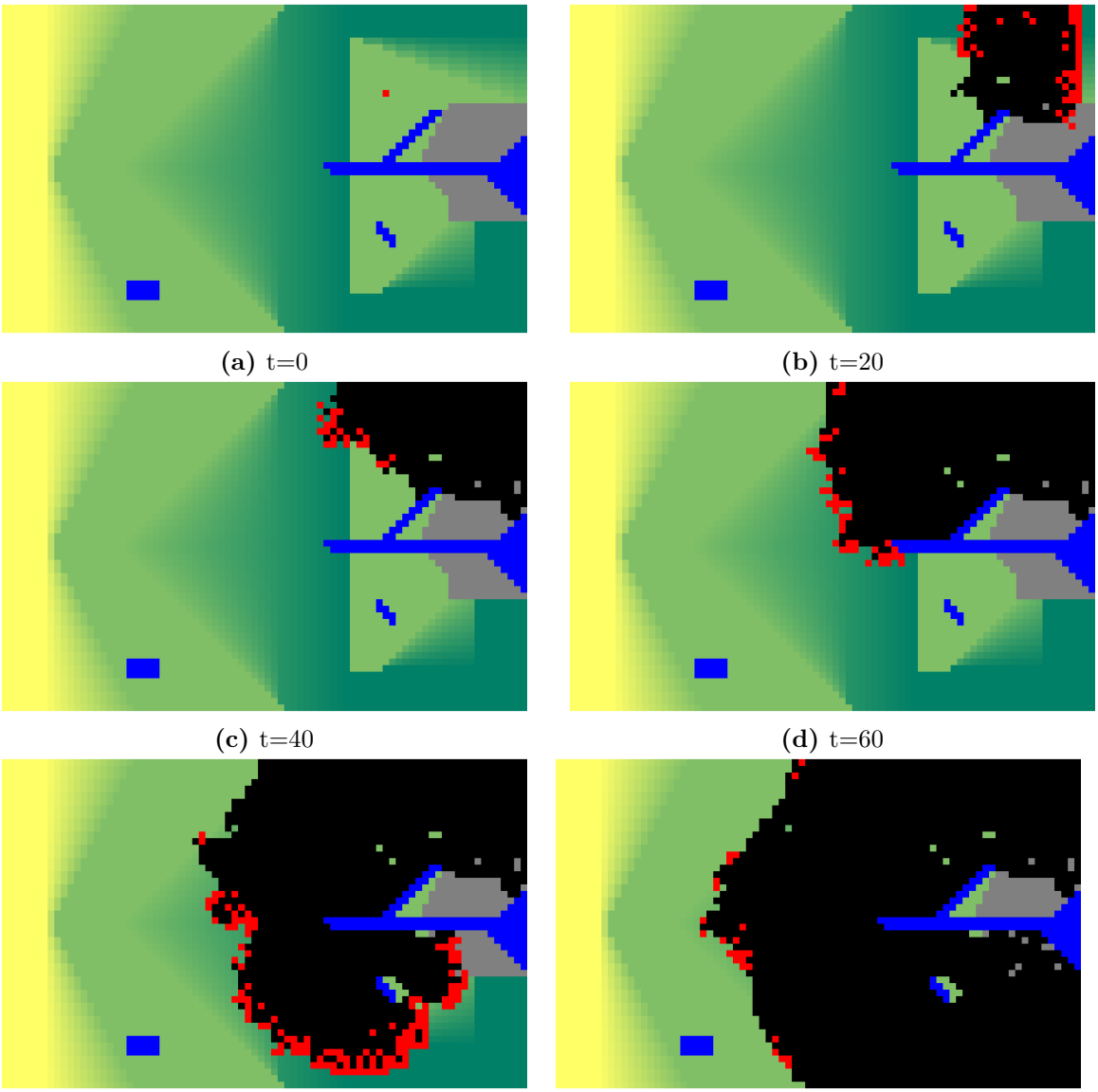

(a) t=0 **(b)** t=20 **(c)** t=40 **(d)** t=60 **(e)** t=80 **(f)** t=100

Figure B.9 – Scenario A - No resource allocation. Stochastic SIR simulation with no applied resource allocation. Total cost equals 165.94. Red indicates 'on fire' and black 'burned'. Time t is displayed in hours.

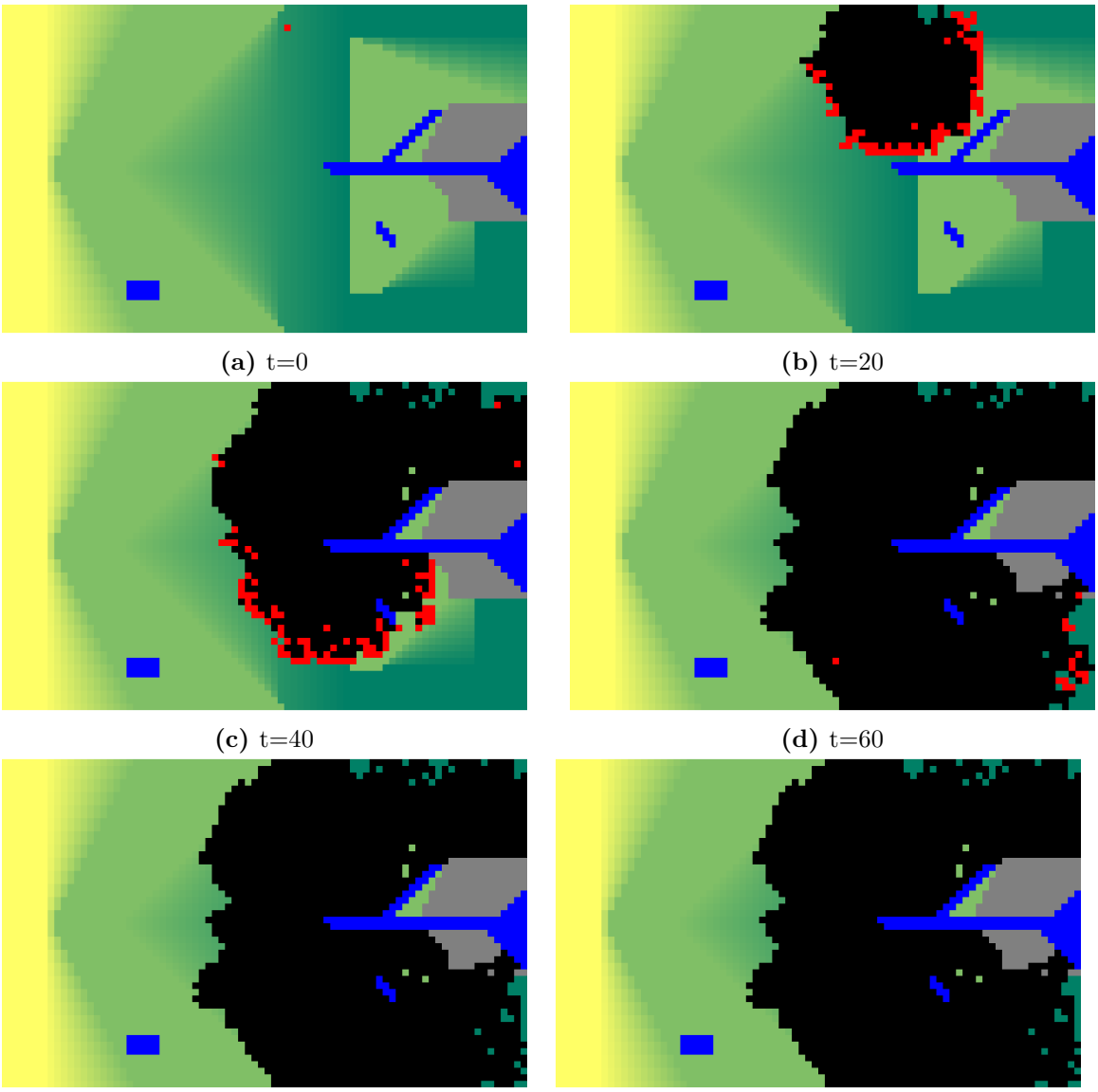

(a) t=0 **(b)** t=20 **(c)** t=40 **(d)** t=60 **(e)** t=80 **(f)** t=100

Figure B.10 – Scenario B - Proposed resource allocation. Stochastic SIR simulation with our proposed resource allocation, Figure 5.20, as part of scatter plot Figure 5.24. Total cost equals 69.99 and the warning time is 5 hours. Red indicates 'on fire' and black 'burned'. Time t is displayed in hours.

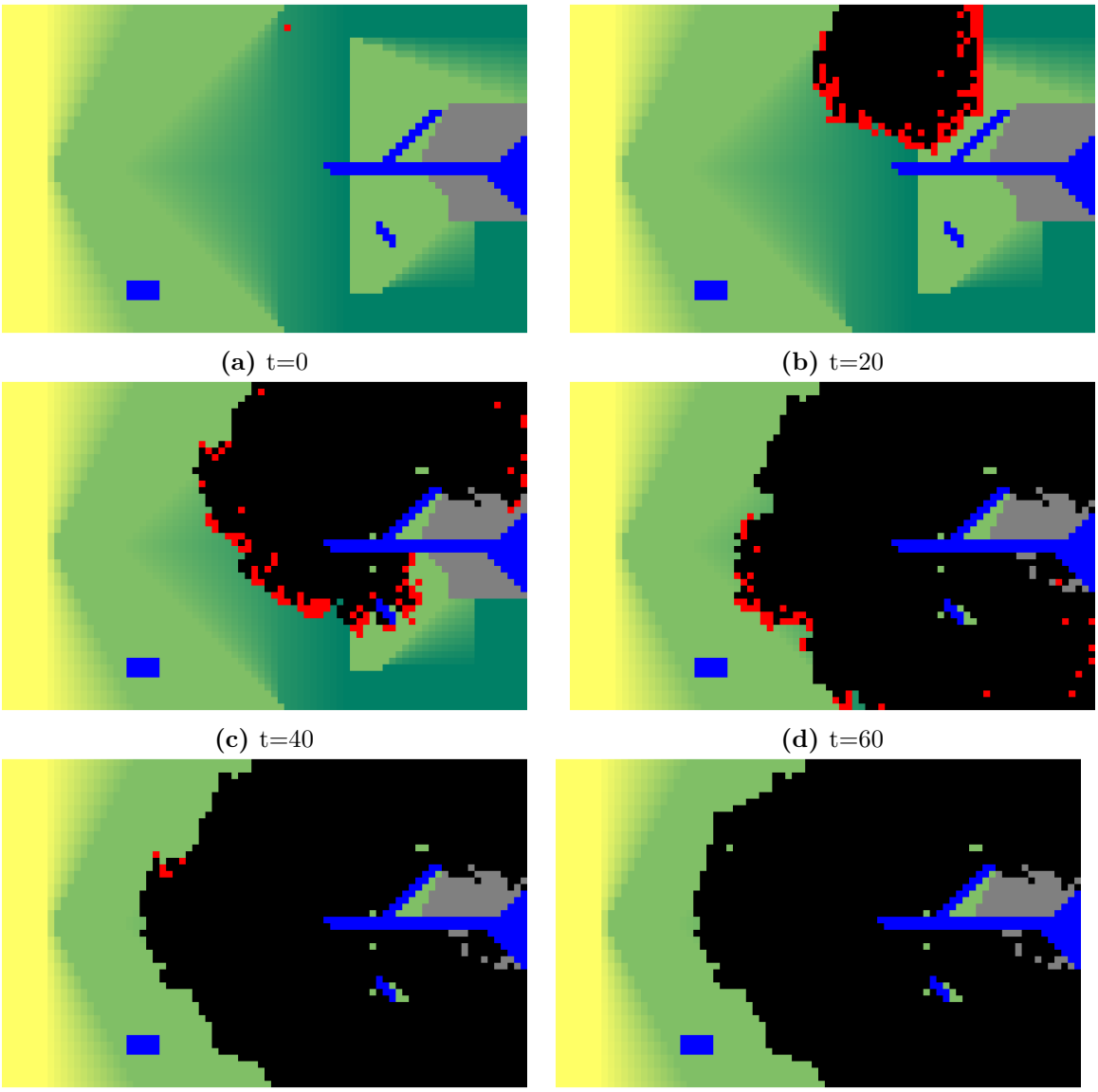

(a) t=0 **(b)** t=20 **(c)** t=40 **(d)** t=60 **(e)** t=80 **(f)** t=100

Figure B.11 – Scenario B - Spectral abscissa resource allocation. Stochastic SIR simulation with resource allocation obtained by minimized the spectral abscissa, Figure 5.23, as part of scatter plot Figure 5.24. Total cost equals 158.05 and the warning time is minus 12 hours. Red indicates 'on fire' and black 'burned'. Time t is displayed in hours.

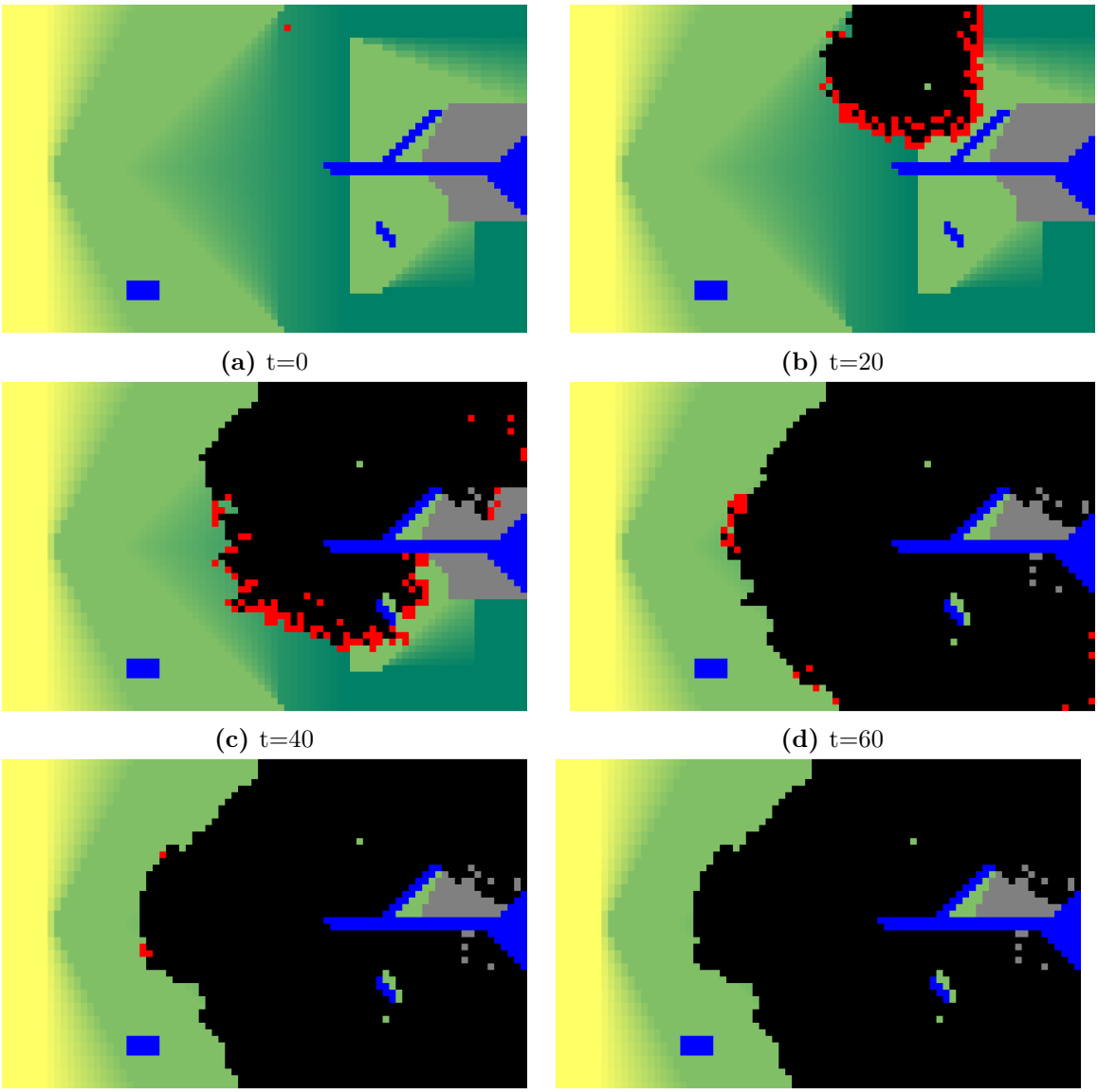

(a) t=0 **(b)** t=20 **(c)** t=40 **(d)** t=60 **(e)** t=80 **(f)** t=100

Figure B.12 – Scenario B - No resource allocation. Stochastic SIR simulation with no applied resource allocation. Total cost equals 185.00. Red indicates 'on fire' and black 'burned'. Time t is displayed in hours.